In vitro und in vivo Testung von Knorpelersatzmaterialien für chondrale und osteochondrale Defekte im Knie

Dissertation

zur Erlangung des akademischen Grades

doctor rerum naturalium (Dr. rer. nat.)

vorgelegt dem Rat der Medizinischen Fakultät
der Friedrich-Schiller-Universität Jena

von

Dipl.-Ing. (FH) Victoria Horbert, geb. Kopsch

geboren am 18.06.1987 in Torgau

Gutachter

1. Prof. Dr. med. Raimund W. Kinne, AG Experimentelle Rheumatologie, Lehrstuhl für Orthopädie, Universitätsklinikum Jena

2. Prof. Dr. rer. nat. Reinhard Wetzker, Institut für Molekulare Zellbiologie, CMB, Universitätsklinikum Jena

3. Prof. Dr. rer. nat. Michael Sittinger, AG Tissue Engineering, Medizinische Klinik mit Schwerpunkt Rheumatologie und Klinische Immunologie, Universitätsmedizin Berlin Campus Charité Mitte

Tag der öffentlichen Verteidigung: 02.07.2019

Meiner verstorbenen Großmutter

I. Abkürzungsverzeichnis

ACT	Autologe Chondrozytentransplantation
ACI	(engl.) autologous chondrocyte implantation
ALP	(engl.) alkaline phosphatase
AU	(engl.) absorbent unit
BMBF	Bundesministerium für Bildung und Forschung
BNC	Bakterielle Nanocellulose
BSA	(engl.) *bovine serum albumin*
CO_2	Kohlenstoffdioxid
DAB	Diaminobenzidin
DMB	Dimethylenblau
DMEM/F12	(engl.) *Dulbecco`s modified eagle medium/ Nutrient mixture F-12*
DNA	(engl.) *desoxyribonucleic acid*
DNase	Desoxyribonuklease
3D	dreidimensional
ELISA	(engl.) *enzyme-linked immunosorbent assay*
EZM	Extrazelluläre Matrix
F	(engl.) *force*
FCS	(engl.) *fetal calf serum*
GAG	Glucosaminoglykan
GuHCl	Guanidiniumhydrochlorid
H/E	Hämatoxylin-Eosin
HRP	(engl.) *horseradisch peroxidase*

ITS	Insulin-Transferrin-Selenium
MACT	Matrix-gestützte autologe Chondrozytentransplantation
MACI	(engl.) *matrix-assisted chondrocyte implantation*
MRI	(engl.) *magnetic resonance imaging*
mRNA	(engl.) *messenger RNA*
NIR	(engl.) *near-infrared*
NIRS	(engl.) *near-infrared spectroscopy*
NIRS-B	(engl.) *near-infrared spectroscopy and biomechanical indentation*
OA	Osteoarthrose
OATS	Osteochondrales autologes Transplantationssystem
OP	Operation
PBS	(engl.) *phosphate-buffered saline*
PCR	(engl.) *polymerase chain reaction*
PGA	Polyglykolsäure
PLS	(engl.) *partial least squares regression*
PTFE	(engl.) *polytetrafluoroethylene*
R^2	(engl.) *coefficient of determination*
RMSECV	(engl.) *root mean square error of cross validation*
RNA	(engl.) *ribonucleid acid*
RNase	Ribonuklease
RPD	residual prediction deviation
rpm	(engl.) *revolutions per minute*
RT	(engl.) *room temperature*
RT-PCR	Reverse-Transkriptase-PCR

SEM	(engl.) *standard error of the mean*
TBS	(engl.) *Tris-buffered saline*
TE	(engl.) *Tissue engineering*
TEP	Totalendoprothese

Verwendete SI-Einheiten

°C	Grad Celsius	g	Gramm
M	Mol	N	Newton
s	Sekunde	l	Liter
Pa	Pascal	Hz	Herz

Verwendete Präfixe

c	zenti	m	milli
k	kilo	n	nano
µ	mikro		

Hilfsmaßeinheiten

%	Prozent

II. Abbildungsverzeichnis

III. Tabellenverzeichnis

IV. Inhaltsverzeichnis

1. Zusammenfassung

Hyaliner Gelenkknorpel ist frei von Nerven, Blut und Lymphgefäßen und besitzt dadurch nur eine begrenzte Regenerationsfähigkeit. Die Zufuhr der Nährstoffe erfolgt ausschließlich per Diffusion durch die extrazelluläre Matrix (EZM) und/oder die Synovialflüssigkeit. Nicht behandelte Knorpeldefekte können daher im Langzeitverlauf zur Arthrose führen, die als Endpunkt einen vollständigen Gelenkersatz erfordert. In den letzten Jahrzehnten wurden zahlreiche Therapiekonzepte zur Behandlung von chondralen und osteochondralen Defekten entwickelt. Allerdings führt keine der bisherigen Behandlungsstrategien zur Bildung von belastbarem Regenerationsgewebe, sondern in der Regel nur zu einer vorübergehenden Linderung der Beschwerden.

Die Arbeitsgruppe Experimentelle Rheumatologie des Uniklinikums Jena befasst sich daher mit der Untersuchung von innovativen und/oder klinisch bereits etablierten Knorpelersatzmaterialien (Bakterielle Nanocellulose, CaReS®, BioSeed®-C) und entwickelte zu diesen Zwecken ein bovines in vitro Knorpelstanzenmodell.

Ziel der vorliegenden Arbeit war es, verschiedene Knorpelersatzmaterialien in vitro und in vivo zu untersuchen. In der ersten Phase wurden die oben genannten Knorpelersatzmaterialien in vitro kultiviert und anschließend biomechanisch, molekularbiologisch und histologisch untersucht. In der zweiten Phase wurde am Standort Jena das Knorpelersatzmaterial BioSeed®-C der Firma TTT in vivo untersucht. Die entstandenen Gewebsregenerate wurden nach 6 und 12 Monaten biomechanisch, molekularbiologisch und histologisch untersucht. Die gewonnenen Erkenntnisse sollen in die Entwicklung standardisierter Verfahren für die Prüfung von *Tissue engineering* (TE) Konstrukten für den orthopädisch-unfallchirurgischen Einsatz einfließen.

Für die in vitro Versuche wurden bovine Knorpelstanzen adulter Rinder mit einem zentralen Defekt versehen. Nach Applikation der Füllmaterialien in die Knorpeldefekte wurden die Knorpelstanzen unter standardisierten Bedingungen für bis zu 12 Wochen in vitro kultiviert. Abschließend wurden die Knorpelstanzen histologisch (n = 4), molekularbiologisch (n = 10) und biomechanisch (n = 10) untersucht. Für die in vivo Untersuchung des klinisch etablierten Knorpelersatzmaterials BioSeed®-C wurden 2 Knorpeldefekte auf der medialen Femurkondyle adulter Merinoschafe generiert. Ein Defekt wurde mit einem allogen besiedelten BioSeed®-C Implantat besetzt und ein Defekt diente als Leerdefekt (Kontrolle). Nach einer Standzeit von 6 und 12 Monaten erfolgte die biomechanische, molekularbiologische und histologische Analyse des Regeneratgewebes. Neben den in vitro und in vivo Versuchen wurde auch die Knorpeldickenvorhersage mittels Nahinfrarot-Spektroskopie (NIRS-B) ex vivo untersucht. Mit diesem Messsystem ist es möglich, die Knorpeleigenschaften im Knie des Großtiermodells Schaf zerstörungsfrei optisch zu

untersuchen und in einem weiteren Schritt die Qualität von Regeneratgewebe in vivo zu beurteilen.

Im Rahmen dieser Arbeit ist es gelungen, mit dem in der Arbeitsgruppe Experimentelle Rheumatologie etablierten in vitro Modell innovative und/oder klinisch bereits etablierte Knorpelersatzmaterialien (BNC, CaReS®, BioSeed®-C) über einen Zeitraum von bis zu 12 Wochen zu kultivieren und so die biomechanischen Eigenschaften (push-out Versuche) und molekularen Prozesse zu untersuchen, die bei der Knorpelregeneration stattfinden. Dieses Modell scheint allerdings nicht für die Untersuchung von resorbierbaren Materialien wie BioSeed®-C geeignet zu sein. Weiterhin zeigte die Auswertung der in vivo Proben trotz klarer klinischer Erfolge im Humansystem mit BioSeed-C im Schafsmodell noch keine eindeutige Ausbildung von vollwertigem Knorpelgewebe. Neben den in vitro und in vivo Untersuchungen ist es zudem gelungen, mittels der nicht invasiven Nahinfrarot-Spektroskopie (NIRS-B) eine zerstörungsfreie Vorhersage der Knorpeldicke im Knie des Großtiermodells Schaf zu realisieren (ex vivo Studie).

Die vorliegende Arbeit liefert vielversprechende Erkenntnisse, um die Entwicklung standardisierter Verfahren für die Prüfung von TE Konstrukten für den orthopädisch-unfallchirurgischen Einsatz voran zu treiben. Die Modifizierung des etablierten in vitro Modells für die Untersuchung von resorbierbaren Materialien sowie weiterführende Untersuchungen zur Vorhersage von Knorpeldicke und Knorpeleigenschaften mittels der nicht invasiven Methode NIRS-B stellen interessante Aufgaben für zukünftige Studien dar.

2 Einleitung

2.1. Aufbau und Eigenschaften des hyalinen Knorpels

Der hyaline Knorpel ist makroskopisch durch seine glatte und milchig durchscheinende Oberfläche charakterisiert und überzieht als wenige Millimeter dicke Schicht die Oberfläche der angrenzenden Knochen der beweglichen Gelenke. Hyaliner Knorpel ist dabei aufgrund seiner Zusammensetzung in der Lage, einen reibungsarmen Bewegungsablauf zu gewährleisten und kann zudem Belastungskräfte von bis zum 5-fachen des eigenen Körpergewichtes aufnehmen.

Adulter Knorpel ist frei von Nerven, Blut- und Lymphgefäßen, und besitzt daher nur eine begrenzte Regenerationsfähigkeit. Die Zufuhr der Nährstoffe erfolgt ausschließlich per Diffusion durch die extrazelluläre Matrix (EZM) und/oder die Synovialflüssigkeit.

Die zellulären Komponenten des adulten Knorpels sind die Chondrozyten, die lediglich 2 - 5% des Gesamtvolumens ausmachen (Stockwell 1979) und in eine EZM eingebettet sind. Die grundlegende Komponente der EZM ist neben Wasser und Ionen (ca. 80%) ein Netzwerk aus strukturellen Makromolekülen (Kollagene, Proteoglykane und verschiedene Glykoproteine; ca. 20%). Das komplexe Zusammenwirken dieser Komponenten bestimmt dabei die wesentlichen biomechanischen Eigenschaften des hyalinen Knorpels (Mollenhauer und Aurich 2003).

Den Hauptbestandteil des kollagenen Fasergerüstes bildet das Kollagen Typ II mit ca. 90 – 95%, das maßgeblich für die Stabilität des Knorpels bei einwirkenden Zug- und Scherkräften verantwortlich ist (Benninghoff 1925). Weitere Bestandteile sind die Kollagene Typ VI, IX, X und XI und Proteoglykane (Kuettner 1992). Das größte und am häufigsten vorkommende Proteoglykan ist das Aggrekan. Ein Proteoglykanmolkül besteht aus einem zentralen Protein, an das negativ geladene sulfatierte Glykosaminoglykan-Ketten (z. B. Chondroitinsulfat, Keratansulfat und Dermatansulfat) gebunden sind. Über die Bindung vieler solcher Moleküle an eine Hyaluronsäurekette entstehen unterschiedlich große Polymeraggregate, die durch ihre polyanionischen Eigenschaften eine hohe Bindungskapazität für Kationen und damit für Wasser besitzen. Dies wiederum beeinflusst die spezifischen und funktionellen Eigenschaften des Knorpels (Putz 2008).

Morphologisch lässt sich der hyaline Knorpel in vier verschiedene Zonen unterteilen, die sich in der äußeren Form der Chondrozyten sowie deren Aktivität und Orientierung zur Gelenkfläche unterscheiden (Buckwalter und Lohmander 1994, Buckwalter und Mankin 1998, Poole et al. 2001) (Abb. 1).

I. Die Tangentialzone ist mit 10 – 20% der Knorpeldicke die dünnste Lage des Gewebes und bildet die Gleitschicht des Knorpels. Die Chondrozyten in dieser Zone sind abgeflacht, spindelförmig und parallel zum flachen Kollagenfasergerüst angeordnet. Durch die parallele Anordnung der Kollagenfasern gilt die Tangentialzone als Zone mit der höchsten Druck- und Zugfestigkeit (Bullough und Goodfellow 1968, Kempson et al. 1973).

II. Die Transitionalzone oder auch Übergangszone macht 40 – 60% der Knorpeldicke aus. Die Chondrozyten in dieser Zone besitzen eine unregelmäßige Anordnung in einem sich überschneidenden Kollagenfasergerüst.

III. Die Radialzone macht 30 – 40% der Knorpeldicke aus. Die Anordnung der Chondrozyten und der Kollagenfasern ist dabei senkrecht zur Gelenkoberfläche. Die Zelldichte ist geringer als in der Transitionalzone.

IV. Die Zone des kalzifizierten Knorpels oder auch Mineralisierungszone bildet den Übergang zum subchondralen Knochen und ist durch degenerativ veränderte Chondrozyten gekennzeichnet.

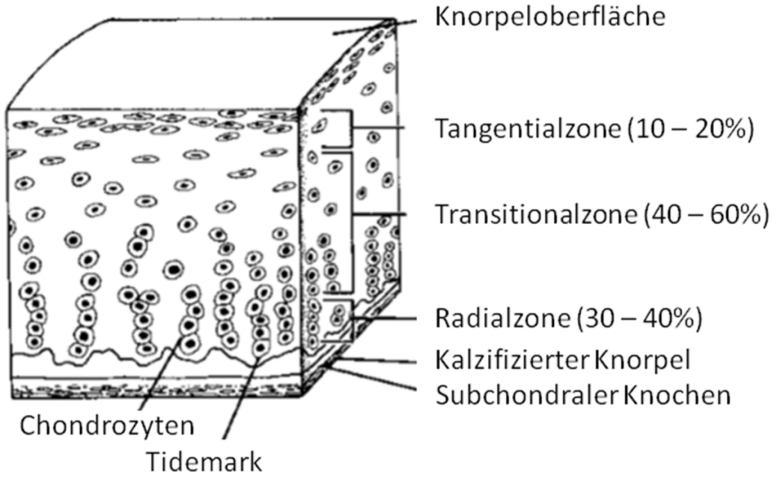

Abb. 1: Schematische Darstellung des Knorpelaufbaus modifiziert nach Newman (Newman 1998).

2.2. Knorpelschäden

Vor allem im Bereich des Kniegelenkes entstehen Knorpeldefekte meist durch Traumata oder im Rahmen der primären Arthrose. Knorpeldefekte mit einer Größe von mehr als 2 – 4 cm^2 heilen dabei selten spontan (Convery et al. 1972, Furukawa et al. 1980, Meachim und Roberts 1971, Mitchell und Shepard 1987) und können so zu einer sekundäre Arthrose führen (Madry et al. 2011, Mankin 1982). Eine entscheidende Rolle spielen dabei unter anderem die Avaskularität des Knorpelgewebes und die geringe Zelldichte (Mankin 1982).

Weiterhin sind die Chondrozyten in ein Gerüst aus Kollagenfasern und Proteoglykanen eingebunden, und können daher nicht sofort zum Ort der Schädigung migrieren (Khan et al. 2008). Dies stellt insbesondere bei jungen Patienten ein großes Problem dar.

Es werden 2 Arten von Knorpelverletzungen unterschieden: rein chondrale Knorpeldefekte und osteochondrale Knorpeldefekte, die bis in den subchondralen Knochen reichen (Noyes und Stabler 1989, Wirth und Rudert 1996). **Chondrale Defekte**, die häufig nach einem Trauma entstehen, führen dabei nicht zwangsläufig zu einer frühen Arthrose (Buckwalter 2002). Verschiedene Studien haben allerdings gezeigt, dass nach Knorpelverletzungen in den Kniegelenken junger Sportler bis zu 40% der untersuchten Patienten innerhalb von 14 Jahren Zeichen einer Arthrose entwickeln (Messner und Maletius 1996). Ob es im späteren Verlauf dann tatsächlich zur Entwicklung einer Arthrose kommt, hängt von verschiedenen Parametern wie Größe, Tiefe und Lokalisation des Defekts, Patientenalter sowie Aktivitätsniveau ab (Buckwalter 2002, Lotz und Kraus 2010, Gaissmaier et al. 2003). Bei **osteochondralen Defekten** hingegen kommt es durch die Eröffnung ossärer Blutgefäße zu einer lokalen Einblutung in die Defekte. Durch das zusätzliche Einwandern von pluripotenten mesenchymalen Stammzellen aus dem Knochenmark kommt es zur Bildung von Reparaturgewebe (Shapiro et al. 1993). Dabei scheint es zu einer vollständigen Rekonstruktion des knöchernen Anteils mit einer unzureichenden Integration des chondralen Anteils zu kommen. Dies kann aufgrund der biomechanischen Belastungen im Gelenk wiederum zu degenerativen Veränderungen und somit zur Entstehung einer Arthrose führen (Shapiro et al. 1993).

2.3. Behandlungsstrategien zur Behandlung von Knorpeldefekten

Wie bereits erwähnt, besitzt der Gelenkknorpel nur eine begrenzte Regenerationsfähigkeit. Nicht behandelte Knorpeldefekte können daher im Langzeitverlauf zur Arthrose führen, die als Endpunkt einen vollständigen Gelenkersatz erfordert. Neben konservativen Behandlungsmöglichkeiten wie Krankengymnastik ist daher das primäre Ziel von modernen Operationsverfahren, die normale Gelenkfunktion mit schmerzloser Beweglichkeit wieder herzustellen und den Einsatz einer Totalendoprothese (TEP) so lange wie möglich zu verzögern.

In den letzten Jahrzehnten wurden daher zahlreiche Operationsverfahren entwickelt, um eine ausreichende Knorpelregeneration zu stimulieren. Keine dieser bisher entwickelten Methoden stimuliert jedoch die Bildung von hyalinem Gelenkknorpel, sondern induziert überwiegend lediglich die Ausbildung von Faserknorpel sowie in der Regel nur eine vorübergehende Linderung der Beschwerden.

Aktuell werden für die Behandlung von chondralen Knorpeldefekten markraumeröffnende Verfahren (Mikrofrakturierung), osteochondrale Transplantate (OATS) sowie die autologe Chondrozytentransplantation (ACT) angewendet (Madry et al. 2011). Die Wahl der Behandlungsmethode ist dabei von der Art der Knorpelverletzung, dem Patientenalter sowie der Defektgröße und -lage abhängig (Madry et al. 2011, Vaquero und Forriol 2012).

2.3.1. Lavage, Débridement und Shaving

Bei kleinen chondralen Knorpeldefekten bieten sich symptomatische Therapieverfahren wie Lavage, Débridement oder Shaving an, die kurzfristige Erfolge bei bis zu 80% der Patienten und mittelfristige Erfolge bei bis zu 50% der Behandelten aufweisen (Buckwalter und Lohmander 1994). Bei der Lavage wird mittels Arthroskopie das Gelenk von den abgelösten Knorpelfasern und Entzündungsmediatoren freigespült. Die Methode des Shaving entfernt abgelöste Knorpelteile, die mechanische Probleme verursachen können (Baumgaertner et al. 1990, Buckwalter und Lohmander 1994). Klinisch und experimentell wurden in verschiedenen Studien allerdings Nekrosen sowie Schädigungen im angrenzenden Gewebe beobachtet (Kim et al. 1991, Korkala 1988). Die Methode des Débridement wurde 1941 von Magnuson erstmals beschrieben. Dabei erfolgt die Entfernung von überschüssigen Knorpelfragmenten mit anschließender Glättung der Knorpelränder und der Knorpeloberfläche. Magnuson (Magnuson 1974) und Haggart (Haggart 1947) konnten dabei eine temporäre Verbesserung des funktionellen Befundes bei bis zu 70% der Patienten zeigen. Bei all diesen Verfahren kommt es allerdings nicht zu einer Ausbildung von Reparaturgewebe oder einer Verlangsamung der Arthroseentwicklung.

2.3.2. Mikrofrakturierung

Die Mikrofrakturierung ist die am häufigsten angewendete Methode für die Behandlung von chondralen Knorpeldefekten. Sie hat das Ziel, pluripotente Stammzellen aus dem Knochenmark in den Defekt zu bringen, um die Bildung von Ersatzknorpel zu stimulieren. Neben der als erstes von Pridie 1959 beschriebenen Technik und der Abrasionsarthroplastik nach Johnson (Johnson 1986) entwickelte Richard Steadman 1985 ein weiteres Verfahren der Mikrofrakturierung (Steadman et al. 1997). Bei dieser Variante der Mikrofrakturierung handelt es sich um ein kostengünstiges, einstufiges Verfahren, welches im Rahmen eines arthroskopischen Eingriffs durchgeführt werden kann und eine geringe Komplikationsrate aufweist (Richter und Diederichs 2009). Der Vorteil gegenüber der Predie-Bohrung ist dabei das Fehlen der Schädigung des subchondralen Knochens (Matthews und Hirsch 1972) durch Hitze und der damit verbundenen Nekrosen.

Steadman bringt dabei mehrere Perforationen in den freiliegenden suchondralen Knochen ein, aus denen zusätzlich Blut aus dem Mark austreten kann. Die darin enthaltenen pluripotenten Stammzellen können durch biologische und biomechanische Faktoren in Knorpel und Knochenzellen differenzieren. Das Ergebnis ist ein defektfüllender, stabiler und belastbarer Faserknorpel (Buckwalter und Lohmander 1994, Shapiro et al. 1993, Burkart et al. 2001).

Allerdings ist der gebildete Faserknorpel den mechanischen Anforderungen langfristig nicht gewachsen und es kommt je nach Defektgröße auch nachfolgend noch zur Ausbildung einer Arthrose (Imhoff et al. 1999). Klinisch zeigte sich durch die Behandlung mittels Mikrofrakturierung bei bis zu 77% der Patienten nach 2-5 Jahren eine Verbesserung der Beschwerden (Steadman et al. 1999, Passler 2000, Knutsen et al. 2007, Mithoefer et al. 2005).

2.3.3. Autologe Chondrozytentransplantation (ACT)

Für die Behandlung von größeren Defekten hat sich die durch die schwedische Arbeitsgruppe um Peterson und Brittberg 1994 entwickelte autologe Chondrozytentransplantation (ACT) zum Goldstandard entwickelt (Brittberg et al. 1994). Dabei werden zunächst die Chondrozyten aus einer arthroskopisch gewonnen Knorpelbiopsie isoliert, in vitro vermehrt und in einer zweiten OP als Zellsuspension in den vorbereiteten Knorpeldefekt injiziert (Brittberg et al. 2003). Ein aus der Tibiaoberfläche gewonnener Periostlappen wird als mechanischer Schutz wasserdicht am umliegenden Knorpel vernäht. Dieser enthält neben den im Periostlappen enthaltenen Wachstumsfaktoren auch mesenchymalen Stammzellen (Peterson et al. 2000, O'Driscoll und Fitzsimmons 2001). Die Technik der ACT wurde dabei kontinuierlich weiterentwickelt, so dass anstelle des aufwändig gewonnen Periostlappens eine resorbierbare Kollagenmatte eingeführt wurde (Haddo et al. 2004, Bentley et al. 2003). Neben der Behandlung von großen Knorpeldefekten (3 bis zu 10 cm^2, (Behrens et al. 2004, Gomoll et al. 2010, Niemeyer et al. 2010)) wird die ACT auch bei kleineren Defekten angewendet, bei denen andere Methoden nicht erfolgreich waren (Niemeyer et al. 2010, Madry und Pape 2008).

In Abhängigkeit von dem Defektort sowie der Art des Defektes wurden in Langzeitstudien über einen Zeitraum von bis zu 20 Jahren gute bis sehr gute klinische Ergebnisse festgestellt (Minas 1998, Peterson et al. 2010, Peterson et al. 2002, Moseley et al. 2010, Micheli et al. 2001, Henderson et al. 2005, Erggelet et al. 2000). Dennoch weist die ACT eine Reihe von Nachteilen auf. Zum einen neigen die isolierten Chondrozyten während der Expansionsphase in Monolayer-Kulturen häufig zu einer Dedifferenzierung (Darling und Athanasiou 2005). Zum anderen ist die Gewinnung und Fixierung des Periostlappens sehr

aufwändig. Weiterhin sind für die ACT zwei operative Eingriffe mit einer hohen Belastung für die Patienten notwendig.

Um diese Nachteile zu umgehen, wurde die ACT unter Verwendung von verschiedenen Biomaterialien zu einem trägergekoppelten Verfahren weiterentwickelt. Bei der sogenannten matrixassoziierten Chondrozytentransplantation (MACT) werden isolierte Chondrozyten auf verschiedene Matrices ausgesät, in vitro kultiviert und anschließend in den Defekt implantiert (Andereya et al. 2006). Klinisch etablierte Trägermaterialien sind dabei beispielsweise Kollagengele (z. B. CaReS®, Arthro Kinetics Biotechnology GmbH, Krems; Novocart® 3D, Tetec AG, Reutlingen), Hyaluronsäuregele (z. B. Hyalograft C ®, Fidia Advanced Biopolymers, Italien; (Nehrer et al. 2006)) oder resorbierbare Biopolymere (z. B. Bioseed C®, BioTissue Technologies, Freiburg; (Kreuz et al. 2009)). Die Vorteile der MACT gegenüber der ACT sind dabei vor allem in der Vereinfachung der Methode sowie der Verkürzung der Operationszeit zu sehen. Studien zeigten bislang keine eindeutigen Unterschiede zwischen ACT und MACT im klinischen und histologischen Outcome (Bartlett et al. 2005, Manfredini et al. 2007, Iwasa et al. 2009).

2.3.4. Transplantation osteochondraler Zylinder

Chondrale bzw. osteochondrale Defekte, insbesondere im Knie, stellen heutzutage ein gravierendes therapeutisches Problem dar. Bei der Anwendung der osteochondralen Transplantation von autologen Knorpel-Knochen Zylindern (OATS) aus demselben Gelenk ist das Ziel die Wiederherstellung der Knorpeloberfläche, um Schmerzfreiheit sowie eine normale Gelenkfunktion zu erreichen. Dazu werden osteochondrale Zylinder von einer gering belasteten Stelle des Gelenkes press-fit in den Knorpel-Knochen-Defekt eingebracht. Diese Methode wurde erstmals 1964 von Wagner beschrieben, um größere Knorpeldefekte im Kniegelenk zu therapieren.

Das Verfahren der OATS wurde durch Hangody (Hangody et al. 1996) und Bobic (Bobic 1996) wieder aufgegriffen, verbessert und zu einem arthroskopischen Vorgehen weiterentwickelt. Mit dieser OATS Technik gelingt es, im Gegensatz zu anderen Operationstechniken (Mikrofrakturierung, Débriment, ACT, MACT) sofort vollwertigen hyalinen Knorpel in den Defekt einzubringen. Weiterhin handelt es sich bei der OATS um ein einstufiges Operationsverfahren. Ein Nachteil der autologen Transplantation von osteochondralen Zylindern besteht allerdings darin, dass autologes Material nur begrenzt zu Verfügung steht und so nur Defekte von höchstens 4 cm^2 mit dieser Methode behandelt werden können.

2.3.5. Tissue Engineering

Nach dem heutigen wissenschaftlichen Stand nimmt der Bedarf für neue Therapie-Ansätze zur Behandlung von chondralen und osteochondralen Defekten stetig zu. Die Entwicklung neuartiger Therapieverfahren für die Herstellung eines biologischen Implantates fordert einen interdisziplinären Ansatz aus Technik, Biochemie, Zellbiologie und Medizin. Tissue Engineering (TE) basiert dabei auf der Vermehrung autologer Zellen in vitro unter Verwendung von biologischem Gewebe, das anschließend als Transplantat in den Patienten eingebracht wird (Richter und Diederichs 2009). Die Technologie des TE ist allerdings sehr aufwändig, da die Zellen der Patienten zunächst isoliert und kultiviert werden müssen, bevor sie anschließend in den Patienten transplantiert werden können. Dabei müssen vor allem potenzielle Infektionen ausgeschlossen werden. Eine weitere Voraussetzung für die erfolgreiche klinische Anwendung solcher TE-basierten Implantate ist zudem die Herstellung einer funktionsfähigen Knorpelmatrix mit ähnlichen biomechanischen Eigenschaften wie hyaliner Knorpel (Weise et al. 2000).

2.4. CaReS ®

CaReS® ist ein autologes, dreidimensionales Hydrogel, das aus Kollagen Typ I besteht. Zunächst werden aus den bei einer Biopsie entnommenen Knorpelfragmenten die Chondrozyten isoliert und ohne weitere Prozesssierung in das Kollagengel eingebracht. Dadurch wird das Risiko der Dedifferenzierung der isolierten Chondrozyten während der mehrmaligen Passagierung minimiert. Das Transplantat kann in jeder gewünschten Größe hergestellt werden (Andereya et al. 2006). In vivo Studien haben zudem gezeigt, dass es auch bei der Verwendung eines zellfreien Kollagen Typ I Hydrogels zur Ausbildung von Reparaturgewebe kommt, das mit dem Gewebe nach der Implantation von zellhaltigen Transplantaten vergleichbar ist. Diese Ergebnisse zeigen, dass es bei den zellfreien Transplantaten zur Einwanderung von Chondrozyten aus dem umliegenden Gewebe kommt, die zur Knorpelregeneration beitragen (Andereya et al. 2006, Maus et al. 2008, Schneider et al. 2011a, Welsch et al. 2010).

2.5. Bakterielle Nanocellulose (BNC)

Cellulose ist ein in der Natur häufig vorkommendes Polysaccharid und ein nahezu unerschöpflicher polymerer Rohstoff mit großer Bedeutung für industrielle Anwendungen.
A.J. Brown (Brown 1886b) beschrieb im Jahr 1886 erstmals die Bildung von Cellulose durch gram-negative Bakterien der Gattung Gluconacetobacter xylinum und stellte fest, dass die molekulare Struktur des entstandenen Produktes mit der von natürlicher Cellulose identisch

war (Brown 1886b, Brown 1886a). Die Synthese der BNC erfolgte an der Übergangszone zwischen Luft und Flüssigkeit und die BNC wies ein feinstrukturiertes dreidimensionales Netzwerk mit einem Wassergehalt von bis zu 99% und einer ausgeprägten Tunnel- und Porenstruktur auf (Abb.2; (Klemm et al. 2011)).

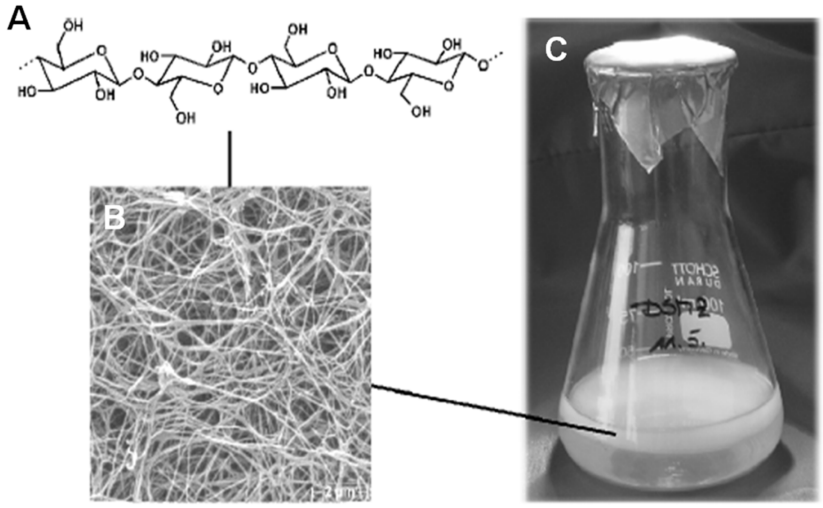

Abb. 2: Struktur und Form bakterieller Nanocellulose (BNC). (A) molekulare Cellulosekette; (B) rasterelektronenmikroskopische (REM) Aufnahme des gefriergetrockneten BNC-Netzwerks (Vergrößerung 10.000); (C) BNC-Vlies aus statischer Kultur (Klemm et al. 2006).

Mitte des 20. Jahrhunderts begannen Hestrin und Schramm mit der Erforschung der grundlegenden Stoffwechselvorgänge der Celluloseproduktion sowie der Erarbeitung eines optimierten Kultivierungsmediums (Hestrin und Schramm 1954, Schramm et al. 1957, Schramm und Hestrin 1954b, Schramm und Hestrin 1954a). Dieses nach seinen Erfindern benannte Medium wird unter Laborbedingungen bis heute für die Produktion von BNC verwendet. Durch Veränderungen des biotechnologischen Prozesses (statisch, dynamisch, in situ-Modifizierung, post-Modifizierung) ist es möglich, die strukturelle Charakteristik der BNC und ihre Eigenschaften zu verändern (Heßler 2008, Seifert 2004, Haigler et al. 1982, Astley et al. 2001, Evans et al. 2005, Nakayama et al. 2004). Durch diese vielseitigen Möglichkeiten der Modifikation sowie die charakteristischen Eigenschaften der BNC (hohe mechanische Stabilität, Biokompatibilität, hohes Elastizitätsmodul und enorme Reißfestigkeit (Kramer 2008)) ist sie ein Biomaterial mit hohem Anwendungspotenzial vor allem im medizinischem Bereich (Jonas und Farah 1998, Kramer 2008).

Klinisch wird die BNC bereits als Wundauflage zur Behandlung von Verbrennungen, Ulzera, als temporärer Hautersatz (Cuticell®Epigraft, Biofill ®, BioProcess®/NexFill®), als Implantat

für die Behandlung von paradontalen Erkrankungen (Gengiflex ®) oder für die Rekonstruktion von Dura-Defekten (SYNTHECEL®, (Rosen et al. 2011)) verwendet.
Weiterhin scheint die bakterielle Nanocellulose aufgrund ihrer biomechanischen Eigenschaften und ihrer Biokompatibilität ein innovatives Implantatmaterial zur Behandlung von Meniskus- (Bodin et al. 2007, Martinez et al. 2012) und Knorpelschäden (Muller et al. 2006, Gama et al. 2012, Ahrem et al. 2014, Andersson et al. 2010, Lopes et al. 2011, Svensson et al. 2005) zu sein.

2.6. BioSeed-C ®

BioSeed®-C ist ein klinisch etabliertes Chondrozyten-Transplantat, das aus einem resorbierbaren Vlies aus Polyglykolsäure (PGA) besteht und mittels chirurgischer Nähte oder Fibrinkleber im Defekt fixiert wird. BioSeed®-C wird für die Behandlung von humanen Gelenkknorpeldefekten im Knie, im Fußgelenk oder der Hüfte erfolgreich eingesetzt und bedient sich der Methode der autologen Chondrozytentransplantation (ACT). Das resorbierbare PGA-Vlies wird dabei vor seiner Implantation in den Knorpeldefekt mit zuvor entnommenen und expandierten Chondrozyten besiedelt und anschließend transossär fixiert. Die PGA Transplantate besitzen eine textile und zugfeste Struktur mit Einzelfaserdurchmessern von 17 µm (Endres et al. 2012). Innerhalb von 7 Tagen verlieren sie bereits 50% ihrer mechanischen Festigkeit und nach 42 Tagen sind die Transplantate in vitro komplett resorbiert (Dunzel et al. 2013, Endres et al. 2007). In vivo ist BioSeed®-C nach einem Zeitraum von etwa 5 Wochen resorbiert (Pillai und Sharma 2010).
In verschiedenen in vitro und in vivo Studien wurde gezeigt, dass es durch die Behandlung des Knorpeldefektes mit einem autologen BioSeed®-C Transplantat zur Bildung von knorpelspezifischer ECM im Transplantat kommt (Hunter und Levenston 2004, Kaps et al. 2006, Endres et al. 2007).

3. Ziele der Arbeit

Zellfreie bzw. zellhaltige TE Konstrukte für die Behandlung von chondralen und osteochondralen Defekten unterliegen derzeit unterschiedlichen Zulassungsbedingungen (Guidlines der EMA zu „Human Cell-based Medicinal Products“). In dieser Richtlinie wird unter anderem auch die standardisierte mechanische Testung der Konstrukte betont. Aus diesem Grund beschäftigte sich das BMBF Verbundprojekt „QuReGe“ mit der Entwicklung bzw. der Etablierung von validen Prüfverfahren von TE Konstrukten für den orthopädisch-unfallchirurgischen Einsatz.

Ziel der vorliegenden Arbeit war es, verschiedene z. T. etablierte klinische Knorpelersatzmaterialien in vitro und in vivo zu untersuchen. Die Arbeitsgruppe Experimentelle Rheumatologie des Universitätsklinikums Jena verfügt über ein etabliertes in vitro Modell (bovines Knorpelstanzenmodell), das für die Testung genutzt wurde. Untersucht wurden die bereits klinisch zugelassenen Knorpelersatzmaterialien BioSeed®-C (zellfrei und zellhaltig) und das Kollagen Typ I Hydrolgel CaReS® (zellfrei und zellhaltig) sowie unmodifizierte BNC.

In der ersten Phase wurden die oben genannten Knorpelersatzmaterialien über einen Zeitraum von bis zu 12 Wochen in vitro kultiviert und anschließend biomechanisch, molekularbiologisch und histologisch untersucht. In der zweiten Phase wurde am Standort Jena das Knorpelersatzmaterial BioSeed®-C der Firma TTT in vivo untersucht. Die entstandenen Gewebsregenerate wurden nach 6 und 12 Monaten biomechanisch, molekularbiologisch und histologisch untersucht.

Die gewonnenen Erkenntnisse sollen in die Entwicklung standardisierter Verfahren für die Prüfung von TE Konstrukten für den orthopädisch-unfallchirurgischen Einsatz einfließen.

4. Publizierte Originalarbeiten

4.1. In Vitro Analysis of Cartilage Regeneration Using a Collagen Type I Hydrogel (CaReS) in the Bovine Cartilage Punch Model (Peer-Reviewed)

Autorenschaft der Publikation

Victoria Horbert, Long Xin, Peter Foehr, Olaf Brinkmann, Matthias Bungartz, Rainer H. Burgkart, T. Graeve, Raimund W. Kinne

Abstract

Objective

Limitations of matrix-assisted autologous chondrocyte implantation to regenerate functional hyaline cartilage demand a better understanding of the underlying cellular/molecular processes. Thus, the regenerative capacity of a clinically approved hydrogel collagen type I implant was tested in a standardized bovine cartilage punch model.

Methods

Cartilage rings (outer diameter 6 mm; inner defect diameter 2 mm) were prepared from the bovine trochlear groove. Collagen implants (± bovine chondrocytes) were placed inside the cartilage rings and cultured up to 12 weeks. Cartilage-implant constructs were analyzed by histology (hematoxylin/eosin; safranin O), immunohistology (aggrecan, collagens 1 and 2), as well as for protein content, mRNA expression, and implant push-out force.

Results

Cartilage-implant constructs revealed vital morphology, preserved matrix integrity throughout culture, progressive, but slight proteoglycan loss from the "host" cartilage or its surface and decreasing proteoglycan release into the culture supernatant. In contrast, collagen 2 and 1 content of cartilage and cartilage-implant interface was approximately constant over time. Cell-free and cell-loaded implants showed: (1) cell migration onto/into the implant; (2) progressive deposition of aggrecan and constant levels of collagens 1 and 2; (3) progressively increased mRNA levels for aggrecan and collagen 2; and (4) significantly augmented push-out forces over time. Cell-loaded implants displayed a significantly earlier and more long-lasting deposition of aggrecan, as well as tendentially higher push-out forces.

Conclusion

Preserved tissue integrity and progressively increasing cartilage differentiation and push-out forces for up to 12 weeks of cultivation suggest initial cartilage regeneration and lateral bonding of the implant in this in vitro model for cartilage replacement materials.

Keywords

bovine cartilage punch model, collagen type I hydrogel, matrix-associated cartilage transplantation (MACT), (immuno)histology, implant push-out force

Introduction

Partial- and full-thickness traumatic or degenerative cartilage lesions of the knee are common and lead to progressive deterioration of the cartilage and finally osteoarthritis. Efficient and reliable methods for successful cartilage repair, including autologous chondrocyte implantation (ACI), microfracture, and osteoarticular transfer/mosaicplasty, are thus highly sought and have shown some promise in initial cartilage regeneration (Hunziker 2002, Musumeci et al. 2014).

These methods, however, mostly do not stop the progression of cartilage degeneration and usually result in an unpredictable outcome concerning: (1) defect coverage; (2) fibrous or hyaline features of the repair tissue; and (3) considerably weaker mechanical properties and higher permeability of the repair tissue compared with native cartilage (Dell'Accio et al. 2006, Ye et al. 2014).

Novel tissue engineering techniques, for example, second-generation ACI techniques such as matrix-assisted chondrocyte implantation (MACI), have led to an improvement of traditional methods and have recently entered clinical practice, usually aiming at providing stable and long-lasting attachment of the regenerated cartilage to the defect area (Bachmann et al. 2004, Dewan et al. 2014, Gobbi et al. 2015, Kon et al. 2009).

These techniques show the advantage of a decreased operation time, limited surgical trauma, and lack of complications associated with the use of periosteum in first-generation ACI (e.g., graft overgrowth) and have employed materials such as collagen membranes (type I/III collagen membrane) (Bartlett W. 2006, Gillogly und Wheeler 2015, Steinwachs und Kreuz 2007).

One commercial MACI product (type I collagen-based CaReS) has been extensively applied in Europe (and “off-label” in the United States) and is currently used with some clinical success (Schneider et al. 2011b). CaReS, a 3-dimensional hydrogel, is first seeded with in vitro–enriched autologous chondrocytes and then introduced into the debrided cartilage defect. Studies in the large animal model Goettinger minipig have recently shown that even a cell-free collagen type I hydrogel yields high-quality cartilage repair tissue comparable to that obtained after implantation of the cell-seeded implant. This suggests that cells migrating into the defect site from the surrounding cartilage may participate in the regeneration of cartilage (Andereya et al. 2006, Maus et al. 2008, Schneider et al. 2011a, Welsch et al. 2010). However, to our knowledge, there are presently no in vitro studies addressing the cellular and molecular mechanisms of cartilage regeneration in cartilage-implant constructs containing this cell-based collagen implant.

The main aim of the study was thus to analyze the behavior of this collagen implant in an in vitro model and to assess whether the results reflect its clinical performance for the therapy of cartilage defects. The following hypotheses were tested: (1) the experimental in vitro model is suitable for pre-testing of implants intended for the clinical regeneration of cartilage defects; (2)

the model allows the description of the cellular and molecular processes underlying cartilage regeneration in vitro; (3) the cell-free and/or cell-loaded collagen implant supports the regeneration of the cartilage defect (via cell migration and tissue formation) in the in vitro model by its physicochemical and molecular structure.

For this purpose, a novel cartilage implant model was developed consisting of: (1) “host” cartilage cylinders resected from bovine femoral condyles using standardized punches; and (2) inserted matrix implants. The cylinders were filled with the cell-free or cell-loaded collagen I scaffold, cultured for periods of up to 12 weeks, and then subjected to: (1) (immuno)histological staining (hematoxylin/eosin, safranin O; aggrecan, collagens 1 and 2); (2) protein assays (dimethyleneblue-binding [DMB]-test for tissue proteoglycan analysis; enzyme-linked immunosorbent assay [ELISA] for aggrecan, collagens 1 and 2); (3) transcriptional analysis (expression of aggrecan, collagen 1, and collagen 2); and (4) measurement of implant push-out force.

Methods

Preparation/Culture of Cartilage Rings with Cell-Free or Cell-loaded Collagen Implants

Bovine cartilage was obtained from the knee joint of German Holstein Friesian Cattle (age 24 months) (Pretzel et al. 2013). Collagen implants (Amedrix GmbH, Esslingen; Germany; cell-free or cell-seeded with bovine chondrocytes; ± cells; cell isolation and seeding according to internal guidelines of the producer) were placed into the inner defect of the cartilage rings (Fig. 3). The constructs were then embedded in an agarose cylinder in 48-well plates (Fig. 3A-E) and cultured for 0, 4, 8, 10, and 12 weeks at 37°C and 5% CO_2 in Dulbecco’s modified Eagle’s culture medium (DMEM; containing 5% fetal calf serum [FCS], 1% gentamycin, and 0.1% ITS (insulin-transferrin-selenium)–culture supplement [final concentrations: 5 µg/ml insulin and transferrin, 5 ng/ml selenic acid; BD Biosciences, Heidelberg, Germany]). Media were changed 3 times a week.

In each experimental series, 120 technical replicates of cartilage rings each were obtained from one animal each for both cell-free and cell-loaded collagen implants (n = 5 and 6 experimental series, respectively) and subsequently analyzed histologically (n = 4), biochemically (n = 10; n = 5 each for real time polymerase chain reaction [RT-PCR] and protein extraction), and biomechanically (n = 10; total of 24 samples for each of the 5 time points; see below). Supernatants were pooled over 1 week and stored at −20°C for further ELISA analysis.

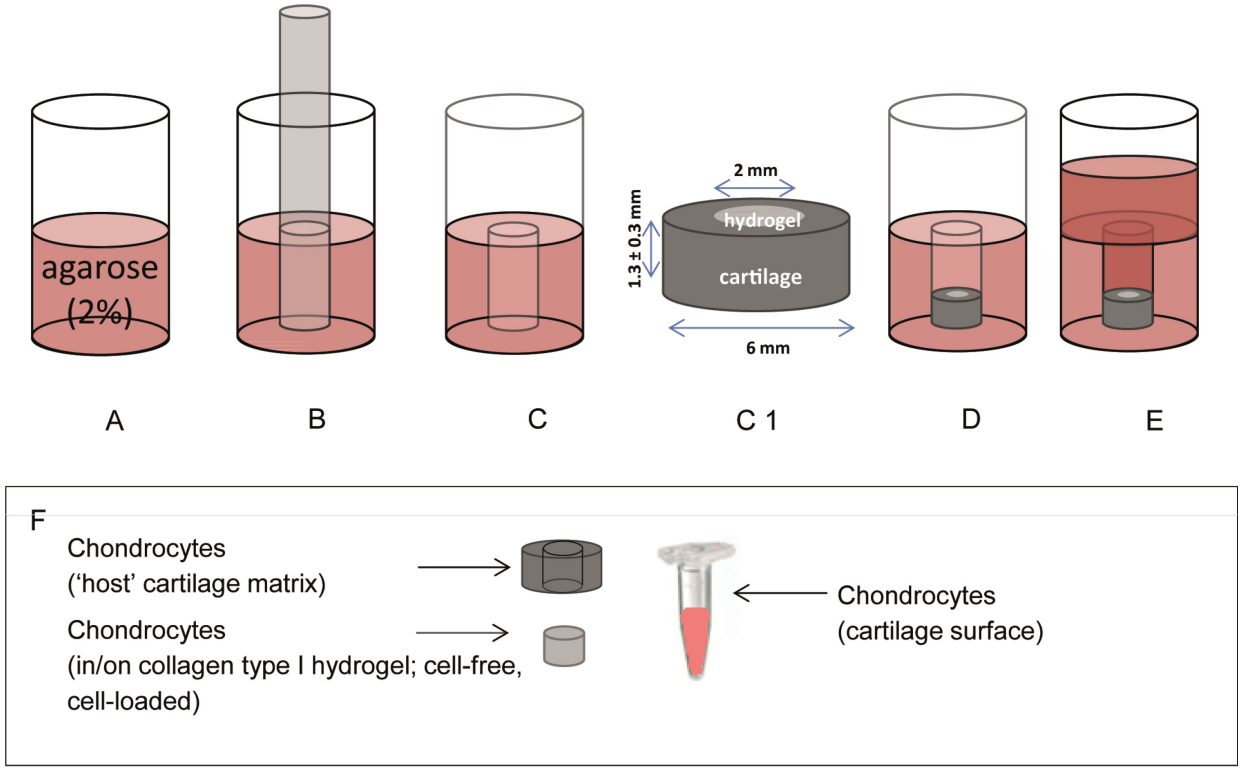

Figure 3: **Scheme of the in vitro model.** For embedding of the cartilage-implant constructs, hot liquid agarose (2%) was added into the wells of a 48-well plate (A). Cylindrical pockets of a defined size (6 mm) were created by inserting a metal-pin plate into the hot agarose until it gelated (B, C). The central defects of the cartilage rings (diameter 2 mm) were filled with the collagen implant (cell-free/cell-loaded; diameter 6 mm) using forceps (C1) and, after embedding the resulting constructs into the agarose (D), culture medium was added (E). After in vitro culture, cartilage-implant constructs were subjected to histological characterization. Also, gene expression of chondrocytes isolated from the "host" cartilage, cells on the cartilage surface, and the collagen implant was analyzed (F). At the protein level, the amount of cartilage components released into the supernatant, as well as the remaining content in "host" cartilage rings and the cells located on the cartilage surface was quantified.

Viability Assay

Cartilage rings were obtained at weekly intervals from in vitro culture, minced using a scalpel and a pair of scissors and initially digested with pronase E (Merck, Darmstadt, Germany; 1 mg/ml) in serum-free DMEM for 1 hour at 37°C, 5% CO_2, and 95% humidity under constant stirring. After three washes in phosphate-buffered saline (PBS: 137 mM NaCl, 2.7 mM KCl, 10 mM Na_2HPO_4× 2 H_2O, 2 mM KH_2PO_4; pH 7.4), they were incubated for 17 hours at 37°C in DMEM containing 5% FCS (Invitrogen, Darmstadt, Germany) and collagenase P (0.1 mg/ml; Roche, Mannheim, Germany). Chondrocytes were then centrifuged (1500 rpm; Eppendorf mini spin; Eppendorf, Hamburg, Germany) for 10 minutes, washed 3 times with PBS containing 5% FCS, and counted. A total of 1 × 10^4 cells were seeded in culture slides (Becton Dickinson–Discovery Labware Products, Bedford, MA, USA) and cultivated for 1 day. Viability was assessed using fluorescein diacetate/propidium iodide life/dead staining (Kunisch et al. 2017). Three images each were taken in 3 chambers of the culture slides using a fluorescence

microscope Axiovert200M, an AxioCam MRm camera, and the AxioVision Rel4.8 program (all Zeiss, Oberkochen, Germany). Viable and dead cells were counted in all images using the cellprofiler soft-ware (www.cellprofiler.org (Carpenter et al. 2006)) and viability was expressed as the mean percentage of viable cells.

Histology and immunohistology

Paraffin sections of the cartilage-implant constructs were cut into 6 µm sections and stained with hematoxylin and eosin (H&E) and safranin O (to assess the proteoglycan content). For aggrecan immunhistology, sections were treated with chondroitinase ABC (0.25 U/ml; Sigma-Aldrich; 37°C, 90 minutes), blocked with hydrogen peroxide and 10% goat serum/Tris-buffered saline (TBS), and incubated overnight at 4°C with the primary antibody (0.1 µg/ml; clone: MA85A95; GenTex, Irvine, CA, USA). For collagen 1 and 2 staining, the epitopes were first demasked by incubation with proteinase K (code S3004; diluted 1:50; Dako, Hamburg, Germany) for 15 minutes at room temperature (RT). The sections were then subjected to blocking of the endogenous peroxidase activity with 0.5% hydrogen peroxide in methanol for 10 minutes, blocking with 25% normal bovine serum albumin (BSA)/TBS for 30 minutes (both at RT), and overnight incubation at 4°C with a primary antibody to bovine collagen 1 (2 µl/ml; polyclonal rabbit IgG; Acris, Herford, Germany) or collagen 2 (10 µg/ml; polyclonal rabbit IgG; Acris, Herford, Germany).This was followed by incubation for 1 hour at RT with a secondary antibody (anti-mouse or anti-rabbit) coupled to horseradish peroxidase (HRP; for collagen 1 and 2 antibodies) or alkaline phosphatase (ALP; for aggrecan) and visualization of the HRP with diaminobenzidine (DAB) and the ALP with Fast Red (both Sigma Aldrich). Sections were then counterstained with hematoxylin and mounted with Aquatex (Merck, Darmstadt, Germany) for light microscopy.
(Isotype-matched) control immunoglobulins consistently yielded negative results.

Score for Cell Migration

Cell migration onto/into the collagen implants was evaluated by 3 independent observers using a scoring system, which consisted of 4 levels (0 = implant without cells, 1 = single adherent cells, 2 = several adherent cells, 3 = cell layer on the implant) (Pretzel et al. 2013). Data were expressed as the means ± standard error of the mean of the values of the three individual observers.

Histology/immunohistology Scores for Safranin O, Collagen 1, Collagen 2, and Aggrecan

The intensity of the red color in the safranin O staining or the positive signal in the immunostaining for aggrecan, collagen 2, and collagen 1 were semiquantitatively evaluated

using a scoring system with 4 levels (0 = no staining; 1 = weak staining; 2 = moderate staining; 3 = strong staining) (Pretzel et al. 2013). Scoring was performed by 3 independent observers, data were expressed as the means ± standard error of the mean of the values of the 3 individual observers.

Quantitative Real-Time Polymerase Chain Reaction (qRT-PCR)

For the isolation of RNA from: (1) cells located in the matrix of the "host" cartilage; (2) cells located on the cartilage surface (see below); and (3) cells migrated onto and into the collagen implants (± cells; Fig. 3F), fine pointed forceps were used to first remove the cartilage-implant constructs from the agarose wells and then carefully separate the collagen implants (± cells) from the surrounding cartilage ring. A total of ten collagen implants were pooled and stored in a tube with 300 µL lysis buffer at −80°C for subsequent RNA isolation. The empty cartilage rings were then treated for 1 minute in a tube with 300 µl lysis buffer under continuous shaking to obtain the RNA from the cells located on the surface of the cartilage rings (Pretzel et al. 2013, Pretzel et al. 2009).

Subsequently, the rings were removed from the buffer and both components were separately stored at −80°C.

The cartilage rings were disintegrated with a pair of scissors in 800 µl TriZol (Life Technologies, Carlsbad, CA, USA), incubation at RT for 15 minutes, and centrifugation at 12,000 rpm for 3 minutes (Ruettger et al. 2010). Total RNA from these samples, the lysed cell fractions (cells on cartilage surface) or the collagen implants was then isolated using the Quiagen Kit (RNeasy mini kit; Qiagen, Hilden, Germany; including a DNase digestion).

The RNA eluate (12 µl each) was primed with oligo(d)T for 10 minutes at 72°C and reverse transcribed for one hour at 42°C using superscript II (Invitrogen). To quantify aggrecan, collagens 1 and 2, and the housekeeping gene aldolase, qRT-PCR (i-cycler PCR system; BioRad, Munich, Germany) was performed using the primers listed in Table 1 and PCR products from bovine chondrocytes as standards. Gene expression in all samples was normalized to the relative expression level of aldolase. Product specificity was confirmed by melting curve analysis and initial cycle sequencing of the PCR products.

Table 1: Primers, product length, and specific amplification conditions for RT-PCR.

Gene	Upstream primer (5´ 3´)	Downstream primer (3´ 5´)	Product length	Annealing temp.	Melting temp.
Aggrecan	CAGAGTTCAGTGGGACAGCA	AGACACCCAGCTCTCCTGAA	193	60	84
Collagen 2	CATCTGGTTTGGAGAAACCATC	GCCCAGTTCAGGTCTCTTAG	600	61	83
Collagen 1	AGCCAGCAGATCGAGAACAT	ACACAGGTCTCACCGGTTTC	185	60	86
Aldolase	CACCGGATTGTGGCTCCGGG	CGCCCCCGATGCAGGGATTC	170	58	88

General amplification protocol (40 cycles): initial denaturation for 90 seconds at 95°C; denaturation for 20 seconds at 94°C, specific primer annealing temperature (see above) for 20 seconds, amplification at 72°C for 30 seconds, additional heating step at 84°C; denaturation for one minute at 95°C; cooling to 60°C (holding for 10 seconds).

Protein extraction

To determine the relative protein amounts of aggrecan, collagen 2, and collagen 1, protein was extracted from: (1) the “host” cartilage (after removal of the collagen implants); and (2) the cells located on the cartilage surface (see above). Protein from the “host” cartilage was isolated by disintegration in 1000 µl of 4 M GuHCL with a pair of scissors and incubation for 48 hours at 4°C under rotation. Protein from the cells located on the cartilage surface was isolated using the acetone precipitate of the lysis buffer according to the supplier’s instruction of the RNeasy mini kit (Qiagen).

Quantification of glycosaminoglycans

Glycosaminoglycans released from the cartilage-implant constructs into the supernatant during culture, as well as the remaining content in the cartilage rings and the cells located on the cartilage surface, were quantified using the DMB assay (Chandrasekhar et al. 1987, Farndale et al. 1986). Supernatants were analyzed by pooling the supernatants of the respective week and group. Briefly, 25 µL of pooled supernatant or extracted/precipitated proteins, respectively, were applied to microtiter plates with or without dilution in 0.05 M sodium acetate buffer (pH 6.8). After addition of 200 µL DMB reagent (containing 1.9-dimethyleneblue (21 µg/ml), 55 nM formic acid; pH 6.8]), absorption was read at 525 nm. A dilution series of a chondroitin-4 sulfate standard (Sigma-Aldrich) was used for the generation of a standard curve and the calculation of the results.

Enzyme-Linked Immunosorbent Assay (ELISA)

Aggrecan, collagen 2, and collagen 1 concentrations in the supernatant during culture, as well as the remaining content in the cartilage rings and the cells located on the cartilage surface,

were quantified using ELISA kits. Supernatants of the cartilage-implant constructs (± cells) after 0, 4, 8, 10, and 12 weeks of cultivation were analyzed by pooling the supernatants of the respective week and group. Aggrecan, collagen 2, and collagen 1 concentrations were then measured according to the protocols of commercially available ELISA kits (Chondrex, Redmond, WA, USA; BlueGene, Shanghai, China). Absorption at 490 nm was measured using a Fluostar Optima Reader (BMG Labtech GmbH).

Biomechanical testing

Biomechanical testing (n = 10 for each time point) was performed using a static universal test system (Zwicki 1120, Zwicki/Roelli, Ulm, Germany). The maximal force required to push out the implant from the cartilage rings ($F_{max(insert)}$) was determined using a cylindrical indenter (diameter 1.8 mm; i.e., 0.2 mm less than the diameter of the central defect). To address remaining friction forces between indenter and empty "host" cartilage ring, a second identical test was then performed and the resulting force $F_{max(empty)}$) was subtracted from the initial push-out force [$F_{max(insert}$) − $F_{max(empty)}$ = $\Delta F_{max(res)}$] and used for further analysis. Values were given in Newtons and, in order to allow a comparison with published studies, in kPa after dividing the values in Newtons by the lateral surface area of the implant cylinder (0.8163 mm^2).

Statistical Analysis

Results were expressed as means ± standard error of the mean. Statistical analysis was performed using the Mann-Whitney U test and the software SPSS 22.0 ($p \leq 0.05$).

Results

Cell-Free Collagen implants

Morphological Characteristics, Viability, and Cell Migration

In the case of cell-free cartilage-implant constructs, lateral contact of the collagen insert to the cylindrical defect was maintained throughout tissue culture for 12 weeks (Fig. 4). Despite relatively long in vitro culture periods (up to 12 weeks), resident cartilage cells showed vital morphology without signs of alterations and positive nuclear staining, thus pointing to suitable culture conditions (Fig. 4). The matrix integrity of the cartilage seemed to be largely unaffected during the whole culture period (Fig. 4), although cartilage zones located close to the edge of the defect were characterized by the appearance of proliferation-induced cell clusters as a possible reaction to the initial mechanical tissue disruption (starting at 4 weeks; Fig. 4; see hash). In addition, late time points showed empty chondrocyte lacunae as a possible sign of chondrocyte emigration from the "host" cartilage ring (Fig. 4; see arrow).

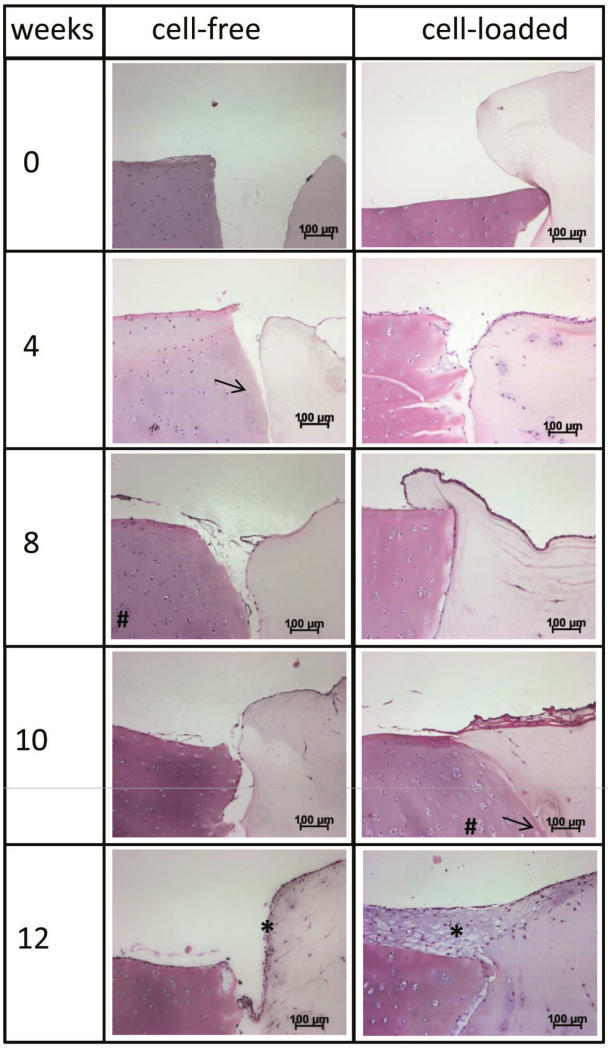

Figure 4: Hematoxylin & eosin staining of the cartilage-implant constructs (cell-free or cell-loaded implants) after placement into the inner defect of the cartilage rings and subsequent culture for 0, 4, 8, 10, or 12 weeks. Morphological characteristics of the cells in cartilage, implant and at the cartilage-implant interface; # proliferation-induced cell clusters; → empty chondrocyte lacunae; * cellular multilayer.

The high viability of the chondrocytes in the cartilage rings was confirmed by fluorescein diacetate/propidium iodide live-dead staining of chondrocytes enzymatically isolated from the cartilage at weekly intervals, resulting in viability rates of > 94% throughout the entire culture period (Fig. 5).

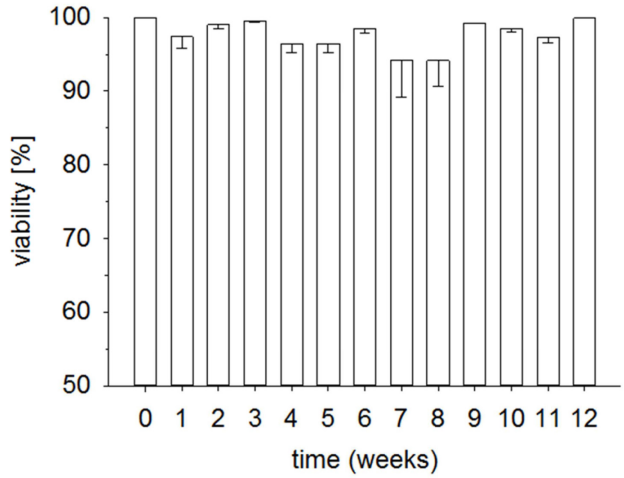

Figure 5: Viability of the chondrocytes in the cartilage ring throughout culture. Chondrocytes were enzymatically isolated from the cartilage at weekly intervals and cultivated for 1 day. Viability was assessed using fluorescein diacetate/propidium iodide staining. Data are expressed as means ± standard error of the mean (SEM); the dashed line indicates a viability of 95%.

Cartilage-implant constructs showed progressive formation of a cellular multilayer on the surface of the cartilage rings throughout cultivation (Fig. 4; see asterisks), as well as initial migration of chondrocytes onto and into the initially cell-free collagen type 1 implants starting at 4 weeks of in vitro culture (Figs. 4 and 6). There was a significant increase of the cell colonization from 0 weeks to all other time points and from 4 weeks to 8 and 12 weeks (Fig. 6).

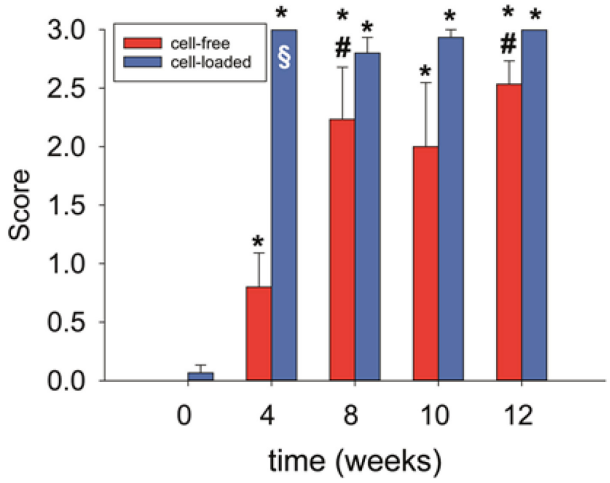

Figure 6: Semiquantitative scoring of cell migration onto/into the collagen implants after culture for 0, 4, 8, 10, or 12 weeks (cell-free; cell-loaded). Degree of migration: 0 = implant without cells, 1 = single adherent cells, 2 = several adherent cells, 3 = cell layer on implant; values are shown as means ± standard error of the mean (SEM); symbols indicate $P \leq 0.05$ versus * 0 weeks and # 4 weeks; § versus cell-free.

Both the cells on/in the collagen implants and on the cartilage surface showed mixed fibroblastic and chondrocytic features (Fig. 4; see asterisk for cell-loaded implants at 12 weeks) and

positively stained for safranin O, aggrecan, and collagen 2, but only very weakly or negative for collagen 1 (Fig. 7).

Content of Proteoglycans, Aggrecan, Collagen 2, and Collagen 1

The finding of a preserved matrix integrity in the surrounding cartilage ring was further supported by a very limited, nonsignificant decrease of the safranin O staining intensity over time (from a semiquantitative score of 2.8 for the freshly isolated cartilage to a score of 1.9 at 12 weeks; Figs. 7 and 8A); this suggested a minimal loss of proteoglycan during 12 weeks of in vitro culture.

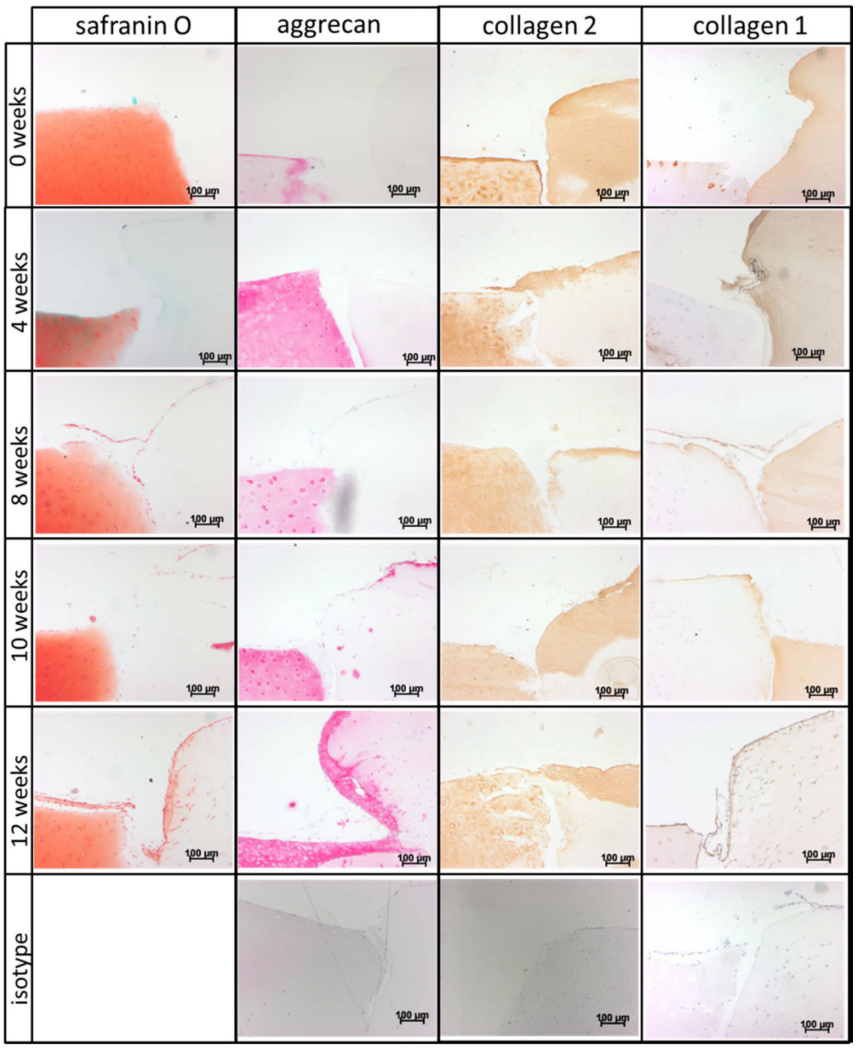

Figure 7: (Immuno)staining of the collagen implants (cell-free) after placement into the inner defect of the cartilage rings and subsequent culture for 0, 4, 8, 10, or 12 weeks. Safranin O staining and immunostaining for aggrecan, collagen 2, and collagen 1 (for quantification see **Fig. 8**); staining with (isotype-matched) control immunoglobulins consistently yielded negative results.

At the cartilage-implant interface there was also a loss of safranin O staining (from 2.6 to 1.3), which reached statistical significance for the 10- and 12-week values in comparison with the 0-week and/or 4-week values (Figs. 7 and 8A). In the implant, staining was first noticed at 8 weeks and then reached a plateau at 10 and 12 weeks (Figs. 7 and 8A), indicating proteoglycan deposition into the implant.

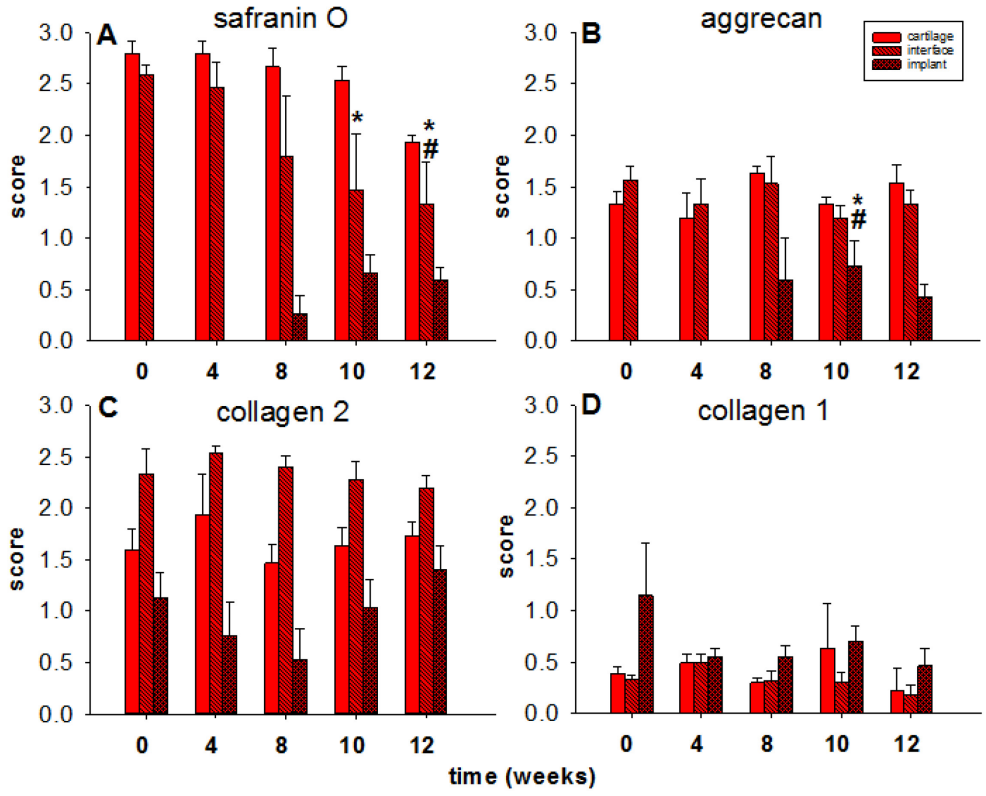

Figure 8: Semiquantitative analysis of "host" cartilage, interface, and collagen implants (cell-free). Score: 0 = no staining, 1 = weak staining, 2 = moderate staining, 3 = strong staining; values are shown as means ± standard error of the mean (SEM); symbols indicate $p \leq 0.05$ versus * 0 weeks, # 4 weeks.

As for the safranin O staining, a largely constant immunostaining for aggrecan was observed in the surrounding cartilage ring and at its interface with the implant throughout the 12-week culture period (constant scores between 1.2 and 1.7 over time; Figs. 7 and 8B), again suggesting a minimal loss of proteoglycan during in vitro culture.

Also, staining for aggrecan in the implant was first noticed at 8 weeks and then reached a plateau at 10 weeks ($p \leq 0.05$ vs. 0 and 4 weeks) and 12 weeks (Figs. 7 and 8B), confirming proteoglycan deposition into the implant.

As in the case of aggrecan, largely constant immunostaining for collagen 2 was observed throughout the 12-week culture period in surrounding cartilage ring (scores between 1.5 and 1.9), cartilage-implant interface (scores between 2.2 and 2.5), and implant (scores between 0.5

and 1.4), without any significant differences among the different time points (Figs. 7 and 8C), again supporting the concept of a preserved matrix integrity.
Very little immunostaining for collagen 1 (except for the implant 0-week value, scores mostly between 0.2 and 0.7) was observed in surrounding cartilage ring, interface, and implant, without any significant differences among the different time points (Figs. 7 and 8D).

DMB Assay (Proteoglycan Content; Tissue Extracts and Culture Supernatant)

As observed by safranin O staining and aggrecan immunostaining, there was a limited, nonsignificant decrease of the glycosaminoglycan (GAG) content in the surrounding cartilage ring over time (from 4911 µg/ml for the freshly isolated cartilage to 3627 µg/ml at 12 weeks, with an intermediate peak of 5785 µg/ml at 4 weeks; Supplementary Figure 1A, available in the online version of the article).
The chondrocytes that migrated onto the surface of the cartilage ring generally showed an approximately 10-fold lower GAG content, with a significant decrease over time (from 537 µg/ml for freshly isolated cartilage to 378 µg/ml at 12 weeks, with an intermediate peak of 689 µg/ml at 8 weeks; $p \leq 0.05$ vs. 4 and 8 weeks for the 10-week time point, $p \leq 0.05$ vs. 4 weeks for the 12-week time point; Supplementary Figure 1A).
Also, in the culture supernatant, there was a limited, nonsignificant decrease of the GAG content over time (from 193 µg/ml at 4 weeks to 146 µg/ml at 12 weeks; Supplementary Figure 1A). This was confirmed by a limited, nonsignificant decrease of the aggrecan release into the supernatant over time (ELISA; from 17 ng/ml at 4 weeks to 10 ng/ml at 12 weeks; data not shown).

ELISA (Collagens 2 and 1; Tissue Extracts and Culture Supernatant)

A significant decrease of the collagen 2 content was observed in the surrounding cartilage ring over time (from 1091 ng/ml at 0 weeks to 296 ng/ml at 12 weeks, $p \leq 0.05$ vs. 0 weeks for the 8-week time point; Supplementary Figure 1C). The chondrocytes migrated onto the surface of the cartilage ring showed an approximately 4-fold higher collagen 2 content, with a nonsignificant decrease over time (from 3757 ng/ml at 0 weeks to 2644 ng/ml at 12 weeks; Supplementary Figure 1C).
There was also a limited, nonsignificant decrease of the collagen 2 release into the supernatant over time (from 1381 ng/ml at 4 weeks to 269 ng/ml at 12 weeks; Supplementary Figure 1C).
In contrast to the collagen 2 release, there was a limited, but significant increase of the collagen 1 release into the supernatant over time (from 185 ng/ml at 4 weeks to a peak of 422 ng/ml at 8 weeks and a subsequent plateau; $p \leq 0.05$ vs. 4 weeks for the 8-week time point; data not shown).

Gene Expression for Aggrecan, Collagen 2, and Collagen 1 (RT-PCR)

Aggrecan expression showed a slight increase over time in cartilage ring (maximum 4-fold increase at 12 weeks), cartilage surface cells (maximum 7-fold; 12 weeks), and, interestingly, in the implant (maximum 3-fold; 10 weeks; Fig. 9A).

Whereas the collagen 2 expression in the cartilage ring was constant or even significantly decreased ($p \leq 0.05$ for 4, 10, and 12 weeks vs. 0 weeks), collagen 2 expression in surface cells and implant rose from baseline values to a transient peak at 8 weeks of 13-fold and 9-fold, respectively, and thereafter decreased again (Fig. 9B).

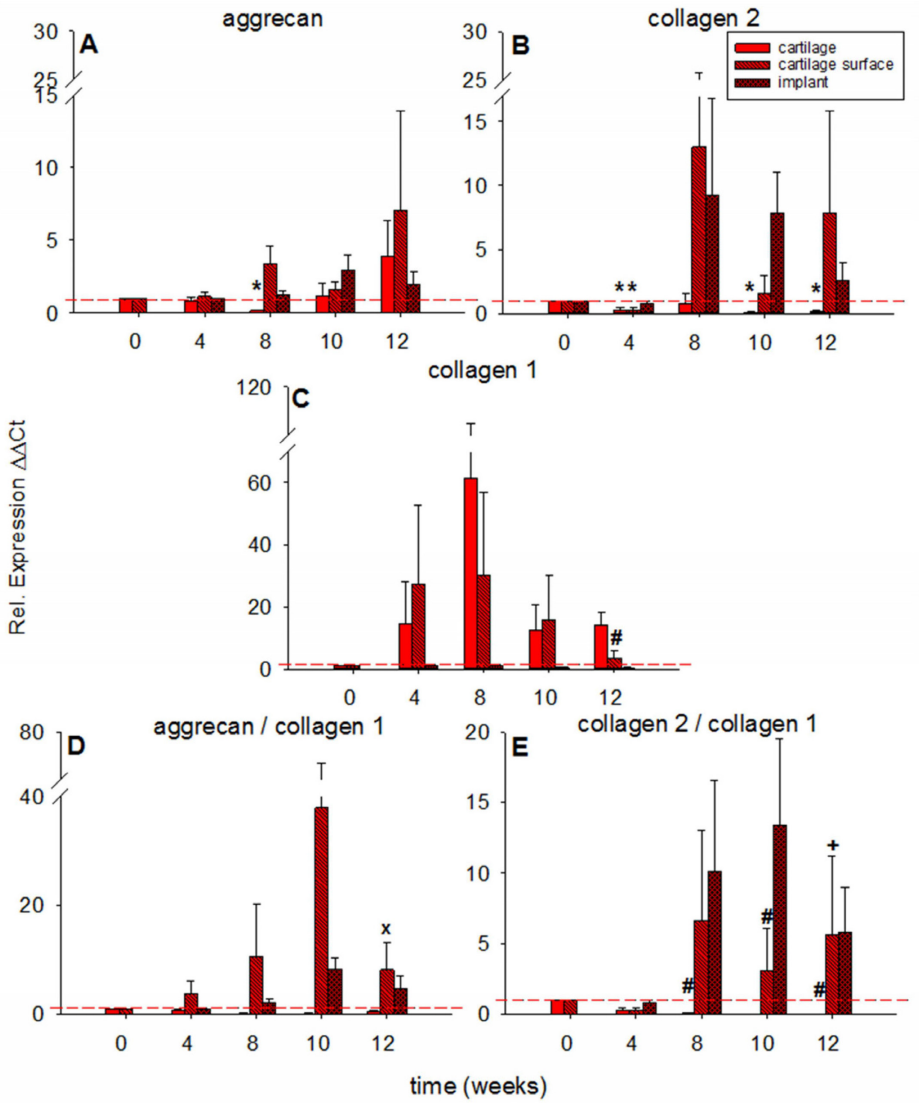

Figure 9: Real-time polymerase chain reaction analysis for aggrecan, collagen 1, and collagen 2 (cell-free implants). mRNA expression for aggrecan (**A**), collagen 2 (**B**), collagen 1 (**C**), aggrecan/collagen 1 ratio (**D**), and collagen 2/collagen 1 ratio (**E**) was determined prior to and after 4, 8, 10, and 12 weeks of *in vitro* culture; relative gene expression of the cells located in the "host" cartilage matrix (cartilage), on the cartilage surface (cartilage surface), and on/in the collagen implant (implant); values are expressed as means ± standard error of the mean (SEM); symbols indicate $p \leq 0.05$ *versus 0 weeks; #versus 4 weeks; x versus 8 weeks; +versus 10 weeks.

Whereas collagen 1 expression in cartilage ring and surface cells rose to a transient peak at 8 weeks of 61-fold and 30-fold, respectively, and thereafter decreased again (surface cells $p \leq 0.05$ for 12 vs. 4 weeks), collagen 1 expression in the implant was constant or even decreased over time (Fig. 9C).

The above changes were reflected in a constant aggrecan/collagen 1 ratio in the cartilage ring, and a transient peak at 10 weeks for surface cells (37-fold) and implant (13-fold; Fig. 9D). As for the aggrecan/collagen 1 ratio, there was a marginally decreased collagen 2/collagen 1 ratio in the cartilage ring ($p \leq 0.05$ for 8, 10, and 12 weeks vs. 4 weeks), and a transient peak at 8 or 10 weeks for surface cells (7-fold) and implant (13-fold; Fig. 9E).

Cell-loaded Collagen implants

Morphological Characteristics and Cell Migration

The findings in cell-loaded cartilage-implant constructs were generally comparable to those in cell-free cartilage-implant constructs, with lateral contact of the implant to the cylindrical defect, vital morphology of the resident cartilage for up to 12 weeks cells, and largely preserved matrix integrity (Fig. 4).

As in the case of cell-free constructs, cell-loaded cartilage-implant constructs also showed progressive formation of a cellular multilayer on the surface of the cartilage rings throughout cultivation (in part with chondrocytic features; Fig. 4; see asterisk at 12 weeks). However, a substantial presence/migration of chondrocytes onto and into the initially cell-free collagen type 1 implants occurred already after 4 weeks of in vitro culture (Figs. 4 and 6). There was again a significant increase of the cell colonization from 0 weeks to all other time points (Fig. 6).

Interestingly, cell-loaded collagen implants showed a significantly faster cell colonization than initially cell-free collagen implants ($p \leq 0.05$ at 4 weeks; Fig. 6).

Content of Proteoglycans, Aggrecan, Collagen 2, and Collagen 1

Also, in this group, there was a very limited, nonsignificant decrease of the safranin O staining intensity over time in the cartilage ring (from a semiquantitative score of 2.4 for the freshly isolated cartilage to a score of 1.5 at 12 weeks; Figs. 10 and 11A).

At the interface, there was also a loss of safranin O staining (from 2.3 to 0.9), which reached statistical significance for the 8, 10, and 12-week values in comparison to the 0-week values (Figs. 10 and 11A).

In the implant, significantly elevated staining was first noticed at 4 weeks and then reached a plateau thereafter (Figs. 10 and 11A; $p \leq 0.05$ vs. 0 weeks for 4, 8, 10, and 12 weeks).

As for the safranin O staining, a largely constant immunostaining for aggrecan was observed in surrounding cartilage ring and interface throughout the 12-week culture period (constant scores between 1.1 and 1.9 over time; Figs. 10 and 11B).

Also, substantial staining for aggrecan in the implant was first noticed at 4 weeks and reached a plateau thereafter (Figs. 10 and 11A; $p \leq 0.05$ vs. 0 weeks for 4, 8, or 12 weeks). Notably, at 4 and 12 weeks the score for cell-loaded implants was significantly higher than that in cell-free implants (compare Figs. 8B and 11B).

Also, for collagen 2, largely constant immunostaining was observed throughout the 12-week culture period in surrounding cartilage ring (scores between 1.9 and 2.2), interface (between 1.6 and 2.4), and implant (scores between 0.7 and 1.4), without any significant differences among the different time points (Figs. 10 and 11C).

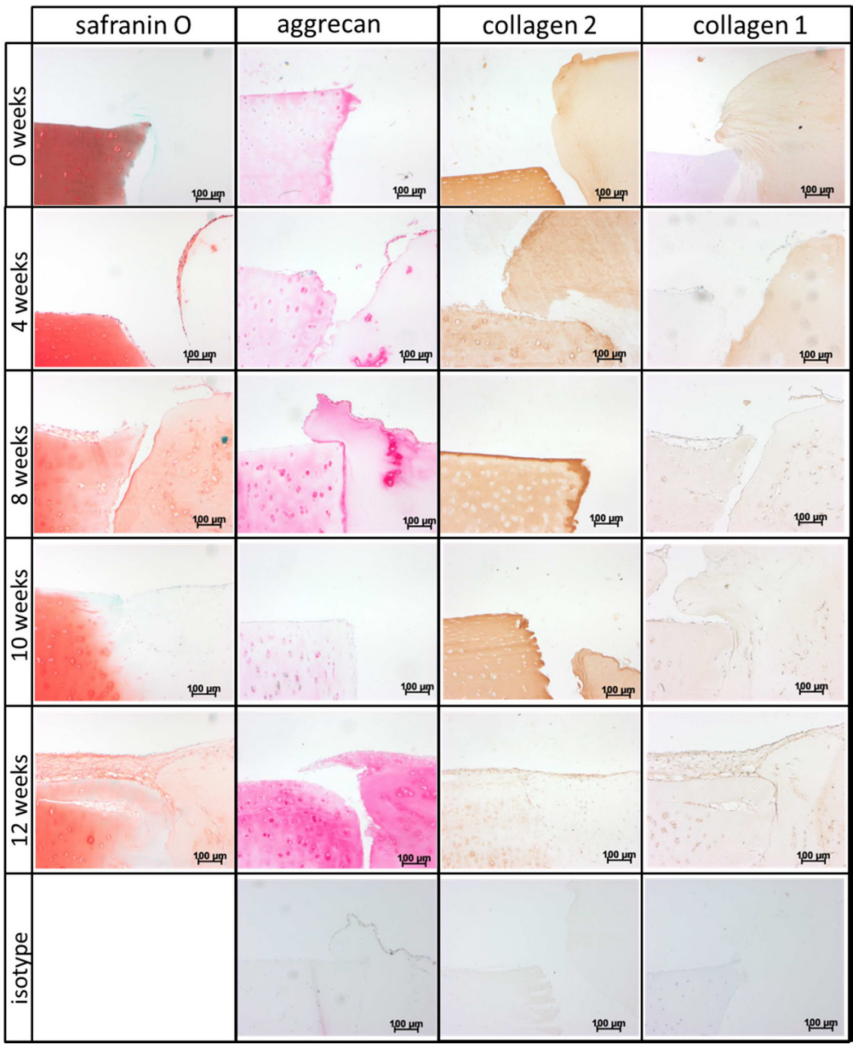

Figure 10: (Immuno)staining of the collagen implants (cell-loaded) after placement into the inner defect of the cartilage rings and subsequent culture for 0, 4, 8, 10, or 12 weeks. Safranin O staining and immunostaining for aggrecan, collagen 2, and collagen 1 (for quantification see **Fig. 10**); staining with (isotype-matched) control immunoglobulins consistently yielded negative results.

Very little immunostaining for collagen 1 (except for one 0-week value, scores mostly between 0.2 and 0.8) was observed in surrounding cartilage ring, interface, and implant, for the latter with significantly lower values versus 0 weeks at 4, 8, 10, and 12 weeks (Figs. 10 and 11D).

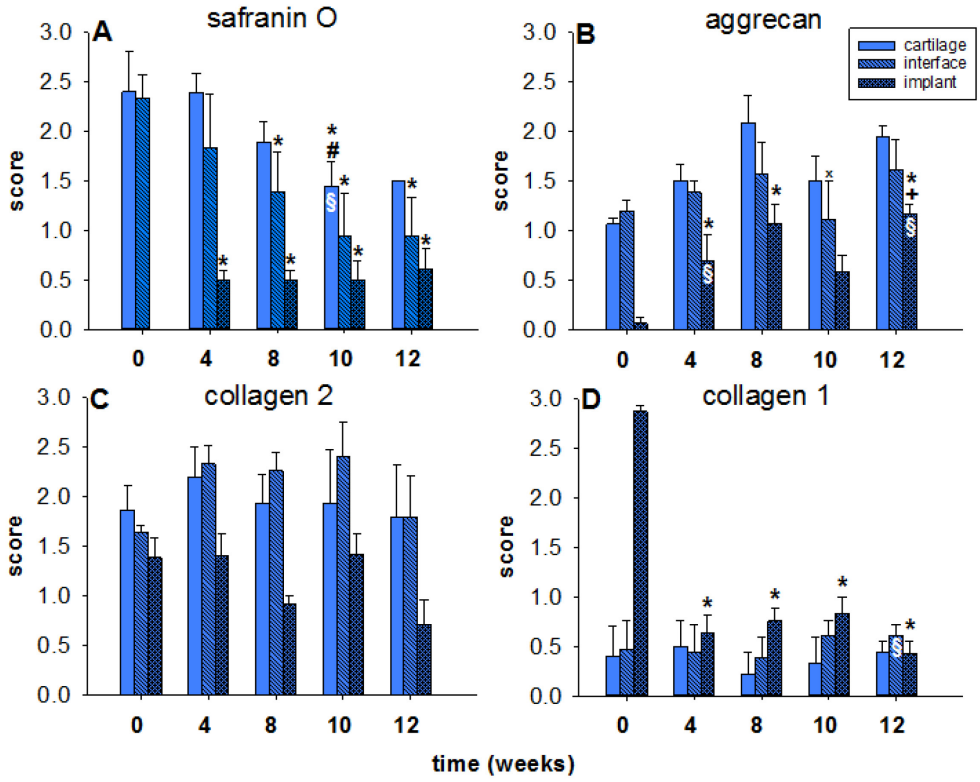

Figure 11: Semiquantitative analysis of "host" cartilage, interface, and collagen implants (cell-loaded). Score: 0 = no staining, 1 = weak staining, 2 = moderate staining, 3 = strong staining; values are shown as means ± standard error of the mean (SEM); symbols indicate $p \leq 0.05$ versus * 0 weeks, # 4 weeks, +10 weeks; § versus cell-free.

DMB Assay (Proteoglycan Content; Tissue Extracts and Culture Supernatant)

In the cell-loaded cartilage-implant constructs, there was a limited, nonsignificant decrease of the GAG content in the surrounding cartilage ring over time with a peak at 4 weeks of in vitro culture (from 5485 µg/ml for the freshly isolated cartilage to 4820 µg/ml at 12 weeks; intermediate peak of 6373 µg/ml at 4 weeks; Supplementary Figure 1B).

Interestingly, the GAG content in the surrounding cartilage ring of cell-loaded constructs was significantly higher than that of cell-free constructs at all time points (Supplementary Figure 1A and B).

The chondrocytes migrated onto the surface of the cartilage ring again showed an approximately 10-fold lower GAG content, with a significant decrease over time (from 449 µg/ml for the freshly isolated cartilage to 405 µg/ml at 12 weeks; intermediate peak of 516 µg/ml at 4 weeks; $p \leq 0.05$ vs. 8 weeks for the 10-week time point; Supplementary Figure 1B). There was

only a marginally lower GAG content in cell-loaded versus cell-free cartilage-implant constructs (compare Supplementary Figure 1A and B).

In the supernatant, there was a limited decrease of the GAG release over time (from 190 µg/ml at 4 weeks to 154 µg/ml at 12 weeks; $p \leq 0.05$ vs. 4 weeks for the 8- and 10-week time points), as confirmed by a limited, significant decrease of the aggrecan release into the supernatant over time (ELISA; from 24 ng/ml at 4 weeks to 10 ng/ml at 12 weeks; $p \leq 0.05$ vs. 10 weeks for the 12-week time point; data not shown).

ELISA (Collagens 2 and 1; Tissue Extracts and Culture Supernatant)

As observed for the cell-free cartilage-implant constructs, there was a limited, nonsignificant decrease of the collagen 2 content in the surrounding cartilage ring up to 8 weeks of in vitro culture with a slight increase thereafter (from 1580 ng/ml at 0 weeks to 523 ng/ml at 12 weeks; Supplementary Figure 1D). The chondrocytes migrated onto the surface of the cartilage ring showed an approximately 3-fold higher collagen 2 release than the cartilage ring itself, with a nonsignificant, slight decrease over time (from 3234 ng/ml at 0 weeks to 2611 ng/ml at 12 weeks; Supplementary Figure 1D). Also, there was a limited, nonsignificant decrease of the collagen 2 release into the supernatant up to 10 weeks of culture with a slight increase thereafter (from 2115 ng/ml at 4 weeks to 854 ng/ml at 12 weeks; Supplementary Figure 1D).

In contrast to the collagen 2 release, there was nonsignificant increase of the collagen 1 release into the supernatant over time (from 270 ng/ml at 4 weeks to a peak of 429 ng/ml at 10 weeks and a subsequent plateau; data not shown).

Gene Expression for Aggrecan, Collagen 2, and Collagen 1 (qRT-PCR)

Whereas aggrecan expression in cartilage ring and implant rose to a transient peak at 8 weeks of 10-fold and 6-fold, respectively, and thereafter decreased again, aggrecan expression in the surface cells was constant over time (Fig. 12A).

The collagen 2 expression in cartilage ring and surface cells was constant over time. In contrast, the collagen 2 expression in the implant rose to a transient peak at 8 weeks of 7-fold and thereafter decreased again (Fig. 12B).

Collagen 1 expression reached a 10-week nonsignificant peak in cartilage ring (10-fold in comparison to 0 weeks) and surface cells (30-fold), and a 12-week nonsignificant peak in the implant (11-fold; Fig. 12C).

The aggrecan/collagen 1 ratio in the cartilage ring showed an increase over time with a 12-week, 32-fold peak in comparison with 0 weeks. In contrast, the aggrecan/collagen 1 ratio of the surface cells and the implant was mostly constant over time (Fig. 12D).

The collagen 2/collagen 1 ratio in cartilage ring, surface cells, and implant only marginally changed over time, without any significant differences among the different time points (Fig. 12E).

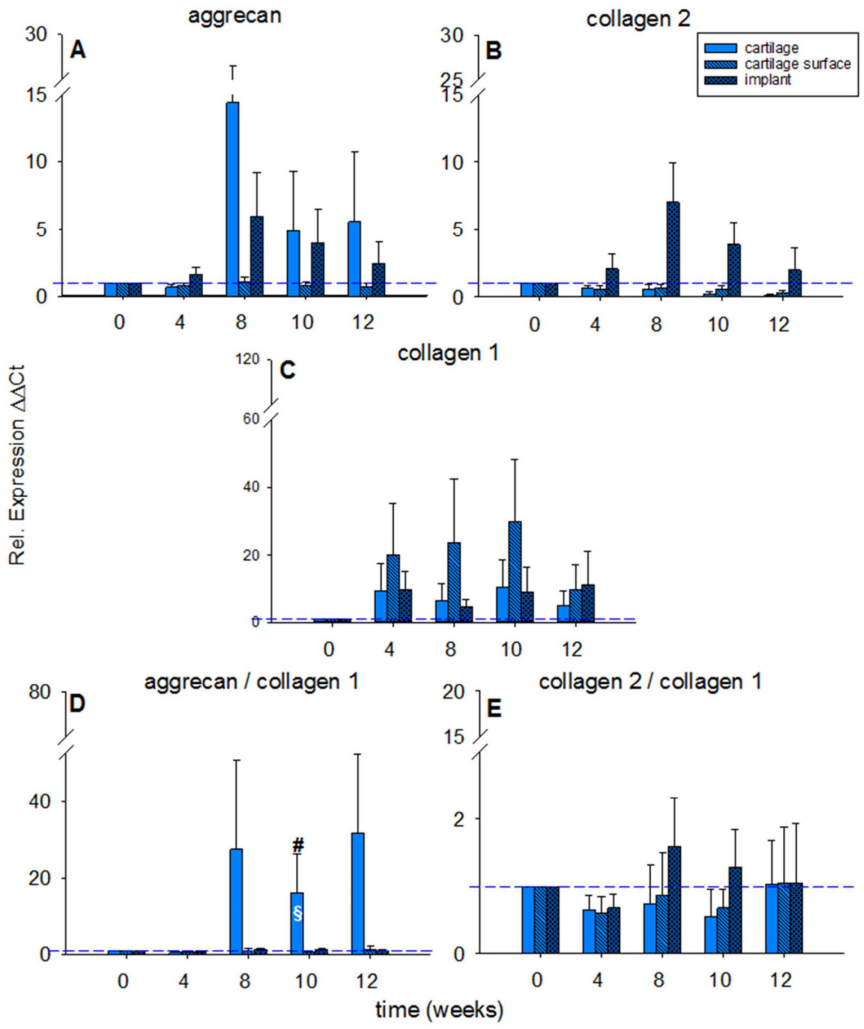

Figure 12: Real time polymerase chain reaction analysis for aggrecan, collagen 1, and collagen 2 (cell-loaded implants). mRNA expression for aggrecan (**A**), collagen 2 (**B**), collagen 1 (**C**), aggrecan/collagen 1 ratio (**D**) and collagen 2/collagen 1 ratio (**E**) was determined prior to and after 4, 8, 10, and 12 weeks of *in vitro* culture; relative gene expression of the cells located in the "host" cartilage matrix (cartilage), on the cartilage surface (cartilage surface), and on/in the collagen implant (implant); values are expressed as means ± standard error of the mean (SEM); symbols indicate $p \leq 0.05$ versus # 4 weeks; § versus cell-free.

Push-Out Forces of the Cultivated Cartilage-Implant Constructs (Biomechanical Testing)

Strikingly, the push-out force for cell-free implants showed a progressive increase during culture (from 0.002 ± 0.000 N or 2.560 ± 0.680 kPa at 0 weeks to a peak of 0.061 ± 0.056 N or 75.858

± 68.780 kPa at 8 weeks and a subsequent plateau; p ≤ 0.05 vs 0 weeks for 4, 8, 10, and 12 weeks; Fig. 13).

This was also the case for cell-loaded implants, which showed a progressive increase during culture from 0.012 ± 0.007 N (15.026 ± 9.095 kPa) at 0 weeks to a peak of 0.126 ± 0.031 N (154.344 ± 38.032 kPa) at 12 weeks (p ≤ 0.05 vs. 4 weeks for 8, 10, and 12 weeks; Fig. 13). At any time point, the values for cell-loaded implants were numerically higher than those for cell-free implants (Fig. 13).

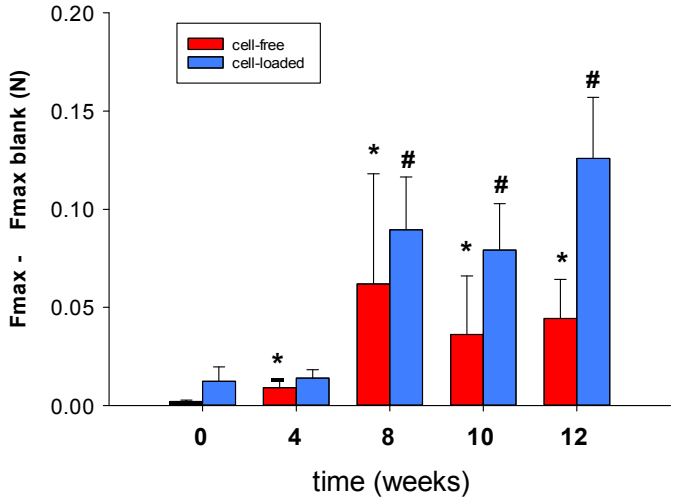

Figure 13: Biomechanical push-out testing of the cartilage-implant constructs (cell-free or cell-loaded implants). Values are expressed as means ± standard error of the mean (SEM); the symbols indicate *P* ≤ 0.05 * versus 0 weeks; # versus 4 weeks.

Discussion

The aim of the present study was to test the long-term performance (12 weeks) of a collagen type 1 hydrogel in a standardized in vitro bovine cartilage punch model. The main findings of the study were that: (1) cartilage-implant constructs revealed vital morphology, preserved matrix integrity, progressive, but only slight proteoglycan loss in the “host” cartilage ring, and decreasing proteoglycan release into the culture supernatant; and (2) cell-free or cell-loaded collagen implants both showed substantial cell immigration/colonization, progressively increased levels of aggrecan (mRNA/protein) and collagen 2 (mRNA increasing/protein constant), and significantly augmented push-out forces of the implants from the “host” cartilage ring over time. Compared with cell-free collagen implants, interestingly, cell-loaded implants displayed significantly earlier cell immigration/colonization, earlier and longer lasting deposition of aggrecan, and tendentially higher push-out forces.

The results of the present study are thus in good agreement with the known biocompatibility of the already clinically approved CaReS implant, in either cell-free or cell-loaded form, as a scaffold material in general and its good performance as an implant material for cartilage repair

in vitro and in vivo (Efe et al. 2012, Petri et al. 2013, Schneider et al. 2011a, Schuettler et al. 2013, Schuttler et al. 2014). In addition, the study provides in vitro data concerning the dynamic molecular processes underlying cartilage regeneration and may be applicable for systematic in vitro screening of future cartilage replacement materials.

As previously published, our present in vitro cartilage regeneration model is highly suitable for the testing of chondral implants with proven or expected clinical potential (Dunzel et al. 2013, Enders et al. 2009, Hunter und Levenston 2004, Madry et al. 2001, Obradovic et al. 2001, Pretzel et al. 2013, Pretzel et al. 2009, Secretan et al. 2010, Vinardell et al. 2009), with easily available, ethically unproblematic, and reproducible tissue supply and the possibility of long-term in vitro culture for up to 12 weeks without major cartilage degeneration. Modified in vitro systems, including subchondral bone (thus addressing the contribution of bone-derived secreted factors or progenitor cells) may provide a more complex understanding of the performance of the cartilage-bone unit in cartilage regeneration than cartilage only-based models. However, such systems may present with technical challenges such as the complete removal of the cartilage layer without damage to the subchondral bone lamella (unpublished data (Mika et al. 2017, Mika et al. 2011)).

On the other hand, cartilage zones located close to the edge of the defect contained proliferation-induced cell clusters as a possible reaction to the initial mechanical tissue disruption and showed empty chondrocyte lacunae. While these changes may indicate some degree of cartilage degeneration in the “host” cartilage (Lotz et al. 2010), they also likely suggest an attempt to repair damaged cartilage and seed the cartilage implant (Morales 2007).

Long-term stability of the “host” cartilage ring over time was indicated by: (1) limited histological signs of cartilage degeneration and chondrocyte viability rates of >94% throughout culture; (2) limited loss of proteoglycan and stable protein content of collagen 2 (and very small amounts of collagen 1); (3) largely constant or even increasing mRNA expression for aggrecan and/or collagen 2; and (4) progressively increased anchoring of the implant in the sense of “lateral bonding.” This shows that the present system allows long-term in vitro culture, which may yield meaningful results with an at least partial transferability to the in vivo situation.

Both cell-free and cell-loaded cartilage-implant constructs showed substantial colonization of the implant, which was paralleled by signs of chondrocyte emigration especially from the superficial regions of the “host” cartilage ring. This confirms the high cyto- or biocompatibility of the type 1 collagen–based implants in the present in vitro system, as previously reported in experimental (Gavenis et al. 2014, Gavenis et al. 2012, Schneider et al. 2011a) and clinical in vivo studies (Efe et al. 2012, Schneider et al. 2011b, Schuettler et al. 2013, Schuttler et al. 2014). Interestingly, cell loading of the collagen implants appeared to accelerate and/or amplify the process of cartilage regeneration in the implant, as indicated by significantly faster cell

colonization. These results argue for an advantage of cell-loaded versus cell-free collagen implants, in agreement with earlier studies on cell-seeded or cell-containing implants based on collagen or other cartilage replacement materials (Endres et al. 2012, Patrascu et al. 2013, Bartz et al. 2016, Zscharnack et al. 2015). Alternatively, in vivo microfracturing of the subchondral bone plate below the cartilage implant can be used to favor cell immigration into initially cell-free implants and optimize the conditions for successful cartilage repair (Erggelet et al. 2009, Gavenis et al. 2014, Gavenis et al. 2012).

Cell-free and cell-loaded collagen implants both showed progressive deposition of the matrix molecule aggrecan and a stable protein content of collagen 2 throughout culture, again demonstrating the cytocompatibility of the implant material and the active production of cartilage-specific matrix molecules by vital chondrocytes (Gavenis et al. 2006). This was further underlined by the progressively increasing mRNA levels for aggrecan and collagen 2 in the implant.

In addition, the locally produced, cartilage-specific matrix molecules appeared to be successfully retained in the collagen implants, as indicated by a progressive decrease of the aggrecan and collagen 2 release into the culture supernatant over time. These results are in good agreement with in vitro data obtained with other clinically applied cartilage implants (Bartz et al. 2016, Endres et al. 2007, Endres et al. 2012). As discussed above in the context of cell immigration, cell loading of the collagen implants accelerated and/or amplified cartilage regeneration, as emphasized by a significantly earlier and more long-lasting appearance/presence of aggrecan, again supporting an advantage of cell-loaded cartilage implants. There were no apparent signs of chondrocyte de-differentiation in either cell-free or cell-loaded collagen implants over time, since: (1) cartilage-specific aggrecan protein content increased to a plateau at approximately 8 weeks and thereafter; (2) collagen 2 (and collagen 1) protein content was stable over time; and (3) the mRNA ratios for aggrecan/collagen 1 and collagen 2/collagen 1 were either constant or considerably increased throughout in vitro culture. The present in vitro model of cartilage repair may thus provide the local conditions to support the phenotypic stability of the chondrocytes in both “host” cartilage and implant.

The favorable mRNA ratios for aggrecan/collagen 1 and collagen 2/collagen 1 in the implant in the present study (an indication for a phenotypic stabilization of the chondrocytes) are in clear contrast to the results obtained upon culture of human osteoarthritic or non-osteoarthritic chondrocytes in the same collagen implant, but without the surrounding cartilage ring (Halbwirth et al. 2015, Jeyakumar et al. 2017, Zwickl et al. 2016, Zwickl et al. 2010). This strongly indicates that the present “in situ organ” culture system generates a local milieu favoring the long-term preservation of the differentiated chondrocyte phenotype, cartilage matrix production, and lateral bonding, a process likely involving reciprocal effects of the cartilage ring and the implant

on each other (unpublished data). These results are in good agreement with previous reports on culture systems applying such a surrounding cartilage ring (Hunter und Levenston 2004, Obradovic et al. 2001, Secretan et al. 2010, Vinardell et al. 2009), but are addressed for the first time on a molecular level in the current study.

Both cell-free and cell-loaded collagen implants showed significantly increased push-out forces from the “host” cartilage ring over time, with tendentially higher values for cell-loaded implants. Thus, well maintained cell vitality, substantial cell migration, and sustained local matrix production appear to have functional consequences in the sense of augmented lateral bonding of the implant to the surrounding “host” cartilage. Lateral bonding at the cartilage-implant interface and the resulting push-out forces are likely influenced by various factors, including: (1) the character of the tissue formed at the interface (Moretti et al. 2005); (2) sprouting of extra-cellular matrix components in the interfacial zone; and (3) the presence or absence of cell death at the interface (Theodoropoulos et al. 2011).

The increase of the push-out forces during the 12-week culture for cell-free or cell-loaded collagen implants (from 2.560 to 54.259 kPa or from 15.026 to 154.344 kPa, respectively) led to final values, which are comparable to those previously reported for poly(glycolic acid)-construct tissues after 5 weeks of culture (Hunter und Levenston 2004) or for cell-loaded agarose hydrogels (Vinardell et al. 2009). This shows that collagen implants, in either cell-free or cell-loaded form, may be well suitable as a scaffold material in general and as an implant material for cartilage repair in vivo (Efe et al. 2012, Schneider et al. 2011b, Schuettler et al. 2013, Schuttler et al. 2014).

The method applied in the present study to measure the push-out force of the collagen implants for the first time took into consideration the blank value obtained by a second push-through of the indenter after the initial push-out of the implant. This approach may help to obtain reproducible results by addressing technical artifacts due to factors such as differences between the defect sizes in individual samples or variations of the implant hydrogel diameter due to variable water content (Hunter und Levenston 2004, Obradovic et al. 2001, Vinardell et al. 2009).

Conclusion

In the present in vitro bovine cartilage punch model, largely preserved tissue integrity, limited proteoglycan release, as well as progressively increasing cartilage differentiation and push-out forces (for up to 12 weeks of cultivation) suggest initial cartilage regeneration and imply lateral bonding of the current collagen implant to the surrounding cartilage. On the basis of significantly faster cell colonization and a significantly earlier and more long-lasting appearance/presence of aggrecan, cell-loaded implants may show an advantage over cell-free cartilage implants. The

present in vitro cartilage regeneration model thus proved well suitable to demonstrate the regenerative capacity of this clinically approved hydrogel collagen type 1 implant and to decipher some of the underlying molecular processes.

Acknowledgments and Funding

The authors are grateful to Cordula Müller and Ulrike Körner for expert technical assistance, as well as to Maren Siedentop, Daniela Warnecke, and Fabian Holzner for expert biomechanical testing of implant push-out forces. We gratefully acknowledge the partial financial support of the Bundesministerium für Bildung und Forschung (BMBF), grant references 13N12601 and 0315577C.

Declaration of Conflicting Interests

The author(s) declared the following potential conflicts of interest with respect to the research, authorship, and/or publication of this article: T.Graeve is a member of the Amedrix GmbH.

Supplemental Material

The supplementary material for this article is available online.

Comparison of Near-Infrared Spectroscopy with Needle Indentation and Histology for the Determination of Cartilage Thickness in the Large Animal Model Sheep (Peer-Reviewed)

Autorenschaft der Publikation

Victoria Horbert, Matthias Lange, Thomas Reuter, Martin Hoffmann, Sabine Bischoff, Juliane Borowski, Harald Schubert, Dominik Driesch, Joerg Mika, Christof Hurschler, Raimund W. Kinne

Abstract

The suitability of near-infrared spectroscopy (NIRS) for non-destructive measurement of cartilage thickness was compared with the gold standard needle indentation. A combination of NIRS and biomechanical indentation (NIRS-B) was used to address the influence of varying loads routinely applied for hand-guided NIRS during real-life surgery on the accuracy of NIRS -based thickness prediction.

NIRS-B was performed under three different loading conditions in 40 osteochondral cylinders from the load-bearing area of the medial and lateral femur condyle of 20 cadaver joints (left stifle joints; female Merino sheep; 6.1 ± 0.6 years, mean ± standard error of the mean). the cartilage thickness measured by needle indentation within the region analyzed by NIRS -B was then compared with cartilage thickness prediction based on NIRS spectral data using partial least squares regression.

NIRS-B repeat measurements yielded highly reproducible values concerning force and absorbance. Separate or combined models for the three loading conditions (the latter simulating load-independent measurements) resulted in models with optimized quality parameters (e.g., coefficients of determination R2 between 92.3 and 94.7) and a prediction accuracy of < 0.1 mm.

NIRS appears well suited to determine cartilage thickness (possibly in a hand-guided, load-independent fashion), as shown by high reproducibility in repeat measurements and excellent reliability compared with tissue-destructive needle indentation. This may provide the basis for non-destructive, intra-operative assessment of cartilage status quo and fine-tuning of repair procedures.

Keywords

Near-infrared spectroscopy (NIRS), needle indentation, histology, articular cartilage thickness, large animal model

Traumatic and osteoarthritis (OA) cartilage defects show limited regeneration capacity, aggravated by secondary loss of cartilage substance in the adjacent tissue. A number of surgical techniques are currently used to repair such cartilage defects (Niemeyer et al. 2013, Steinwachs et al. 2008). However, as they are mostly not curative, there is a continuing need to optimize the approaches, for example, by using large animal models to verify specific aspects of the interventions. Intra-operative mapping of cartilage thickness with high regional resolution by non-destructive near-infrared spectroscopy (NIRS) may be superior to previously applied, non-invasive, high-quality magnetic resonance imaging (MRI) and may thus allow fine-tuning of repair procedures for articular cartilage injury, for example, a more precise definition of the defect borders.

In animal models, the gold standard for the determination of cartilage thickness is the method of invasive, tissue-destructive needle indentation (Jurvelin et al. 1995), and only a limited number of studies report on non-invasive procedures such as MRI (Roemer et al. 2009), ultrasound (Suh et al. 2001), or NIRS (Afara et al. 2012, Afara et al. 2013a, Afara et al. 2013b, Hoffmann et al. 2012 , Plettenberg 2007, Tiderius et al. 2007). Thus, there is a high need for non-destructive and convenient techniques to analyze the thickness of healthy or diseased articular cartilage in preclinical and human set-ups.

NIRS has been previously applied for the non-destructive assessment of normal or degenerated cartilage in porcine, ovine, equine, rat, and bovine animal models (Afara et al. 2012, Afara et al. 2013b, Hoffmann et al. 2012 , Plettenberg 2007), in tissue-engineered cartilage constructs (Baykal et al. 2010), and for the quantification of cartilage alterations in degenerative human OA (Stumpfe et al. 2013, Tiderius et al. 2007). In these studies, NIRS showed good correlations with clinical injury scores, biomechanical properties (Stumpfe et al. 2013), histological grading (Stumpfe et al. 2013), and biochemical features. NIRS may thus be suitable as a non-destructive, clinically applicable method for cartilage analysis, also considering that Afara et al (Afara et al. 2013a) have already used NIRS for the determination of the articular cartilage thickness under static conditions.

The present study aimed at determining the accuracy of NIRS-based cartilage thickness prediction and the influence of varying loads and/or data preprocessing. A specific and novel approach of this study was to perform the measurements under non-static conditions. For this purpose, a combination of NIRS and biomechanical indentation (NIRS-B) was used, as previously established in our group (Hoffmann et al. 2012 , Hoffmann et al. 2010). This combined approach was chosen to address the question of whether ex vivo non-destructive NIRS is suitable for the determination of cartilage thickness in a force-independent fashion, which takes into account the varying loads during hand-guided NIRS. This may then eventually provide the basis for intra-operative assessment of cartilage status quo in humans

and experimental models. In the present study, NIRS-B was thus successfully applied for the first time to predict the cartilage thickness on the femur condyles in the large animal model sheep, and to validate it by comparison with the gold standard indentation and the values obtained by histology.

Materials and Methods

Sample Preparation Method

Twenty left cadaver stifle joints (adult female Merino sheep; age 6.1 ± 0.6 years (mean ± standard error of the mean [SEM]; body weight 78.5 ± 2.7 kg; frozen at −20°C) without cartilage alterations were used. The joint samples were derived from either unpublished studies of experimental chondral repair (permission from the governmental commission for animal protection, Free State of Thuringia, Germany; registration number 02-007/11) or published studies on the injection of calcium phosphate cement into bone defects of lumbar vertebral bodies (Bungartz et al. 2016, Maenz et al. 2017).

After thawing (24 hours), the joints were opened, the femur was fixed in a clamp, and the cartilage kept humid with isotonic saline solution. One osteochondral cylinder each (diameter 10 mm; depth ~20 mm; original orientation on the condyle marked by an incision) was extracted with a trepan drill from the main load-bearing area of the medial and lateral femur condyle (Fig. 14A-D), visually examined for approximately equal cartilage thickness along its circumference, transferred to isotonic saline solution, and stored at 20°C until further analysis (within 30 minutes).

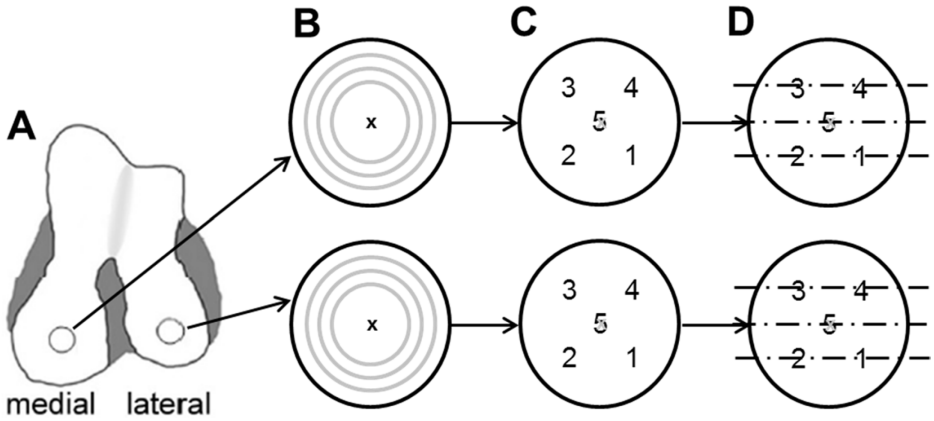

Figure 14: Sample preparation (left knee). One osteochondral cylinder each (diameter 10 mm; depth 20 mm) was extracted with a trepan drill form the main load-bearing area of the medial and lateral femur condyle (A) for subsequent near-infrared spectroscopy (NIRS) (B; × = center of fiber probe), needle indentation at 5 defined locations covering the region analyzed by NIRS (C), and conventional histology at 3 different levels representing the locations analyzed by NIRS and needle indentation (D).

Combination of NIRS and Biomechanical Indentation (NIRS-B)

NIRS-B was performed on the cartilage surface of the osteochondral cylinders (Fig. 14B) in a climatized room (20°C) using a NIRS system (Arthrospec; Jena, Germany). As shown in Supplementary Figure 2, this system was synchronized with a linear translation stage (Thorlabs, Dachau, Germany) driving a 2-mm diameter fiber probe and a force sensor (ME Systeme, Hennigsdorf, Germany) to simultaneously measure indentation force (force range 0-10 N; sampling rate 32 Hz) and corresponding tissue NIRS absorbance spectra (range of 947-1649 nm; spectral resolution 3 nm; dynamic range 16 bit; sampling rate of 9 Hz) (Hoffmann et al. 2012).

Thirty minutes after warm-up, the NIRS-B system was calibrated using a polytetrafluoroethylene (PTFE) optical reference standard. Subsequently, the osteochondral cylinders were placed in the sample holder and immersed in isotonic saline until the cartilage surface was covered.

NIR spectra of 40 samples were acquired for unloaded cartilage (interval 1, minimal indentation), loaded cartilage (interval 2, indentation 0.1 mm) and loaded cartilage after relaxation (interval 3, indentation 0.1 mm) as shown in Figure 15. These 3 load conditions were chosen to represent the forces occurring during hand-guided, intraoperative NIRS assessment when: (1) just lightly touching the surface; (2) applying variable forces during locus screening (“navigation force”) or actual quantitative measurement (“procedure force” (Chami et al. 2006, Plettenberg 2007)); or (3) assessing cartilage relaxation during more extended application of the fiber probe.

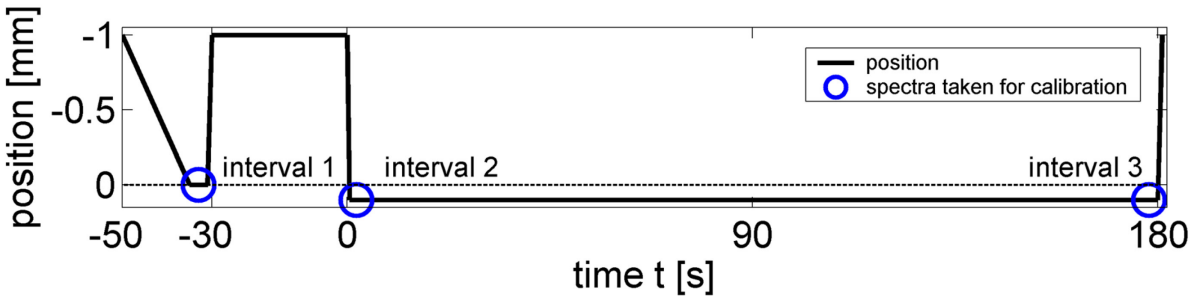

Figure 15: Movement of the fiber probe during the NIRS-B (near-infrared spectroscopy in combination with biomechanical indentation) measurements. The position of the fiber probe during the NIRS measurements is shown in relation to the surface of the osteochondral samples (position 0); the intervals 1 (minimal indentation), 2 (maximal indentation), and 3 (relaxation), in which NIRS spectra were recorded, are also indicated.

Each measurement sequence started by lowering the fiber probe onto the surface of the sample with a speed of 0.2 mm/s to reach the feed position s = 0 mm, as defined by F_0 = 0.5 N. After recording 10 NIR spectra in this minimal load position (interval 1; Fig. 15), the fiber

probe was removed for a 30-second sample resting period and then advanced toward the sample surface with a speed of 0.2 mm/s until maximal indentation of 0.1 mm was reached. At this point, 10 NIR spectra and the indentation force F_{max} were recorded (interval 2; Fig. 15). The indentation depth was chosen in the present set-up, since the application of a specified strain as a percentage of the cartilage thickness was impossible in undamaged cartilage of unknown thickness (i.e., without prior needle indentation).

After a relaxation time of t = 180 seconds with no probe movement, further 10 NIR spectra and the indentation force F_{Relax} were recorded (interval 3; Fig. 15). The 10 spectra of each interval were averaged and the absorbance was calculated as A = −log10 (Sample Signal – Dark Signal/Reference Signal – Dark Signal).

To determine the reproducibility of NIRS-B measurements, 3 repeat measurements were conducted on one sample, using a cartilage relaxation period of approximately 1 minute between individual measurements to reduce reswelling artifacts.

The spectral data set acquired under all 3 loading conditions (complete range of wavelengths from 947 to 1649 nm; exemplary depiction of the loadings and factor weights of several principal components based on the factor analysis of one NIR spectra shown in Supplementary Fig. 3) and the reference thickness set determined by needle indentation or histology (location 5 on the respective condyle; Fig. 14C and D) of all 40 cartilage samples were then used to develop calibrations. In the case of the spectra from interval 1 (virtually unloaded cartilage), calibration was performed using the original reference thickness set, in the case of spectra from intervals 2 and 3 (constant indentation depth 0.1 mm), 0.1 mm were subtracted from the reference thickness values.

The Bruker OPUS 7.0 software was then used for data pre-processing, partial least squares (PLS) regression, and leave-one-out cross validation. PLS was preferred in the present study because: (1) it is the standard method for NIRS analysis; (2) due to its widespread use, it favors comparability of the data with other publications in the field; and (3) it prepares the ground for future applications with a higher number of parameters such as varying tissue features (including unhealthy tissue), temperatures, feeds, and so on.

The resulting PLS models were evaluated and optimized on the basis of the parameters coefficient of determination (R^2; maximum of 100) (Haaland und Thomas 1988), root mean square error of cross validation (RMSECV) (Haaland und Thomas 1988), residual prediction deviation (RPD; with values < 2.5 classified as poor and not recommended for screening), and number of principal components (rank; desirable rank between 3 and 9 to avoid underfitting or overfitting) (Haaland und Thomas 1988). The RPD is the ratio of the standard deviation to the standard error of prediction, and is a common quality parameter routinely used in NIR spectroscopy.

To investigate the influence of varying loads, either models based on separate spectra from intervals 1, 2, and 3 (models 1-3, respectively; 40 spectra each), or based on combined spectra from all 3 intervals (model 4; 120 spectra), were developed.
To investigate the influence of noise reduction, modeling was fully repeated with spectral data previously smoothed using a pixel weighted mean filter, resulting in 8 models each for the calibration algorithms using either needle indentation or histology as reference (Tables 4 and 5).

Needle indentation

Cartilage thickness was validated at 5 different locations on each specimen (Fig. 14C), covering the region analyzed by NIRS (Suh et al. 2001). A hypodermic needle (25 G; 0.5 × 16 mm; Sterican; B. Braun Melsungen AG; Melsungen; Germany) was driven through the cartilage by a linear servomotor at a constant speed (0.3 mm/s) while continuously recording force and position. Cartilage thickness was determined as the distance from the initial surface contact to the tidemark, as defined by a characteristic change in the curve slope due to the different material properties of uncalcified and calcified cartilage (Supplementary Fig. 4) (Suh et al. 2001).

Histology

Immediately after performing NIRS-B and needle indentation, the osteochondral cylinders were fixed in 4% paraformaldehyde, decalcified in Osteodec solution for 3 weeks (Bio-Optica, Milan, Italy; weekly exchange of the solution), dehydrated, and embedded in paraffin. The samples were then cut into 8-µm sections and stained with hematoxylin and eosin.
The thickness of the articular cartilage (tidemark to surface) at the locations of all NIRS/needle indentation measurement points (see Fig. 14B-D) was measured in the respective location of one paraffin section each using an Axiophot microscope, a 4 × EC Plan-Neofluar objective (both Carl Zeiss, Jena, Germany) and the Axiovision 4.2. software (Carl Zeiss Vision GmbH, Jena, Germany).

Statistical Analyses

Results (means ± SEM) were statistically analyzed using the Wilcoxon signed rank test and SPSS 22.0 (IBM SPSS, Armonk, NY, USA). Correlations among parameters were assessed using the Spearman rank correlation test. Statistical significances were accepted at $p \leq 0.05$.

Results

This section presents representative full NIRS spectra and describes the data from the NIRS-B assessment and its reproducibility. It then shows the results from the gold standard determination of the cartilage thickness by needle indentation (or histology), and, finally, it reports on the development of models for the prediction of cartilage thickness by NIRS on the basis of values derived from either needle indentation or histology.

Full NIRS Spectrum Depiction

Full NIRS spectra show the characteristic wavelength pattern of three repeat measurements for one cartilage sample in interval 1 (minimal indentation; F_0= 0.5 N) with maxima at λ = 950 nm (second overtone of O-H bonds), λ = 1170 nm (second overtone of C-H, C-H_2, and C-H_3 bonds), and λ = 1450 nm (first overtone of O-H bonds; Fig. 16; for the depiction of the spectra of either the same location under the influence of the different loads at the different intervals or in cartilage samples of varying thickness see Supplementary Figs. 5 and 6, respectively). Low variability of the data, exemplified for the low-noise wavelength of 950 nm (insert in Fig. 16), was observed throughout the NIRS absorbance spectrum.

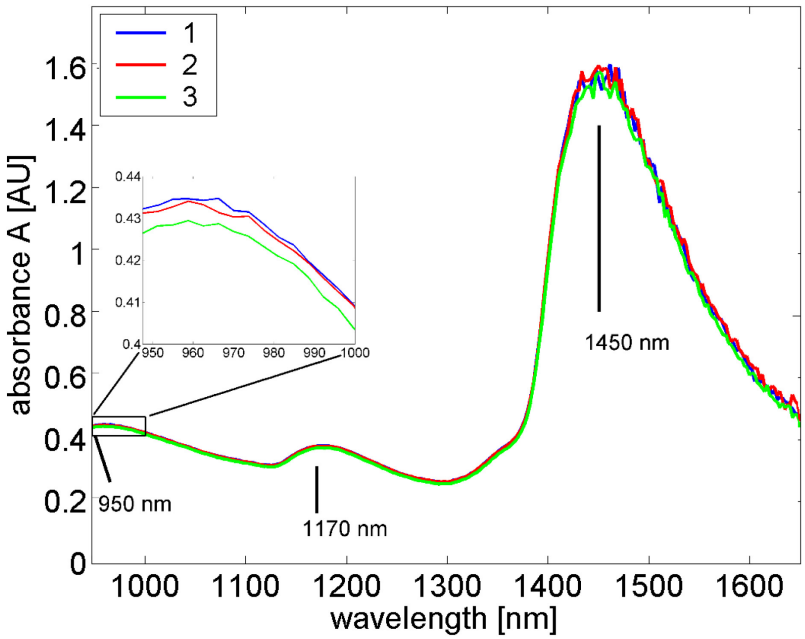

Figure 16: Near-infrared spectroscopy (NIRS) absorbance spectrum in interval 1 (minimal indentation; F_0 = 0.5 N). The complete NIRS absorbance spectrum of 3 repeat measurements for one cartilage sample in interval 1 displays the characteristic wavelength pattern of cartilage with maxima at λ = 950 nm, λ = 1170 nm, and λ = 1450 nm. In subsequent **Figures 17B** and **18B**, the variability of the absorbance data is exemplarily depicted for the characteristic low-noise wavelength of 950 nm (see insert).

In subsequent Figures 17B and 18B, the variability of the absorbance data is exemplarily depicted for the characteristic low-noise wavelength of 950 nm (see insert).

Reproducibility of NIRS-B Measurements

Repeated measurements of the cartilage in one sample (sheep 3) yielded highly reproducible values for force (F_{max}, and F_{Relax}; SEM maximum 4.4% of the mean; Fig. 17A; Table 2) and absorbance in intervals 1 to 3 at the positions minimal indentation (s = 0), maximal indentation, and relaxation, respectively (SEM maximum 0.4% of the mean; Fig. 17B; Table 2).

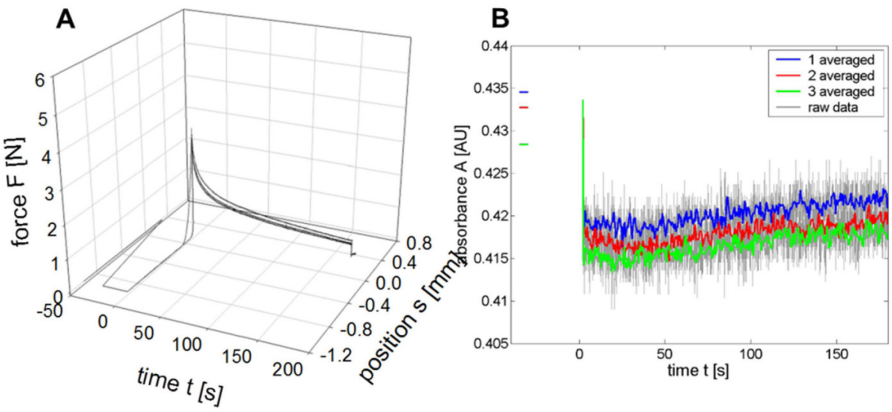

Figure 17: Accuracy of NIRS-B (near-infrared spectroscopy in combination with biomechanical indentation) repeat measurements. (A) Three-dimensional force-feed-time graph of triple repeat measurements in one sample; (**B**) change of absorbance at the wavelength of λ = 950 nm in triple repeat measurements in one sample; after numerically higher absorbance values in interval 1, the values slightly increased in the period between intervals 2 and 3, in parallel with a numerically decreased F_{Relax} in comparison with the respective F_{max}.

Table 2

Reproducibility of NIRS-B: Three repeat measurements of force and absorbance on one sample in intervals 1, 2, and 3, exemplified for λ = 950 nm

Repeat	Interval 1	Interval 2	Interval 3	Interval 1	Interval 2	Interval 3
	F_0 (N)	F_{max} (N)	F_{Relax} (N)	A_1 (AU) at 950 nm	A_2 (AU) at 950 nm	A_3 (AU) at 950 nm
1	0.50	3.05	0.75	0.4345	0.4186	0.4221
2	0.50	3.16	0.79	0.4327	0.4180	0.4198
3	0.50	3.36	0.87	0.4283	0.4147	0.4184
Mean		3.19	0.80	0.4319	0.4171	0.4201
SEM		0.09	0.04	0.0018	0.0012	0.0011
SEM/mean (%)		2.8	4.4	0.4	0.3	0.3

The unloaded tissue in interval 1 showed a numerically higher absorbance than the loaded tissue in intervals 2 and 3. The absorbance slightly increased between intervals 2 and 3, whereas the force decreased from F_{max} to F_{Relax} (Fig. 17A and B; Table 2).

NIRS-B assessment. Indentation force and complete NIRS spectra (947-1649 nm) of 40 samples were then measured in one defined location on the load-bearing area of the medial and lateral femur condyle (see Fig. 14) in intervals 1, 2, and 3 (Fig. 15). During cartilage surface compression in interval 2, the force significantly increased (2.19 ± 0.23 N) and then significantly decreased again (0.59 ± 0.06 N) toward the end of the relaxation period (interval 3; Fig. 18A; Table 3).

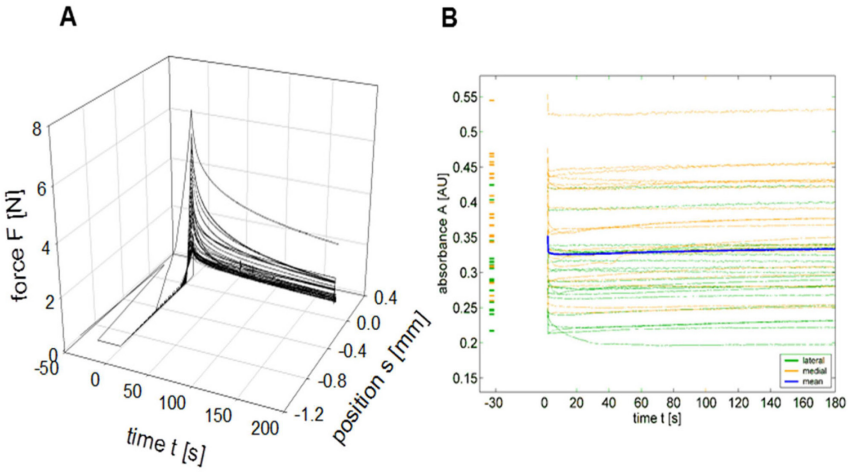

Figure 18: NIRS-B (near-infrared spectroscopy in combination with biomechanical indentation) measurements of all samples. (**A**) Three-dimensional force-feed-time graph of all samples (n = 40); (**B**) change of absorbance at the wavelength of λ = 950 nm in all samples; with variable values for the absorbance of the 40 individual samples, the force increased during compression of the cartilage surface in interval 2, and then decreased again at the end of the relaxation period (interval 3). In contrast, the absorbance significantly decreased during initial compression, and significantly increased until the end of the relaxation period.

Interval 1 (minimal indentation) showed variable NIRS absorbance (exemplified for λ = 950 nm; mean of 0.3459 ± 0.0119 AU; Table 3). In contrast to the force pattern, the absorbance significantly decreased during the initial compression (interval 2), and then significantly increased until the end of the relaxation period (Fig. 18B; Table 3).

Table 3

NIRS-B measurement: Force and absorbance (exemplified for λ = 950 nm) of 40 cartilage samples measured in intervals 1, 2 and 3; + = p ≤ 0.05 in comparison to F_0 or $A_{Interval\ 1}$; * = p ≤ 0.05 in comparison to F_{max} or $A_{Interval\ 2}$.

Repeat	Interval 1 F_0 (N)	Interval 2 F_{max} (N)	Interval 3 F_{Relax} (N)	Interval 1 A_1 (AU) at 950 nm	Interval 2 A_2 (AU) at 950 nm	Interval 3 A_3 (AU) at 950 nm
Mean	0.5	2.19^{+}	0.59*	0.3459	0.3276^{+}	0.3331*
SEM		0.23	0.06	0.0119	0.0117	0.0119
(min;max)		(0.88;6.68)	(0.24;2.40)	(0.2169; 0.5448)	(0.2137; 0.5251)	(0.1976; 0.5308)
SEM/mean (%)		10.5	10.2	3.4	3.6	3.6

Needle indentation. Cartilage thickness showed regional heterogeneity for the 5 measurement points on the medial and lateral femur condyles (n = 20 each; Fig. 19A and B; for details see figure legends).

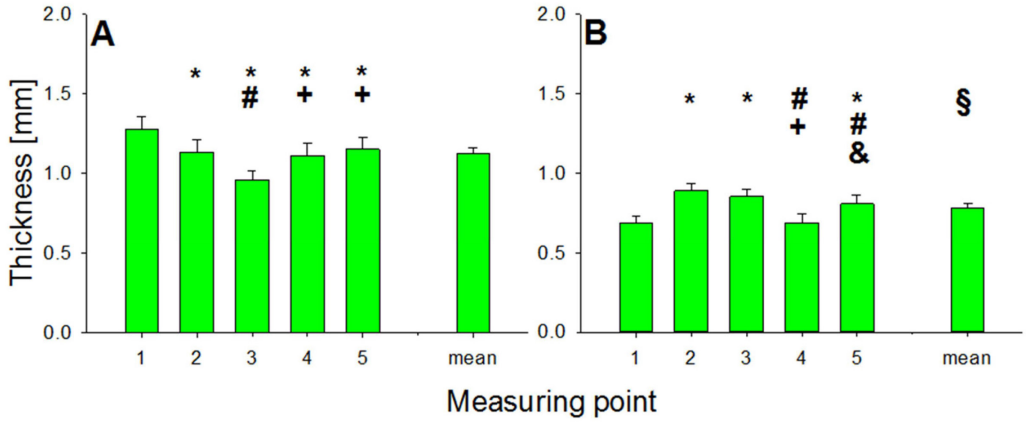

Figure 19: Determination of cartilage thickness by needle indentation (*n* = 40). Cartilage thickness at the 5 measurement locations on the medial femur condyle (**A**) and the lateral femur condyle (**B**). Values shown are means ± standard error (SEM) of the mean for each location, as well as those for all locations). The symbols indicate *p* ≤ 0.05 in comparison with: * measurement point 1 (lateral-distal); # measurement point 2 (medial-distal); + measurement point 3 (medial-proximal); & measurement point 4 (lateral-proximal); and § medial femur condyle.

The cartilage thickness of all 5 measurement points on each condyle was averaged for comparison with subsequent NIRS-B; the overall mean for the medial condyle (1.14 ± 0.07 mm) was significantly higher than that for the lateral condyle (0.78 ± 0.05 mm; Fig. 19A and B).

On the medial condyle, the values for measurement point 3 were significantly lower than those for measurement points 1, 2, 4, and 5 ($p \leq 0.05$); in addition, measurement points 2, 4, and 5 showed significantly lower values than measurement point 1 (Fig. 19A).
On the lateral condyle, the values for measurement point 4 were significantly lower than those for measurement points 2, 3, and 5 (Fig. 19B); in addition, measurement points 2, 3, and 5 showed significantly higher values than measurement point 1, and measurement point 5 (central) showed significantly lower values than measurement point 2 (Fig 19B).

NIRS-B Thickness Prediction Based on Needle Indentation

For all 8 models, a prediction accuracy of < 0.1 mm and models with highly optimized quality parameters were obtained (R^2 from 92.43 to 94.74; RMSECV < 0.1; optimized values for RPD between 3.8 and 4.4; acceptable number of principal components between 4 and 10). Performance of models with raw or smoothed data was comparable (i.e., noise did not cause substantial deterioration of the models; Table 4), indicating that non-modified data can be used for future analyses. Correlations between NIRS and needle indentation values for the different models were also highly significant (rho between 0.953 and 0.967; all P = 0.000; Fig. 20).

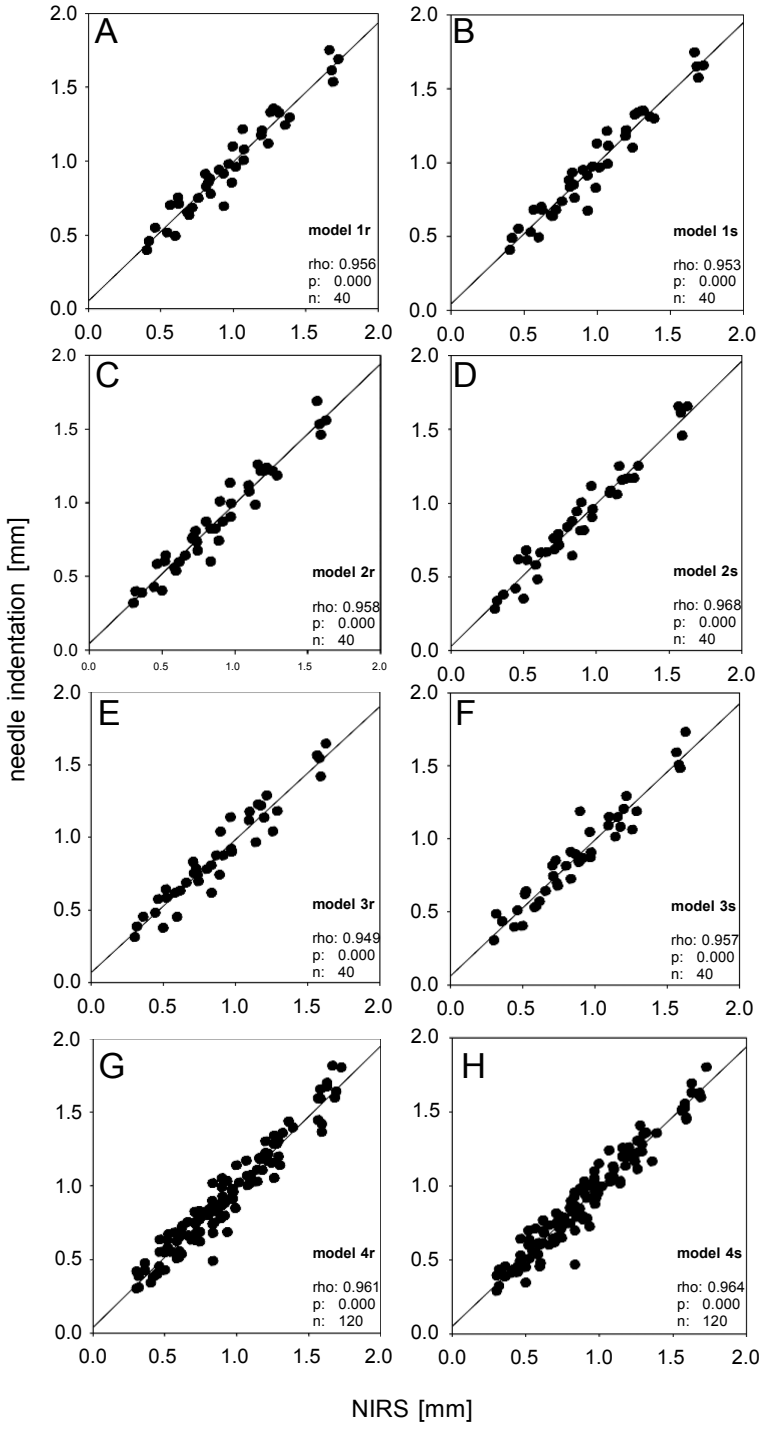

Figure 20: Correlations between the values obtained by near-infrared spectroscopy (NIRS) and needle indentation. Visual depiction of the correlations between the values obtained by NIRS and needle indentation for the different prediction models (including rho, *P*, and *n* for each correlation; compare with **Table 4**).

Regarding differences among the thickness predictions for individual cartilage samples derived from the 3 models for the different loading conditions, and from model 4 based on all 3 conditions (total of n = 6 prediction values for each sample), the variability was very limited (SEM between 0.9% and 5.7% of the mean; data not shown).

Table 4

NIRS-B thickness prediction based on needle indentation (minus 0.1 mm offset for intervals 2 and 3; measurement point 5): Evaluation of (n = 40) samples. Coefficient of determination (R^2), Root Mean Square Error of Cross Validation (RMSECV), Residual Prediction Deviation (RPD), and number of principal components (Rank); calibrations were either based on the separate use of 40 spectra each from intervals 1, 2 or 3 (models 1, 2, and 3, respectively), or of 120 spectra from all intervals (model 4).

	Pre-processing	R^2	RMSECV	RPD	No. of principal components (Rank)	No. of spectra (data source)
Model 1r	raw	94.04	8.61	4.1	5	40 (A_1)
Model1s	smoothed	94.12	8.57	4.1	4	40(A_1)
Model 2r	raw	94.09	8.59	4.12	4	40 (A_2)
Model2s	smoothed	94.74	8.10	4.36	8	40(A_2)
Model 3r	raw	92.43	9.72	3.64	4	40 (A_3)
Model 3s	smoothed	92.94	9.39	3.76	10	40 (A_3)
Model 4r	raw	93.63	9.00	3.96	9	120 (A_1, A_2, A_3)
Model 4s	smoothed	93.91	8.80	4.05	8	120 (A_1, A_2, A_3)

Independently performed linear regression analysis for repeated measures confirmed a highly significant, positive correlation between needle indentation and NIRS-B in model 4 (n = 120; $P \leq 2.2 \times 10^{-16}$; $R^2 = 0.958$; Supplementary Figure 7B), confidence intervals close to the prediction accuracy of NIRS-B (approximately 0.17 mm; Supplementary Fig. 7A), and showed no significant indications for an offset of the values for the 2 methods from zero (Supplementary Fig. 7B), a significant inter observer variability (Supplementary Fig. 7B), or a deviation from a normal distribution (Supplementary Fig. 7C).

Histology

As observed by needle indentation, the histologically determined cartilage thickness for the 5 measurement points on the medial and lateral femur condyles (n = 20 each) showed regional heterogeneity (see legend to Fig. 21A and B).

When the cartilage thickness of all 5 measurement points on each condyle was averaged, the overall mean value for the medial condyle (0.91 ± 0.04 mm) was significantly higher than that for the lateral condyle (0.63 ± 0.03 mm; Fig. 21A and B).

The histology values resulted significantly lower than the needle indentation values for measurement points 1, 4, and 5 on the medial condyle and for measurement points 2, 3, and 5 on the lateral condyle (Fig. 21A and B). However, there was a weak, but significant correlation between the thickness values derived from histology and needle indentation on both condyles (rho 0.544 and 0.367, respectively; Fig. 21C and D).

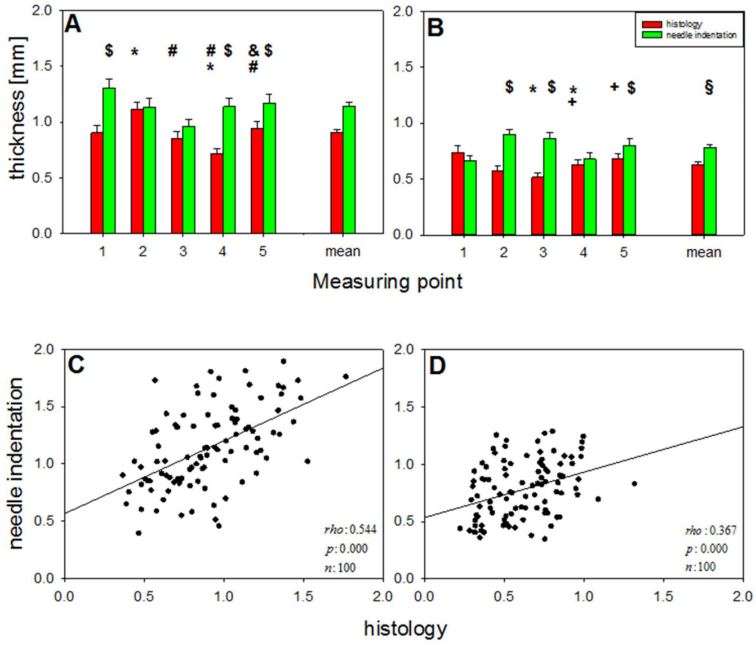

Figure 21: Comparison between the cartilage thickness values obtained by histology and needle indentation (*n* = 40 for all measurement points). Cartilage thickness at the various locations on the medial femur condyle (**A**) and the lateral femur condyle ([**B**; data shown as means ± standard error (SEM) of the mean for each location, as well as those for all locations]); Spearman rank correlations between the values obtained by needle indentation and histology on the medial (**C**) and lateral condyle (**D**); *P* ≤ 0.05 in comparison with: * measurement point 1; # measurement point 2; + measurement point 3; & measurement point 4; § medial femur condyle; and $ for the comparison between needle indentation and histology. For reasons of clarity, significant differences among the needle indentation values for the individual measurement points are not shown in this figure, but only in **Figure 19** (see above).

On the medial condyle, the values for measurement point 3 were significantly lower than those for measurement point 2 ($p \leq 0.05$); in addition, measurement point 4 showed significantly lower values than measurement points 1, 2, and 5, and measurement point 2 showed significantly higher values than measurement points 1 and 5 (Fig. 21A).

On the lateral condyle, the values for measurement points 3 and 4 were significantly lower than those for measurement point 1; in addition, the values for measurement points 4 and 5 were significantly higher than those for measurement point 3 (Fig. 21B).

NIRS-B Thickness Prediction Based on Histology

When using histology as a reference set, a high prediction accuracy (< 0.1 mm), good-quality parameters (R^2 from 86.44 to 90.84; RMSECV ≤ 0.1; acceptable number of principal components; Table 5), and significant correlations were obtained for models 1, 2, and 4 (rho between 0.900 and 0.936; all P = 0.000; Supplementary Fig. 8).

Table 5

NIRS-B thickness prediction based on histology (minus 0.1 mm offset for intervals 2 and 3; measurement point 5): Evaluation of (n = 40) samples. Coefficient of determination (R^2), Root Mean Square Error of Cross Validation (RMSECV), Residual Prediction Deviation (RPD), and number of principal components (Rank); calibrations were either based on the separate use of 40 spectra each from intervals 1, 2 or 3 (models 1, 2, and 3, respectively), or of 120 spectra from all intervals (model 4).

	Pre-processing	R^2	RMSECV (%)	RPD	No. of principal components (Rank)	No. of spectra (data source)
Model 1r	Raw	90.37	8.57	3.23	7	40 (A_{I1})
Model1s	Smoothed	90.57	8.48	3.3	9	40(A_{I1})
Model 2r	Raw	86.76	10.00	2.77	8	40 (A_{I2})
Model 2s	Smoothed	86.44	10.20	2.72	6	40 (A_{I2})
Model 3r	Raw	89.39	8.99	3.07	9	40 (A_{I3})
Model 3s	Smoothed	89.76	8.83	3.13	10	40 (A_{I3})
Model 4r	Raw	91.36	8.23	3.4	8	120 (A_1, A_2, A_3)
Model 4s	Smoothed	90.84	8.47	3.31	9	120 (A_1, A_2, A_3)

Lack of improvement after data smoothing again indicated the principal suitability of non-modified data (Table 5). Instead, model 3 based on NIRS absorbance during relaxation showed deteriorated quality parameters (Supplementary Fig. 8).

Discussion

In the present study, aimed at determining the accuracy of NIRS-based thickness prediction under the influence of varying loads using a combination of NIRS and biomechanical indentation (NIRS-B), NIRS-B proved highly reproducible in measuring the absorbance of normal articular cartilage in different states of compression or relaxation. Following development of optimized data analysis models in comparison with the articular cartilage thickness determined by needle indentation (and, to a lesser degree, also in comparison with histology), NIRS-B was capable of predicting the articular cartilage thickness with a high accuracy (< 0.1 mm). Thus, non-destructive, force-independent NIRS-B appears highly suitable for the assessment of cartilage thickness in experimental or human cartilage pathophysiology.

NIRS-B Reproducibility

Repeated measurements of the cartilage yielded highly reproducible values with very limited variation for force and absorbance levels throughout the NIRS-B assessment protocol. This result shows that NIRS-B yields stable and reliable experimental results, and further confirms the methodological validity of combined NIRS analysis and biomechanical indentation, as

previously suggested by our group and others (Hoffmann et al. 2012 , Hoffmann et al. 2010, Sugisaki et al. 2001).

Time Course of Force and Absorbance

When compressing the cartilage on the femur condyle during indentation with the NIRS fiber probe, the force increased to a maximum (F_{max}; 2.19 N) and subsequently decreased again toward the end of the relaxation period (F_{relax}; 0.59 N). This well-known cartilage stress-relaxation phenomenon (Sophia Fox et al. 2009), previously observed using force measurements (Hoffmann et al. 2012), NIRS (Hoffmann et al. 2012), and ultrasound (Nieminen et al. 2006, Zheng et al. 2005), is also reflected in an initial decrease of the absorbance during maximal indentation of s = 0.1 mm and a subsequent increase between intervals 2 and 3. The initial decrease of NIRS absorption during maximal indentation likely results from the extrusion of water (the main absorber of NIR radiation) from the cartilage extracellular matrix (Hoffmann et al. 2012 , Padalkar et al. 2013). However, the increasing NIRS absorption during subsequent cartilage relaxation is partially unexpected, since the cartilage should continue to lose water under continuous compression, as confirmed by a progressive decrease of the compression forces.

However, a compressed extracellular matrix and/or a partial loss of chemically bound, fixed water from collagens or glycosaminoglycan side chains (GAGs) of cartilage proteoglycans (see Padalkar et al. (Padalkar et al. 2013) and references therein) may also underlie the increasing NIRS absorption in this phase. Finally, such “water-reduced” GAGs may partially revert the extrusion of water from the cartilage and cause an osmotically driven influx of water (Hoffmann et al. 2012 , Padalkar et al. 2013).

The existence of free and bound water in the cartilage matrix, as well as their differential detection by bands of different wavelengths in static NIRS, has been demonstrated previously (Bagratashvili et al. 1997, Padalkar et al. 2013, Ressler et al. 1976). It remains to be shown whether such differential detection of free and bound water is also applicable to the dynamic combined NIRS-B protocol performed in the present study, and whether further biochemical analysis can identify the specific molecules undergoing an alteration of their NIRS signal under these conditions.

NIRS-B Thickness Prediction

In the present study, suitable calibration algorithms were developed for the comparison of the dynamic NIRS-B and needle indentation data using PLS regression. This resulted in robust models with a high accuracy for the prediction of the articular cartilage thickness (< 0.1 mm).

These results confirm previous high-accuracy findings of Afara et al. (Afara et al. 2012, Afara et al. 2013a) with static NIRS. However, these authors mounted fiber probe and specimen in a rig to keep both components stable and avoid vibrations during NIRS, a setup difficult to achieve during manual application in arthroscopic surgery. In the latter case, a standard hook probe is pressed on the tissue surface with forces between 0.5 and 4 N (Chami et al. 2006, Plettenberg 2007), a range well covered in the present study. Thus, the current study demonstrates for the first time that, at an experimental level, prediction of cartilage thickness can not only be performed by static NIRS but also by dynamic combined NIRS-B.

The models based on separate data from intervals 1 to 3 (constant load, 40 spectra each) and the model 4 based on all 3 intervals (varying load, 120 spectra) all showed high quality parameters. Notably, model 4 combining data with largely varying forces (range 0.5-6.68 N) also showed high performance, indicating that exact prediction of cartilage thickness by NIRS-B may also be feasible under intraoperative, hand-guided conditions. This may more closely reflect real-life surgery, during which different surgeons apply a fiber probe with variable forces during locus screening ("navigation force") or actual quantitative measurement ("procedure force" (Chami et al. 2006, Plettenberg 2007)). Also, model performance was largely unchanged by data smoothing, indicating that more easily available raw data without any loss of information can be used for future analyses.

One particular example for NIRS-B thickness prediction based on needle indentation is now depicted in Supplementary Figure 3, in which 5 individual factors with their respective factor weights contribute to the prediction model (model 2s, smoothed; coefficient of determination: 48.32%, 82.42%, 87.62%, 89.88%, 91.64% for 1, 2, 3, 4, and 5 factors, respectively). Since this contribution is mainly situated in the wavelength range around 1170 nm (second overtone of C-H, $C-H_2$, and $C-H_3$ bonds), it can be speculated that NIRS signal changes reflect alterations of the main organic components of cartilage, that is, large aggregating proteoglycans and collagens. In this case, changes in water content appear to be less important, since the 2 main water peaks at 950 and 1450 nm are not included. Thus, NIRS-B thickness prediction may be based on differences in matrix content and/or distribution between the NIRS probe on the cartilage surface and the NIR-reflecting border to the subchondral lamella in cartilage of varying thickness. However, it is has to be clearly pointed out that: (1) NIR spectra reflect numerous, very broad, and strongly superimposing overtone and combination bands; (2) cartilage contains a multitude of organic and inorganic components, including up to 70% of water; (3) the NIR bands in the cartilage cannot be directly interpreted, but must be analyzed using complex statistical approaches. The conversion of such speculations to scientific insight into the molecular basis of the NIRS signal changes will thus require much more detailed NIR spectra of aqueous solutions with

defined concentrations of one or few organic components and their respective NIRS profiles (Zierbock et al. 2012). As in the case of the needle indentation-based models, the histology-based NIRS model 4 showed high performance (RPD >3.3), further underlining that dynamic NIRS is in principle able to predict cartilage thickness under intra-operative, hand-guided conditions with varying loads.

Needle indentation

Marked regional heterogeneity of the cartilage thickness was observed on both medial and lateral femur condyles, with individual values for the medial condyle from 0.51 mm (medial-proximal) to 1.89 mm (lateral-distal; overall mean 1.14 ± 0.07 mm) and values for the lateral condyle from 0.35 mm to 1.29 mm (both lateral-proximal; overall mean 0.78 ± 0.05 mm).
To our knowledge, measurements of cartilage thickness on the medial and lateral femur condyle in sheep by needle indentation have not been published before; however, the present values were well in the range of those obtained by conventional formalin/paraffin histology (Ruediger et al. 2013, Cake et al. 2003). This confirms that, apart from its invasiveness, invasive needle indentation is a gold standard for the localized determination of cartilage thickness, giving more accurate measures than A-mode ultrasound or manual/stereomicroscopic measurement (Afara et al. 2013a, Suh et al. 2001).

Histology

To our knowledge, a direct comparison between histology and needle indentation has also not been reported. Other studies have either determined the cartilage thickness by 1 of these 2 methods (sometimes in comparison to third acoustical or optical procedures) (Hoffmann et al. 2010, Pastoureau et al. 2003, Shepherd und Seedhom 1999, Suh et al. 2001), or applied other modalities such as high-resolution MRI or laser displacement sensoring (Norman et al. 1999, Pepin et al. 2009). The discrepancies between needle indentation and histology found in the present study are likely due to alcoholic dehydration for histology. However, significant, positive correlations between needle indentation and histology or between NIRS-B and histology indicate that technically simple, inexpensive, and broadly applicable histology may still be valuable for the (comparative) estimation of cartilage thickness in experimental (large) animal models and humans. Alternatively, more sophisticated histological techniques only available in specialized laboratories, such as undecalcified plastic embedding or the cryostat cutting of undecalcified samples (Mika et al. 2011, Buchner et al. 1995) may provide information regarding the observed discrepancies.

Limitations

The present investigation was performed with normal sheep cartilage in order to first establish the system for unaltered, healthy cartilage. It has to be expected that the situation in unhealthy cartilage will be different and possibly more complex and will likely require new analyses and calibrations (Stumpfe et al. 2013, Tiderius et al. 2007).

In addition, all data in the present study were obtained with osteochondral plugs extracted with a drill from the medial and lateral femur condyle, in order to allow a positioning of needle indenter and NIRS fiber probe as close as possible to an exactly perpendicular orientation. Future studies will have to address the question, whether this exact positioning of the sensors can be reproduced in vivo on intact condyles under the tightly restricted spatial access during minimally invasive surgery (Kopsch et al.). In the current study, measurement point 5 of the needle indentation has been used as a reference for the calibration of the NIR spectra for cartilage thickness prediction, resulting in robust models with high quality parameters and a high accuracy for the prediction of the articular cartilage thickness. In order to consider not only the NIRS signal from the central cartilage area directly below the fiber probe but also a possible contribution from a wider conus extending to the measurement points 1 to 4 of the needle indentation, the average of the measurement points 1 to 5 may be used (data not shown). The fact that this approach also yielded high-quality parameters (R^2 between 88.66 and 93.53) and accuracy (RMSECV between 7.93 and 10.5%), can be interpreted as a sign of the high stability and reproducibility of the present calibration algorithms.

In the present experimental setup, the application of a specified strain as a percentage of the cartilage thickness (as performed in Maenz et al. (Maenz et al. 2016, Maenz et al. 2014)) was impossible, since NIRS was executed in undamaged cartilage with unknown thickness (i.e., without prior needle indentation). The choice of a defined, fixed 0.1 mm indentation depth, aimed at generating highly reproducible and highly accurate experimental conditions for all samples and measurements, completely eliminated any influence of creep, since a time-dependent motion of the 2 mm diameter fiber probe into the cartilage under constant load was impossible. This assumption is further supported by the fact that the force showed a rise to a peak, followed by a slow stress-relaxation process until a substantially lower force value above 0 N was reached.

In contrast, it may be very difficult to define an appropriate force suitable to generate such reproducible experimental conditions, because of the variable viscosity of the tissue with time and among different samples (due to, e.g., creep and relaxation). Furthermore, single

measurements at full cartilage relaxation may require time periods in the range of hours, with the serious risk of substantial cartilage alterations (e.g., progressive water loss or tissue break-down). Finally, an unequivocal determination of the time point of full cartilage relaxation may further complicate or extend the measurements. In our opinion, the choice of the indentation depth therefore does not question, but rather strengthens the validity of the present results.

The range of the measurement error in the present study extends from approximately 8% to 10% and thus compares well with the relative measurement errors reported in previous studies comparing either needle probe and ultrasonic measurements (range between 8.7% and 20.5%, depending on cartilage thickness and indenter radius (Suh et al. 2001)) or needle probe and static NIRS measurements (range between 5.5% and 7.1% (Afara et al. 2013a)). The accuracy of cartilage prediction in the present study is thus regarded as highly satisfactory for a non-destructive technique potentially applicable for hand-guided NIRS during real life surgery.

Conclusion

NIRS-B allows the prediction of articular cartilage thickness with a high accuracy (< 0.1 mm) and high-quality parameters after development of an optimized data analysis model in comparison with the gold standard needle indentation. Prediction of cartilage thickness can therefore not only be performed by static NIRS but also by dynamic combined NIRS-B, at least at an experimental level. Non-destructive, force-independent NIRS may thus also be suitable for intra-operative determination of the cartilage thickness in human disease or experimental models.

Acknowledgments and Funding

The authors thank Cordula Müller, Ulrike Körner, and Mattias Reebmann for expert technical assistance, and Dirk Woetzel, BioControl Jena, GmbH, for expert statistical analyses. The author(s) disclosed receipt of the following financial support for the research, authorship, and/or publication of this article: This study was supported by the Federal Ministry of Education and Research grants FKZ 1315577D and FKZ 13N12601 to RWK.

Declaration of Conflicting Interests

The author(s) declared no potential conflicts of interest with respect to the research, authorship, and/or publication of this article

Animal Welfare

The present study followed international, national, and/or institutional guidelines for animal treatment and complied with relevant legislation.

Ethical Approval

Ethical approval was not sought for the present study, because this was an ex vivo study with pre-existing animal material (see also the paragraph ‘Sample Preparation Method’ in the Materials and Methods section).

Supplementary Material

Supplementary figures for this article are available online.

4.3. In vitro analysis of the potential cartilage implant bacterial nanocellulose using the bovine cartilage punch model (Peer-Reviewed)

Autorenschaft der Publikation

Victoria Horbert, Peter Foehr, Friederike Kramer, Ulrike Udhardt, Matthias Bungartz, Olaf Brinkmann, Rainer H. Burgkart, Dieter O. Klemm, Raimund W. Kinne

Abstract

Biocompatible bacterial nanocellulose (BNC) shows high potential as wound dressing and dura mater replacement, and even for the development of blood vessel or cartilage implants. Thus, the regenerative capacity of BNC implants was analyzed using a standardized bovine cartilage punch model.

Cartilage rings with an outer diameter of 6 mmand an inner defect diameter of 2 mm were derived from the trochlear groove (femur-patellar articulation site). BNC implants were cultured inside the cartilage rings for up to 12 weeks. Cartilage-BNC-constructs were then evaluated by histology (hematoxylin/eosin; safranin O), immunohistology (aggrecan, collagens 1 and 2), and for protein content, mRNA expression, and push-out force of the implants.

Cartilage-BNC-constructs displayed vital chondrocytes (≥ 90% until week 9; > 80% until 12 weeks), preserved matrix integrity during culture, limited loss of matrix-bound proteoglycan from 'host' cartilage or cartilage-BNC-interface, and constant release of proteoglycans into the culture supernatant.

In addition, the content of the matrix protein collagen 2 in cartilage and cartilage-BNC-interface was approximately constant over time (with very limited quantities of collagen 1). Interestingly, BNC implants showed: (1) cell colonization of the implant; (2) progressively increasing mRNA levels for the proteoglycan aggrecan and collagen 2 (max. fivefold); and (3) significantly increasing push-out forces during culture (max. 1.6-fold).

Retained tissue integrity and progressively increasing chondrogenic differentiation in implant and cartilage- implant-interface suggest beginning cartilage regeneration in the BNC in the present model and indicate a high potential of BNC as a cartilage replacement material. Thus, the present model appears suitable to predict the in vivo performance of cartilage replacement materials (e.g., BNC) for tissue engineering.

Keywords: Bovine cartilage punch model, bacterial nanocellulose, regeneration model, articular cartilage, implant push-out force

Introduction

Partial- or full-thickness degenerative or traumatic knee cartilage lesions lead to progressive cartilage deterioration and finally to osteoarthritis. Established surgical approaches to cartilage repair include: (1) autologous chondrocyte implantation (ACI) following chondrocyte harvest from healthy cartilage regions; (2) microfracture of the bone plate below the cartilage to release mesenchymal stem cells from the bone marrow; and (3) transfer of healthy osteochondral plugs into the defect (osteoarticular transfer- OATS/mosaicplasty). These procedures are very attractive and show promise for initial cartilage regeneration (Hunziker 2002, Musumeci et al. 2014).

However, the quality of the repair tissue is still unsatisfactory, with inconsistent and poor histology (fibrous instead of hyaline cartilage), decreased mechanical competence, and a higher permeability of the repaired tissue in comparison to normal cartilage (Dell'Accio et al. 2006, Ye et al. 2014). Novel techniques for tissue engineering have recently entered clinical practice, e.g., second generation ACI techniques like matrix-assisted chondrocyte implantation/transplantation (m-ACI/MACT), which normally aim at reliable and long-term cell attachment to the defect area (Bachmann et al. 2004, Dewan et al. 2014, Gobbi et al. 2015, Kon et al. 2009). These techniques are based on materials like collagen 1/3 membranes (Bartlett W. 2006, Gillogly und Wheeler 2015, Steinwachs und Kreuz 2007), and combine several advantages, i.e., a shorter operation time, more limited surgical trauma, and the absence of complications due to the use of the outer bone membrane (periosteum; e.g., graft overgrowth).

Because of its unique material properties, bacterial nanocellulose (BNC) is very attractive as a novel biomaterial for many potential biomedical applications. Numerous in vitro and in vivo publications indicate high biocompatibility and biofunctions of BNC (Ahrem et al. 2014, Avila et al. 2015, Avila et al. 2014, Feldmann et al. 2013, Klemm et al. 2001, Kowalska-Ludwicka et al. 2013, Lang et al. 2015, Moritz et al. 2014, Napavichayanun et al. 2016, Pretzel et al. 2013, Saska et al. 2017, Wippermann et al. 2009b, Schumann et al. 2009, Bodin et al. 2007). BNC may be preferable over collagen implants because collagens are regularly derived from natural sources, in particular animal tissues, and thus the removal or inactivation of viral contamination remains an ever-increasing challenge for the safety of biomedical products and complete risk elimination has not been achieved (Mark Plavsic; http://www.biopharminternational.com/integrated-approachensure-viral-safety-biotherapeutics-0).

In contrast, the successful removal or inactivation of bacteria or bacterial products (in particular lipopolysaccharides) during the production of BNC products intended for clinical use is well established and documented (company information, Jenpolymer Materials UG & C. KG, Jena; Germany).

In particular, a high potential of BNC as a matrix for cartilage implants has been suggested on the basis of its favorable mechanical properties, its significant support of chondrocyte proliferation/ingrowth, and the lack of significant activation of pro-inflammatory reactions (Horbert et al. 2018, Svensson et al. 2005, Moller et al. 2017,). However, there are currently no in vitro studies characterizing the precise cellular and molecular mechanisms underlying cartilage regeneration in the BNC implant. The present study was thus performed to investigate the in vitro performance of BNC implants and to assess whether the results mirror their in vivo performance as a cartilage replacement material. The following questions were addressed: (1) is the in vitro model suitable for the pre-testing of cartilage replacement materials intended for future clinical application; and (2) does the model allow a comprehensive description of the mechanisms underlying in vitro cartilage regeneration. A cartilage implant model was thus applied using: (1) 'host' cartilage cylinders derived from the bovine femoral trochlea using a standardized punch system; and (2) inserted BNC implants (Horbert et al. 2018). The cartilage-BNC-constructs were kept in culture for up to 12 weeks, and then analyzed by: (1) (immuno-) histological staining; (2) protein assays in tissue and supernatants; (3) transcriptional analysis; and (4) evaluation of the implant push-out force.
'Host' cartilage and BNC implants remained vital with intact matrix and only slight loss of matrix-bound proteoglycan throughout 12 week in vitro culture. The BNC implants supported initial cell migration and cartilage differentiation/regeneration.

Methods

Biosynthesis of BNC implants

A nutrient medium according to Schramm and Hestrin (Schramm und Hestrin 1954b) was applied for the cultivation of Gluconacetobacter xylinus (DSM 14666; synonym Komagataeibacter xylinus, Deutsche Sammlung für Mikroorganismen und Zellkulturen GmbH, Braunschweig, Germany). The medium was inoculated with a pre-culture of the bacteria in a volume ratio of 20:1 and cultivated in 150 ml-beakers containing 64 glass tubes (inner diameter of 2.4 mm; 30 ml of inoculum per beaker) for 14 days at 28°C. The size of the BNC implants inside the tubes was 2.3 mm in diameter and 3 to 7 mm in height.
To remove bacterial and media remnants, the BNC was treated with 0.1 M aqueous sodium hydroxide solution at 100°C 10 min, rinsed several times with pyrogen-free water, steam pressure sterilized and stored until further use (room temperature).

Preparation and culture of bovine cartilage rings with BNC implants

Bovine cartilage was resected from the knees of German Holstein Friesian Cattle (age of 24 months). Cartilage rings were prepared from the lateral aspects of the facies articularis of the femur-patellar articulation site as previously published (Horbert et al. 2018, Pretzel et al. 2013) and an inner defect (diameter 2 mm) was generated using biopsy punches. BNC implants (Polymet Jena e.V., Jena; Germany) were placed into the central defect of the 'host' cartilage rings and kept in culture for 0, 4, 8, 10, and 12 weeks (Fig. 22; (Horbert et al. 2018)). Thereafter, cartilage-implant constructs were analyzed by histology. In addition, gene expression in chondrocytes derived from 'host' cartilage, its surface, or BNC implants was investigated (for preparation see below). The quantity of cartilage matrix proteins released into the culture supernatant, and the remaining content in 'host' cartilage and the chondrocytes on the cartilage surface was also analyzed.

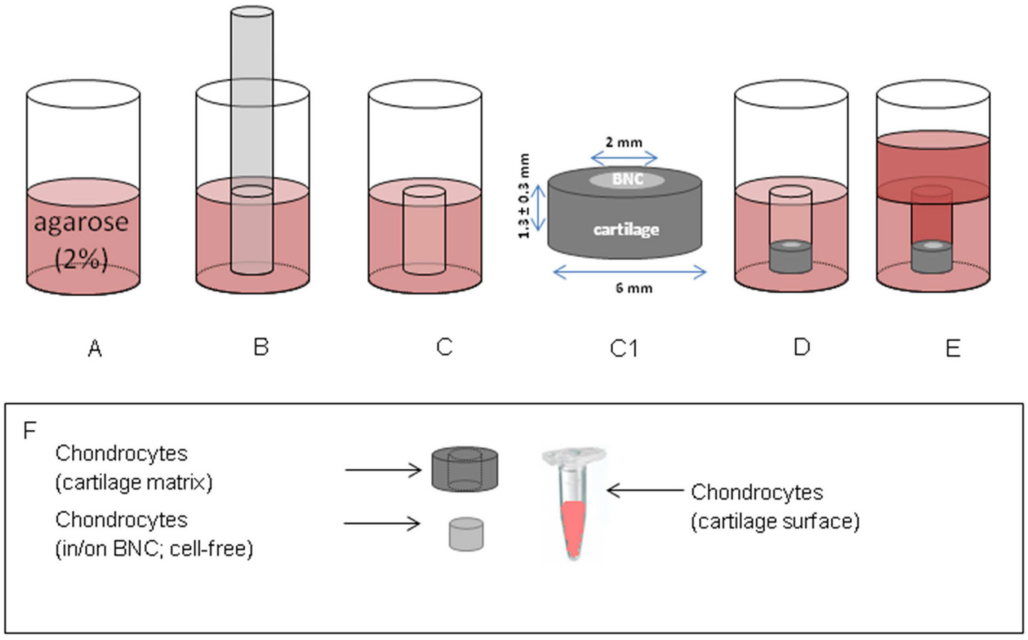

Figure 22: Schematic depiction of the in vitro model. First, hot liquid agarose (2%) was added into the wells of a 48-well plate (A). Cylindrical pockets with a defined size of 6 mm were generated by insertion of a metal-pin plate into the hot agarose and removal following gelation of the agarose (B, C). The BMC implant was inserted into the inner defect of the cartilage rings using forceps (C1) and, after embedding of the resulting constructs into the agarose (D), the well was filled with culture medium (E). Cartilage-implant constructs were histologically characterized after in vitro culture. Also, the mRNA expression in chondrocytes isolated from 'host' cartilage, the cells on its surface, and the BNC implant was investigated (F). Finally, the amount of cartilage proteins in supernatant, 'host' cartilage rings and the cells located on its surface was analyzed.

A total of 120 cartilage rings each were obtained from bovine knee joints (n = 7 animals) and analyzed by histology (n = 4), biochemistry (n = 10; n = 5 each for RT-PCR and protein determination), and biomechanics (n = 10; 24 samples for each time point). Culture supernatants were combined over 1 week and kept at - 20 _C for subsequent ELISA analysis.

Viability assay

Viability was assessed using fluorescein diacetate/ propidium iodide live/dead staining (Kunisch et al. 2017; Horbert et al. 2018). Four images each were taken in 3 chambers of the culture slides using a fluorescence microscope Axiovert200 M, an Axio- Cam MRm camera, and the AxioVision Rel4.8 program (all Zeiss, Oberkochen, Germany). Viable and dead cells were counted in all images using the cellprofiler software (www.cellprofiler.org) (Carpenter et al. 2006) and viability was expressed as the mean percentage of viable cells.

Histology and immunohistology

Cartilage-BNC-constructs, either non-cultured or cultured for 4, 8, 10 or 12 weeks, were fixed in PBS with 4% paraformaldehyde and embedded in paraffin. The samples were cut into 6 µm sections and stained with hematoxylin/eosin (HE) or safranin O (to assess the proteoglycan content).
Immunohistology for aggrecan, collagen 1, and collagen 2 was performed as previously reported (Horbert et al. 2018).
All immunohistological stainings using isotype-matched control antibodies with irrelevant specificity were negative.

Score for cell migration

Colonization of the BNC implants was analyzed using a published score (Pretzel et al. 2013, Horbert et al. 2018), consisting of 4 levels (0 = implant without cells, 1 = single adherent cells, 2 = several adherent cells, 3 = cell-layer on the implant). Scoring was independently performed by three individual observers, expressing the results as the mean ± standard error of the individual scores.

Scores for safranin O, collagen 1, collagen 2 and aggrecan

The intensity of the safranin O staining or the immunostaining for aggrecan, collagen 2, and collagen 1 was quantified using a published semi-quantitative score (Pretzel et al. 2013, Horbert et al. 2018), consisting of 4 levels (0 = no staining; 1 = weak staining; 2 = moderate

staining; 3 = strong staining). The sections were independently scored by three individual observers, expressing the results as the means ± standard error of the individual values.

Scanning electron microscopy

The micro-and nanostructure of the BNC samples and the morphology of the chondrocytes migrated onto the surface of the BNC were investigated by scanning electron microscopy (SEM). The samples were fixed in 2% (v/v) glutaraldehyde in 0.2 M sodium cacodylate buffer (pH 7.2). After 72 h, the samples were rinsed twice in 0.2 M sodium cacodylate buffer and dehydrated in ascending ethanol series [50, 60, 70, 80, 90, 100% (v/v)]. Prior to critical point drying (EMITECH K850; Emitech, Ashford, UK), the ethanol was exchanged against acetone. Dried samples were mounted with carbon tabs on aluminum stubs, sputter-coated (EMITECH K500; Emitech, Ashford, UK), and analyzed (beam energy of 10 kV; XL-30 ESEM; Philips, Hamburg, Germany).

Quantitative real-time polymerase chain reaction (qRT-PCR)

To quantify the mRNA expression of aggrecan, collagen 2, and collagen 1, RNA was separately isolated from: (1) cells in the 'host' cartilage; (2) cells located on its surface (see below); and (3) cells in BNC implants (Fig. 22F). For RNA isolation from the different groups, the BNC implants were removed from the cartilage rings. Ten implants were pooled and kept in a tube with 300 µl lysis buffer at - 80°C for subsequent RNA isolation.

Empty cartilage rings were treated for 1 minute in tubes with 300 µl lysis buffer each under continuous rotation to obtain the RNA from the cells located on the cartilage surface (Horbert et al. 2018). The rings were then removed from the tubes, followed by separate storage of the two components at - 80°C.

Cartilage rings were cut with scissors in 800 µl TriZol (Life Technologies, Carlsbad, CA, USA), incubated for 15 minutes at RT, and centrifuged for 3 minutes at 12.000 rpm (Horbert et al. 2018). Total RNA from the cartilage rings, the lysed cells on the cartilage surface, or the BNC implants was isolated using the Quiagen Kit (RNeasy® mini kit; Qiagen, Hilden, Germany; including DNase digestion).

qRT-PCR (i-cycler PCR system; BioRad, Munich, Germany) for the quantification of aggrecan, collagens 1 and 2, and the housekeeping gene aldolase was done as previously published (Horbert et al. 2018; Table 1). Gene expression was normalized to the relative expression of aldolase.

Protein extraction

To quantify aggrecan, collagen 2, and collagen 1, protein was extracted from: (1) chondrocytes located in the 'host' cartilage matrix; and (2) chondrocytes located on its surface. For this purpose, the BNC implants were removed from the cartilage rings. Protein from (1) was isolated by cutting in 1000 µl of 4 M GuHCL with scissors and incubation at 4°C for 48 h under rotation. Protein from (2) was isolated using acetone precipitation according to the instructions of the RNeasy® mini kit supplier (Qiagen).

Quantification of glycosaminoglycans

The release of glycosaminoglycans from the cartilage-BNC-constructs into the supernatant, and the remaining content in 'host' cartilage and the cells located on its surface, was measured using the DMB assay (Chandrasekhar et al. 1987, Farndale et al. 1986, Horbert et al. 2018). The supernatants of the respective week and group were pooled for the analysis.

Enzyme-linked immunosorbent assay (ELISA)

The concentrations of aggrecan, collagen 2, and collagen 1 in the culture supernatant, and the remaining content in ´host´ cartilage and the cells located on its surface, were quantified utilizing ELISA-Kits as previously described (Horbert et al. 2018). The supernatants of the cartilage-BNC-constructs of the respective week (0, 4, 8, and 10 weeks) and group were pooled.

Biomechanical testing

Biomechanical testing of samples from the different time points and test series (10 samples each) was executed using a static universal test system (Zwicki 1120®, Zwick/Roell, Ulm, Germany) at the Department of Orthopedics and Sportsorthopedics, Technische Universität München as previously described (Horbert et al. 2018). In brief, the push-out force of the implant from the 'host' cartilage ring ($F_{max(insert)}$) was measured applying a cylindrical indenter with a diameter of 1.8 mm (0.2 mm less than the central defect diameter). To account for remaining friction forces between indenter and empty 'host' cartilage ring, the test was repeated once more and the resulting force ($F_{max(empty)}$) was then subtracted [$F_{max(insert)}$ - $F_{max(empty)}$= $\Delta F_{max(res)}$]. Values were given in N and, or comparison with previous publications, in kPa (after division by the lateral surface of the BNC cylinder (0.8163 mm2).

Statistical analysis

Results were displayed as means ± standard error of the mean. The Mann-Whitney U test was used for statistical analysis and the statistical software SPSS 22.0 was applied. Significance was accepted at $p \leq 0.05$.

Results

BNC implants

Morphological characteristics

The BNC insert maintained lateral contact to the defect walls throughout culture (Fig. 23A). Resident cartilage cells were vital without signs of alterations and showed positive nuclear staining despite the relatively long culture periods (up to 12 weeks), suggesting well suitable culture conditions (Fig. 23A). SEM confirmed the superficial seeding of the BNC implants with numerous cells with spread-out morphology and an underlying, dense extracellular matrix (Figs. 23B1, 24; time point 8 weeks). The matrix of the cartilage appeared largely intact over time (Fig. 23A). However, cartilage close to the defect edge contained proliferation-induced cell clusters, possibly as a consequence of the initial tissue injury by the biopsy punch (Fig. 23A; see hash).

A generally high viability of the chondrocytes in the cartilage rings was confirmed by fluorescein diacetate/propidium iodide live-dead staining of chondrocytes enzymatically isolated from the cartilage at weekly intervals, resulting in viability rates of close to or [90% until week 9, and[80% for the remaining time points (Fig. 24).

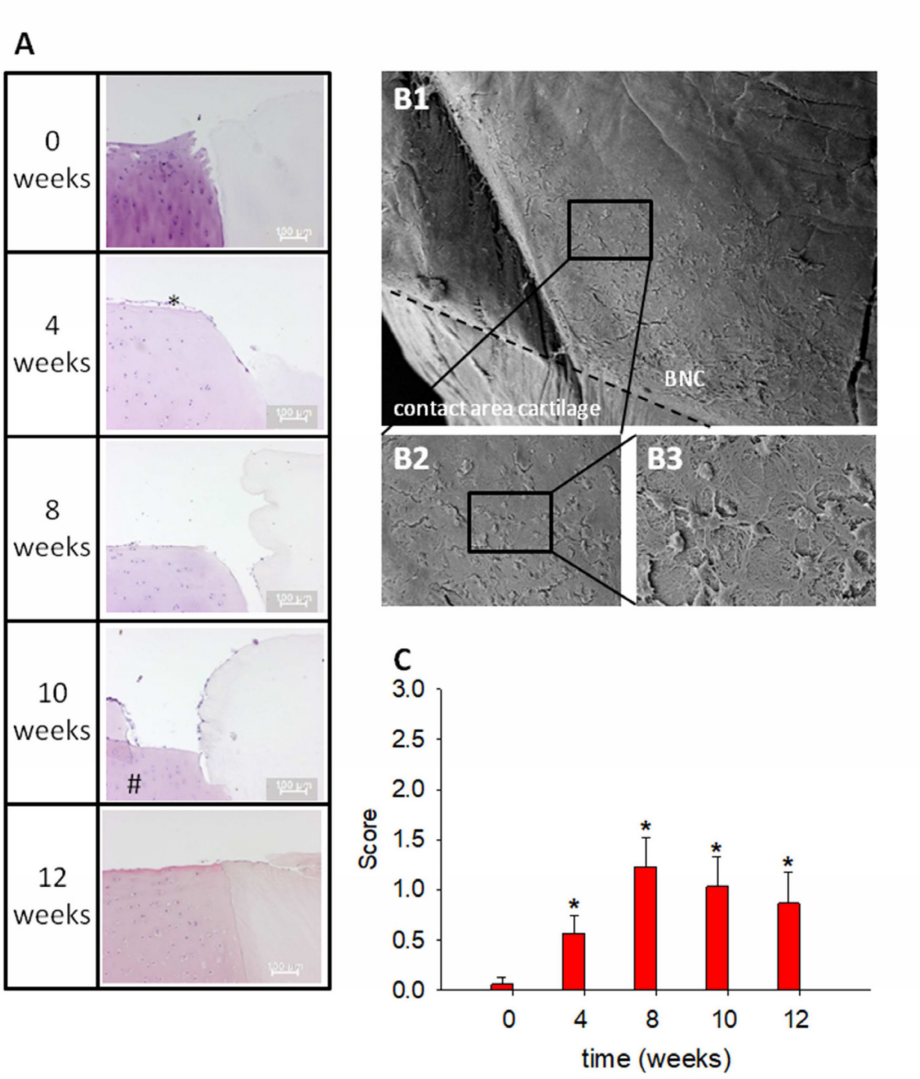

Figure 23: HE staining of the cartilage-BNC-constructs after culture in the central cartilage defect for 0, 4, 8, 10, or 12 weeks. (A) Morphology of the cells in cartilage, BNC implant and at the cartilage-implant interface; # = proliferation induced cell clustering; * = migration of chondrocytes onto the BNC implant. (B) Scanning electron microscopy images of the cells migrated onto the BNC surface; magnification top panel: x 100 (B1); left bottom panel: x 1000 (B2); right bottom panel: x 2000 (B3). (C) Semiquantitative analysis of cell colonization of the BNC implants; migration score: 0 = implant without cells, 1 = single adherent cells, 2 = several adherent cells, 3 = cell-layer on implant; * p B 0.05 versus 0 weeks.

Cartilage-BNC-constructs showed the earliest substantial colonization of the initially cell-free BNC implants after 4 weeks (Figs. 23A, C; see asterisks). Cell colonization significantly increased from 0 weeks to all subsequent time points (Fig. 23C).

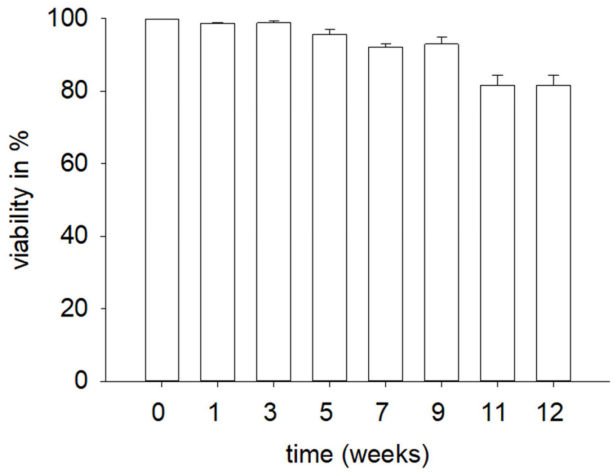

Figure 24: Viability of the chondrocytes in the cartilage ring throughout culture. Chondrocytes were enzymatically isolated from the cartilage at weekly intervals and cultivated for 1 day. Viability was assessed using fluorescein diacetate/propidium iodide staining. Data are expressed as mean ± standard error of the mean (SEM)

Content of proteoglycans, aggrecan, collagen 2, and collagen 1

The data suggesting a retained matrix integrity in the surrounding cartilage were further supported by a limited, non-significant decrease of the safranin O staining during culture (from a semi-quantitative score of 2.2 for freshly isolated cartilage to a score of 1.3 after 12 weeks of culture; Figs. 25, 26A); this indicated an only limited loss of proteoglycans during this time period.

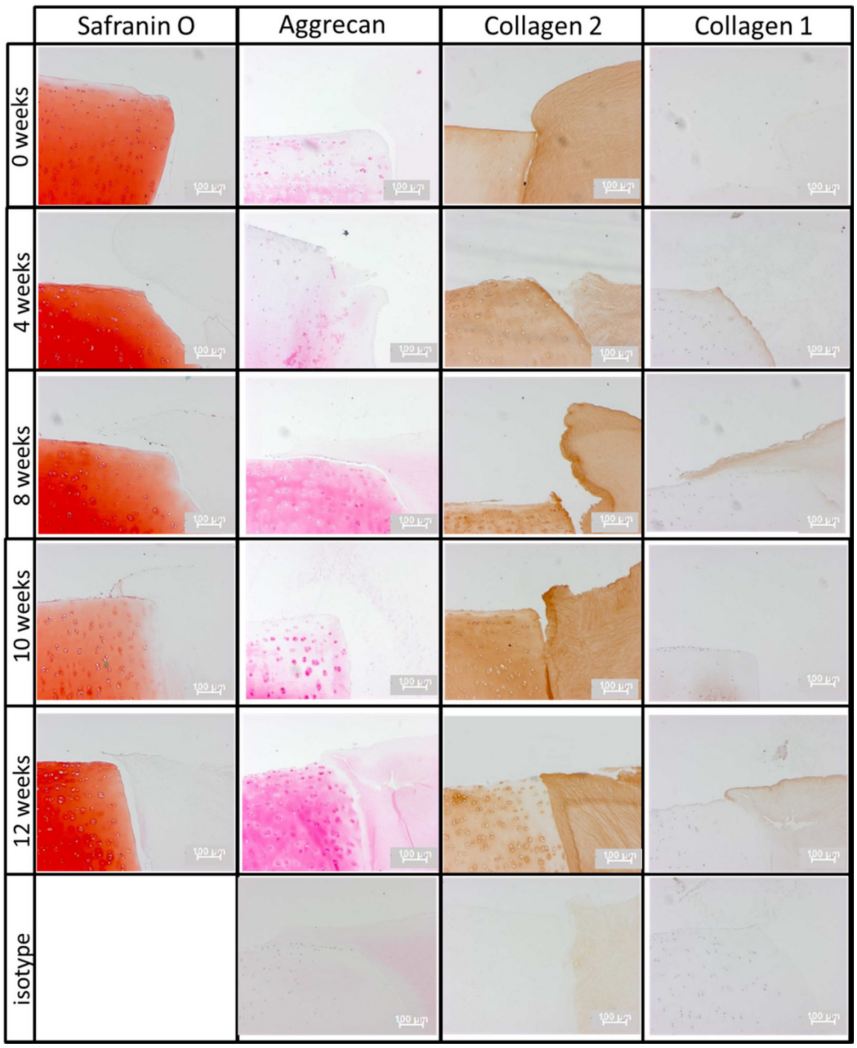

Figure 25: Safranin O, aggrecan, collagen 2, and collagen 1 (immuno)staining of the BNC implants after placement into the inner defect of the cartilage rings and subsequent culture for 0, 4, 8, 10, or 12 weeks.

Also the cartilage-implant interface showed no significant decrease of the safranin O staining (from 2.2 to 1.2; Figs. 25, 26A).

In contrast, in the implant there was no safranin-O staining at any time point.

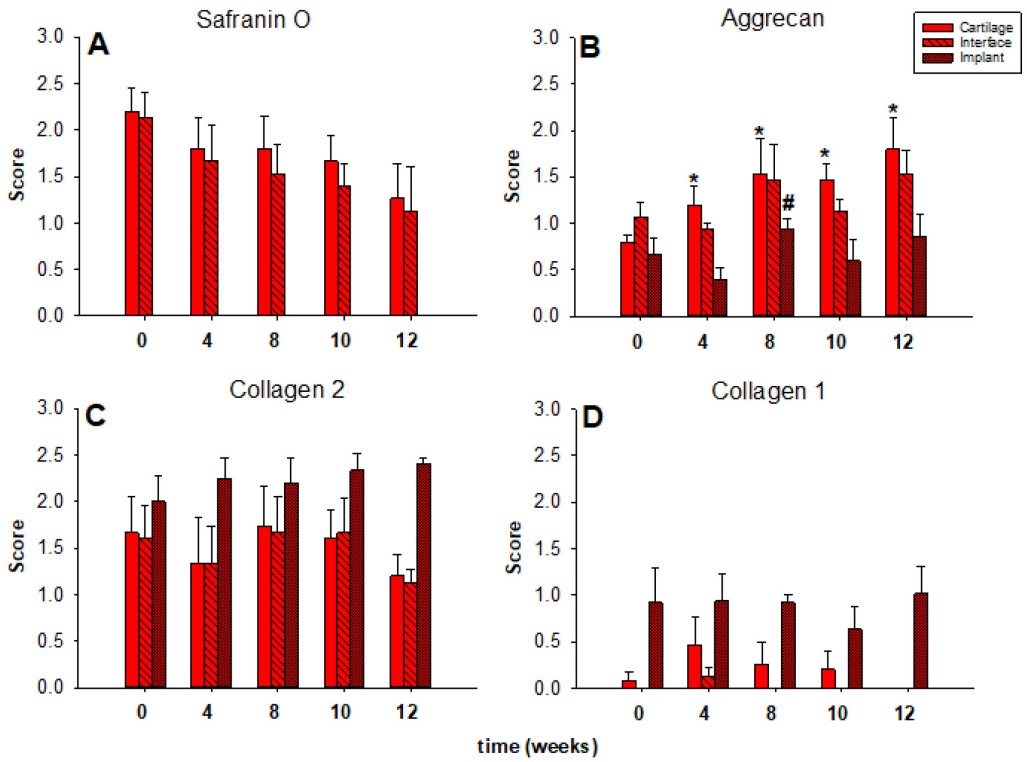

Figure 26: Semiquantitative analysis of Safranin O, aggrecan, collagen 2, and collagen 1 (immuno)staining in 'host' cartilage, interface, and BNC implants. Degree of staining: 0 = no staining, 1 = weak staining, 2 = moderate staining, 3 = strong staining; values are shown as means ± standard error (SEM) of the mean; * $p \leq 0.05$ versus 0 weeks; # $p \leq 0.05$ versus 4 weeks.

For the aggrecan staining, a significant increase was noted in the surrounding cartilage throughout culture ($p \leq 0.05$ for 4, 8, 10, and 12 weeks versus 0 weeks; Figs. 25, 26B). The aggrecan immunostaining in cartilage-implant-interface and implant during 12 week culture was largely constant (scores between 0.9 and 1.5 for the interface and between 0.4 and 0.9 for the implant, with a significant intermediate peak at 8 weeks for the implant; Figs. 25, 26B)

Also for collagen 2 the immunostaining was largely constant during 12 week culture in cartilage ring (scores between 1.3 and 1.7), cartilage-implant-interface (between 1.3 and 1.7), and BNC implant (between 2.0 and 2.4), without any significant differences among the individual time points (Figs. 25, 26C).

There was very little collagen 1 immunostaining (scores mostly between 0 and 1.0) in cartilage ring, interface, and implant. There were again no significant differences among the different time points (Figs. 25, 26D).

Proteoglycan content of tissue extracts and culture supernatant (DMB-assay)

Confirming the results of safranin O and aggrecan staining, the decline of the glycosaminoglycan (GAG) content in the cartilage ring throughout culture (from 5080 µg/ml for the freshly isolated cartilage to 3454 µg/ml at 12 weeks; Fig. 27) was limited and not significant.

The GAG content in chondrocytes migrated onto the surface was approx. sevenfold lower and showed a numerical decline throughout culture (from 706 µg/ml in fresh cartilage to 383 µg/ml at 12 weeks; Fig. 27A).

Also in the culture supernatant a very limited, nonsignificant decrease of the GAG content was observed throughout culture (from 118 µg/ml at 4 weeks to 113 µg/ml at 12 weeks; Fig. 27A), as confirmed by the constant release of aggrecan into the supernatant (ELISA; from 6 ng/ml at 4 weeks to 6 ng/ml at 12 weeks; Fig. 27B).

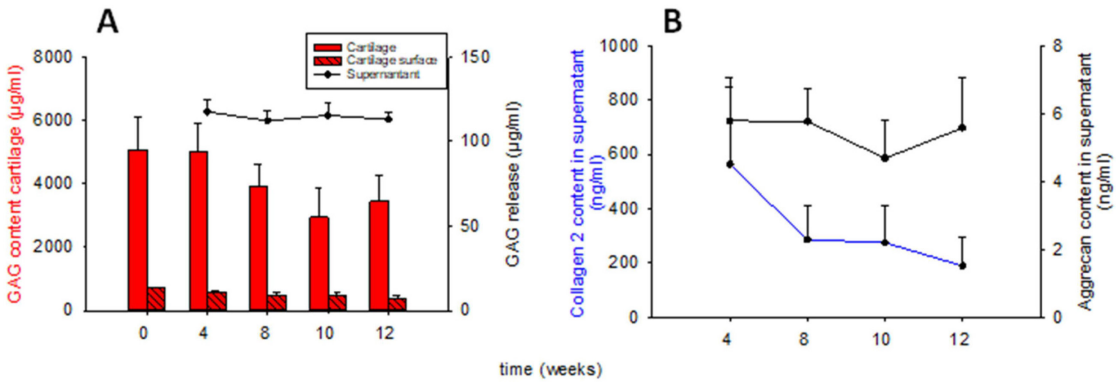

Figure 27: Quantitative analysis of proteoglycan content or release (DMB assay) or newly synthesized collagen 2 and aggrecan (ELISA) in cartilage-BNC-constructs. Proteoglycans (DMB assay) and newly synthesized collagen 2 and aggrecan (ELISA) were quantified in fresh and cultured 'host' cartilage (cartilage), cells located on its surface (cartilage surface), and culture supernatant (supernatant), when using BNC implants (A for proteoglycan; B for collagen 2 and aggrecan); values are expressed as mean ± SEM

Collagen 2 and 1 content of culture supernatant (ELISA)

The decline of the collagen 2 release (from 562 ng/ml at 4 weeks to 189 ng/ml at 12 weeks Fig. 26B), and the increase of the collagen 1 release during culture (from 165 ng/ml at 4 weeks to 228 ng/ml at 12 weeks; data not shown) were also limited and not significant.

Gene expression for aggrecan, collagen 2, and collagen 1 (RT-PCR)

Aggrecan expression in the ´host´ cartilage significantly decreased over time ($p \leq 0.05$ for 4 and 10 weeks versus 0 weeks), whereas the cartilage surface cells did not significantly change. Interestingly, the **implant** showed a transient, substantial peak of aggrecan expression at 8 weeks (max. fivefold), with a subsequent decrease thereafter (Fig. 28A).

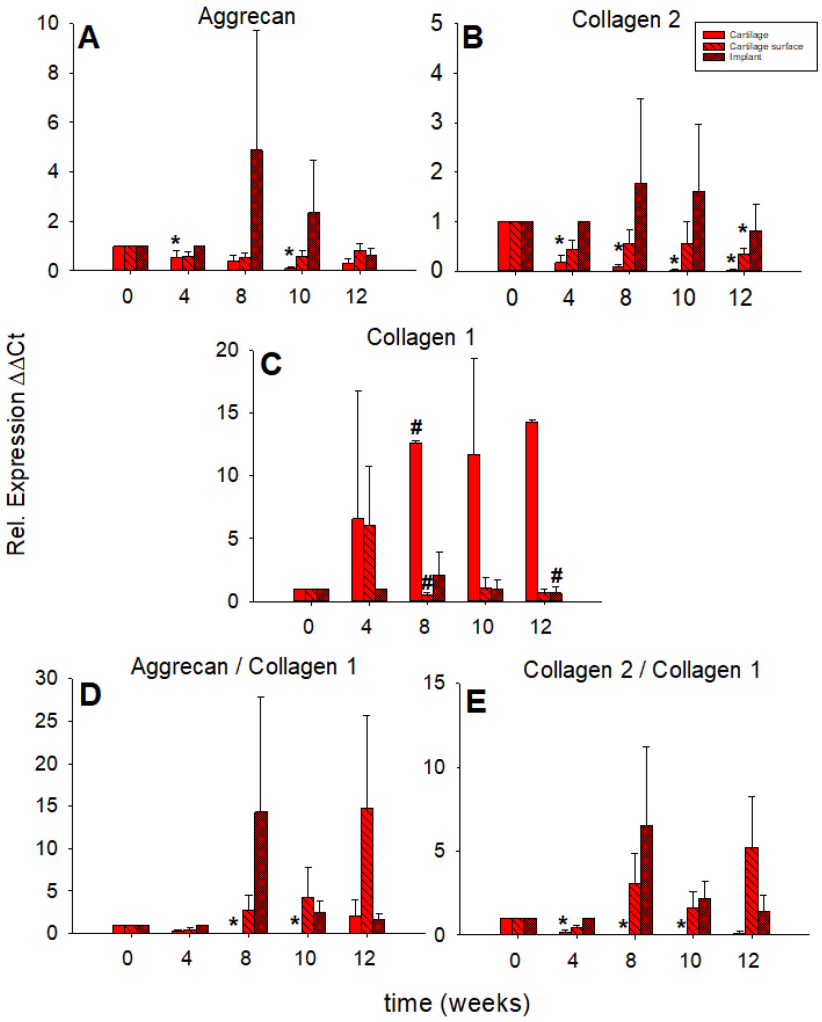

Figure 28: qRT-PCR analysis for aggrecan, collagen 2, and collagen 1 gene expression in 'host' cartilage, cartilage surface, and BNC implants. mRNA expression for aggrecan (A), collagen 2 (B), collagen 1 (C), aggrecan/collagen 1 ratio (D), and collagen 2/collagen 1 ratio (E) A-E was analyzed prior to and after 4, 8, 10, and 12 weeks of tissue culture; relative gene expression of the cells located in the 'host' cartilage (cartilage), on its surface (cartilage surface), and on/in the BNC implant (implant); values are expressed as means ± SEM; * $p \leq 0.05$ versus 0 weeks; # $p \leq 0.05$ versus 4 weeks.

Collagen 2 expression in 'host' cartilage and cartilage surface cells showed a significant decrease over time (cartilage ring: $p \leq 0.05$ for 4, 8, 10 and 12 weeks versus 0 weeks; surface cells: $p \leq 0.05$ for 12 weeks versus 0 weeks), whereas the collagen 2 expression in the **implant** increased from baseline to a transient twofold peak at 8 weeks and thereafter declined again (Fig. 28B).

Expression of collagen 1 in the 'host' cartilage significantly increased over time ($p \leq 0.05$ for 8 weeks versus 4 weeks), whereas the collagen 1 expression in cartilage surface cells and **implant** only increased to transient peaks at 4 (sixfold) and 8 weeks (twofold), respectively, with a decrease thereafter (Fig. 28C).

Whereas the aggrecan/collagen 1 ratio in the ´host´ cartilage displayed a minor increase at 12 weeks (after a significant decrease at 8 and 10 weeks versus 0 weeks) and the aggrecan/collagen 1 ratio in the cartilage surface cells showed a long-term rise (Fig. 28D), the aggrecan/collagen 1 ratio in the **implant** increased to an intermediate peak (8 weeks; 14-fold), with a subsequent decrease (Fig. 28D).

In contrast to the aggrecan/collagen 1 ratio, the collagen 2/collagen 1 ratio in the ´host´ cartilage significantly decreased over time ($p \leq 0.05$ for 4, 8 and 10 weeks versus 0 weeks; Fig. 28D). However, this ratio long-lastingly increased in cartilage surface cells (fivefold peak at 12 weeks) and **implant** (sevenfold peak at 8 weeks; Fig. 28E).

Push-out forces of the cultivated cartilage-BNC-constructs (biomechanical testing)

Notably, the push-out force for the BNC implants significantly increased during culture (from **0.05 ± 0.01 N** or 59.09 ± 6.56 kPa at 0 weeks to **0.08 ± 0.01 N** or 97.08 ± 17.26 kPa at 12 weeks; $p \leq 0.05$ for 8 and 12 weeks versus 0 weeks; Fig. 29).

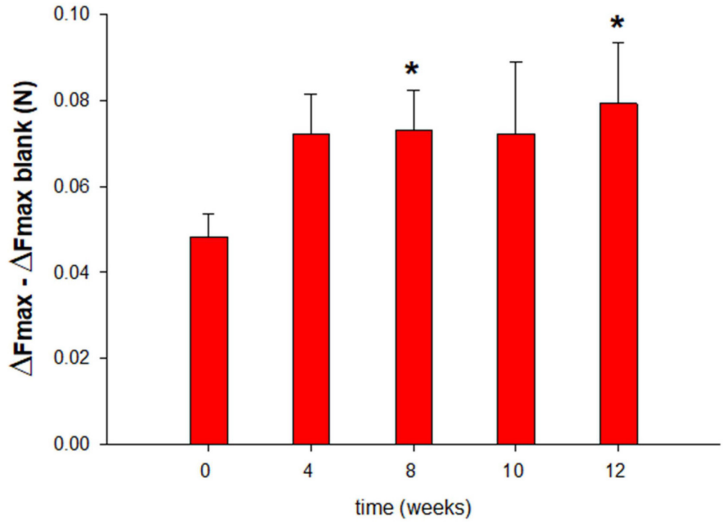

Figure 29: Push-out tests of the cartilage-BNC-constructs. Values are expressed as mean ± SEM; * $p \leq 0.05$ versus 0 weeks.

Discussion

The aim of the current study was to assess the long-term in vitro performance of a bacterial nanocellulose (BNC) implant using a standardized bovine cartilage punch model. The central results were that: (1) cartilage-BNC-constructs showed vital chondrocytes, preserved matrix integrity, limited loss of proteoglycan from the matrix of 'host' cartilage ring or cartilage-BNC-interface, and a constant release of proteoglycans into the culture supernatant; (2) BNC implants showed cell immigration/colonization and increased aggrecan and collagen 2 mRNA levels; and (3) BNC implants displayed significantly elevated push-out forces from the 'host' cartilage over time. The results of this study concord well with the known biocompatibility of BNC implants for medical applications (Ahrem et al. 2014, Avila et al. 2015, Avila et al. 2014, Bodin et al. 2007, Feldmann et al. 2013, Klemm et al. 2001, Kowalska-Ludwicka et al. 2013, Lang et al. 2015, Markstedt et al. 2015, Moritz et al. 2014, Napavichayanun et al. 2016, Saska et al. 2017, Schumann et al. 2009, Wippermann et al. 2009a) and their potential as a cartilage replacement material. BNC hydrogels may thus be well suitable for in vivo cartilage repair by matrix-associated chondrocyte transplantation. In addition, the lack of in vivo biodegradability may render BNC a sustainable scaffold to support cell ingrowth and subsequent remodeling of the joint cartilage.

The present long-term in vitro cartilage regeneration model, based on reproducible, easily available, and ethically unproblematic tissue supply, appears well suited for the evaluation of chondral implants with proven or expected clinical potential (Horbert et al. 2018) and references therein). The ´host´ cartilage ring shows only minor cartilage degeneration, and zones at the defect edge containing proliferation-induced cell clusters may indicate an attempt at the repair of damaged cartilage and the seeding of the cartilage implant (Lotz et al. 2010, Morales 2007).

On one hand, the 'host' cartilage ring demonstrated long-term stability over time as shown by: (1) limited indications of cartilage degeneration and chondrocyte viability rates of [90% for 9 weeks of culture; (2) limited proteoglycan loss and significant increase of aggrecan content, as well as stable collagen 2 content (small amounts of collagen 1), in good agreement with published own data on a co-culture system with a collagen type I hydrogel (Horbert et al. 2018). On the other hand, there were some signs of a limited dedifferentiation of the resident chondrocytes particularly at later time points, as shown by significantly decreasing aggrecan and collagen 2 mRNA levels and the resulting collagen 2/collagen 1 and aggrecan/collagen 1 ratios. This demonstrates that the current model in principle supports long-term culture in vitro with at least partial transferability to the in vivo situation, but may become more vulnerable to in vitro artifacts at 10 and 12 weeks.

The BNC implants showed a progressive colonization, paralleled by signs of chondrocyte emigration particularly from the surface of the 'host' cartilage. This underlines the high cyto-compatibility of the BNC implant in the current in vitro model, as previously shown in experimental (Ahrem et al. 2014, Bodin et al. 2007, Feldmann et al. 2013, Moritz et al. 2014, Nimeskern et al. 2013, Pretzel et al. 2013, Saska et al. 2017) and in vivo studies (Avila et al. 2015, Avila et al. 2014, Klemm et al. 2001, Kowalska-Ludwicka et al. 2013, Lang et al. 2015, Napavichayanun et al. 2016, Schumann et al. 2009, Wippermann et al. 2009a).

As a sign of beginning cartilage regeneration, the initially cell-free BNC implants showed deposition of the matrix proteins collagen 2 and aggrecan throughout culture. This was further stressed by progressively rising levels of collagen 2 and aggrecan mRNA. The locally synthesized, cartilage-specific matrix proteins seemed to be successfully retained in the BNC implants, as shown by a constant aggrecan release and a decreased collagen 2 release into the culture supernatant over time.

There were no clear indications for chondrocyte dedifferentiation in BNC implants over time, since: (1) the content of the cartilage-specific proteins aggrecan and collagen 2 (and of the connective tissue collagen 1) was stable throughout culture; and (2) the aggrecan/ collagen 1 and collagen 2/collagen 1 mRNA ratios were substantially increased over 8 weeks of tissue culture (up to 14- and 6-fold, respectively). The current regeneration model may thus support a middle- term phenotypic stability of the chondrocytes colonizing the implant, in line with previous publications describing similar models (Horbert et al. 2018) and references therein). In addition, the current cellular and molecular data on cartilage regeneration and chondrocyte colonization/differentiation further underline the potential of BNC for cartilage repair.

The BNC implants developed significantly augmented push-out forces from 'host' cartilage throughout culture. Thus, high cell vitality, considerable cell colonization, and prolonged local matrix production apparently result in increased lateral attachment between implant and surrounding cartilage ring. The augmentation of the push-out forces of the initially cell-free BNC implants during the 12-week culture [from 59.09 to 97.08 kPa, i.e., by approx. 64%] generated final values well comparable to those previously published for PGA-constructs after 5 weeks (Hunter und Levenston 2004) or for cellseeded agarose hydrogels after 6 weeks of culture (Vinardell et al. 2009). The underlying mechanisms may include: (1) the tissue formed at the cartilage implant interface [(Moretti et al. 2005); compared with Figs. 23B1, 24]; (2) sprouting of different components of ECM in the interfacial region (compare with separate manuscript on three-dimensonally perforated BNC in this issue; Horbert et al. 2018) and (3) the local absence or presence of cell death (Theodoropoulos et al. 2011, Horbert et al. 2018) and references therein. Highly standardized experimental conditions were applied in the present study, including preparation of BNC implants and 'host' cartilage

rings, placement and culture of the implants inside the cartilage, careful harvesting and overnight transport of 10 fresh, unfrozen cartilage-BNC-constructs for each time point to the Department of Orthopedics and Sportsorthopedics, Technische Universität München, and immediate final biomechanical testing. These standardized procedures make an influence of a differential bulk growth of the BNC implant at the different culture time points on the resulting push-out forces very unlikely. This again shows that BNC implants may serve as a suitable scaffold material in general (Avila et al. 2015, Bodin et al. 2007, Klemm et al. 2001, Kowalska-Ludwicka et al. 2013, Lang et al. 2015, Moritz et al. 2014, Napavichayanun et al. 2016, Saska et al. 2017, Schumann et al. 2009, Wippermann et al. 2009a) and, in particular, as cartilage repair material (Ahrem et al. 2014, Pretzel et al. 2013).

Conclusion

Largely retained tissue integrity, limited proteoglycan release, and generally high viability of local chondrocytes in the 'host' cartilage ring (> 90% until 9 weeks), as well as long-term stabilization of the chondrogenic phenotype and significantly augmented push-out forces of the BNC implant (up to 12 weeks) indicate beginning cartilage regeneration of the BNC implant in the current model system. Thus, the present in vitro cartilage repair model seems to be suitable to predict the in vivo performance of cartilage replacement materials such as BNC for tissue engineering.

Acknowledgements

The authors are grateful to Cordula Müller, Bäbel Ukena, and Ulrike Körner for expert technical assistance, as well as Maren Siedentop, Daniela Warnecke, and Fabian Holzner for expert biomechanical testing of implant push-out forces.
We gratefully acknowledge the partial financial support of the Bundesministerium für Bildung und Forschung (BMBF), grant references 13N12601 and 0315577C.

Declaration of Conflicting Interests

There are no potential conflicts of interest for any of the authors regarding the research, authorship, and/or publication of this article.

5. Gesamtdiskussion

Ziel der vorliegenden in vitro Studien war es, die Knorpelregeneration von verschiedenen z. T. bereits im klinischen Einsatz befindlichen Konstrukten in einem in der Arbeitsgruppe Experimentelle Rheumatologie des Uniklinikums Jena etablierten in vitro Systems zu testen. Das vorliegende Modellsystem basiert auf bovinen Knorpelzylindern, in die die verschiedenen regenerativen Materialien eingebracht werden und bis zu 12 Wochen in vitro kultiviert werden können. Nach verschiedenen Zeitpunkten (0, 4, 8 10 und 12 Wochen) erfolgte die biomechanische (push-out Versuche), molekularbiologische (qRT-PCR und Proteinanalyse) und histologische (semiquantitativer Score) Untersuchung der Konstrukte.
Ein Vorteil des auf bovinen Knorpelstanzen basierenden in vitro Modells ist neben der ethisch unproblematischen Probengewinnung die hohe Reproduzierbarkeit des Systems. Der Knorpelring, der das zu untersuchende Implantat umgibt, zeigt nur an den Schnittkanten eine geringe Knorpeldegeneration. Die dort zu erkennenden Chondrozyten-Cluster könnten darauf hinweisen, dass die Chondrozyten versuchen, den beschädigten Knorpel zu reparieren und das Implantat zu besiedeln und mit Matrix zu füllen. Bei allen untersuchten Konstrukten wurde neben der vitalen Morphologie der Chondrozyten sowie der intakten Matrix-Integrität auch ein leidglich geringer Proteoglykan-Verlust sowie eine verminderte Proteoglykan-Freisetzung im Überstand beobachtet. Weiterhin wurde bei allen untersuchten Konstrukten eine gute bis sehr gute Zellmigration / Zellkolonisation beobachtet. Das hier verwendete in vitro Modell scheint daher für die Testung von chondralen Knorpelimplantaten (sowohl innovativen, als auch klinisch etablierten Implantaten) gut geeignet zu sein. Es bietet die Möglichkeit, die bei der Knorpelregeneration stattfindenden molekularen Prozesse zu entschlüsseln und so zusammen mit den biomechanischen und histologischen Daten Vorhersagen für die in vivo „Performance“ von klinisch etablierten und neu entwickelten TE Konstrukten zu treffen.

Dieses in vitro Modell scheint allerdings nur begrenzt für die Testung von resorbierbaren Materialien wie Bioseed®-C in Frage zu kommen. Eine auf diesem in vitro Modell basierende Vorhersage der in vivo Performance scheint aufgrund der schnellen Resorbierbarkeit des PGA-Vlieses (42 Tage) nicht möglich. Für solche Materialien müsste das vorliegende in vitro System eventuell so modifiziert werden, dass der subchondrale Knochen mit in das System einbezogen wird und in einem Knorpel-Knochenzylinder ein zentraler Defekt bis zur subchondralen Lamelle generiert wird. In diesen Defekt können dann beispielsweise resorbierbare Materialien eingebracht und kultiviert werden. Die vollständige Entfernung der Knorpelschicht ohne Schädigung der subchondralen Lamelle ist jedoch technisch sehr anspruchsvoll (unveröffentlichte Daten).

Parallel zu den in vitro Versuchen wurde das Knorpelersatzmaterial BioSeed®-C der Firma TTT in vivo untersucht. Die entstandenen Gewebsregenerate wurden nach 6 und 12 Monaten molekularbiologisch (qRT-PCR und Proteinanalyse) und histologisch (O´Driscoll Scores, modifizierte O´Driscoll Scores und Penada Score) untersucht. Histologisch konnte eine Abnahme des Proteoglykan-Gehaltes beobachtet werden. Molekularbiologisch (qRT-PCR) zeigte sich, dass die mit dem Implantat BioSeed-C besetzten Defekte eine verminderte Expression von Kollagen 1 und eine langfristig erhöht Expression des Knorpelmarkers Kollagen 2 aufwiesen. Weiterhin zeigte die PG-Konzentration im Knorpelgewebe (DMB-Assay) eine numerische Abnahme des GAG-Gehaltes nach 6 und 12 Monaten im Vergleich zum Nullpunkt. Die molekularbiologischen Ergebnisse unterstreichen dabei das therapeutische Potenzial der verwendeten Implantate. Allerdings zeigen die Ergebnisse auch, dass es durch die versetzte Operation beider Kniegelenke zu einer erhöhten Belastung des Knorpels bzw. zu einer Schädigung des umliegenden Knorpels im Kniegelenk kommt. Mit diesen Daten wird momentan eine Veröffentlichung vorbereitet.

Neben den in vitro und in vivo Versuchen mit den verschiedenen Knorpelersatzmaterialien wurde auch die Knorpeldickenvorhersage unter dem Einfluss variierender Belastung mittels Nahinfrarot-Spektroskopie (NIRS-B) ex vivo untersucht. Mit dem NIRS Messsystem war es möglich, die Knorpeldicke im Knie des Großtiermodells Schaf zerstörungsfrei optisch zu detektieren. Die mittels NIRS-B gewonnenen Daten wurden dabei mit den Ergebnissen der mittels der Goldstandard-Methoden Nadelindentation bzw. Histologie erhobenen Daten verglichen und für die Entwicklung geeigneter Kalibrierungsalgorithmen verwendet. Mit diesen Algorithmen war dabei eine sehr genaue Knorpeldickenvorhersage (<0,1 mm) möglich. Mit diesem Messsystem scheint es also möglich zu sein, eine nichtinvasive Beurteilung der Knorpeldicke und der Knorpeleigenschaften von gesundem bzw. regeneriertem Knorpel realisierbar durchzuführen.

Es gibt allerdings einige Limitationen, auf die bei späteren Untersuchungen eingegangen werden sollte. Zum einen wurde für die Messungen in der vorliegenden Studie normaler Schafsknorpel verwendet, um das NIRS-B Messsystem zunächst für unveränderten und gesunden Knorpel zu etablieren. Allerdings könnte die Situation bei degeneriertem Knorpel anders und möglicherweise komplexer sein und somit neue Analysen und Kalibrierungen erfordern. Eine weitere Einschränkung ist, dass die gewonnenen Daten eine möglichst senkrechte Ausrichtung an den Knorpel-Knochen Zylindern aus der Hauptbelastungszone der medialen und lateralen Femurkondyle erfordern. Diese exakte Positionierung der Messsonde an intakten Kondylen muss bei einem räumlich eng begrenzten Zugang im Rahmen einer minimal-invasiven Operation noch reproduziert werden.

6. Schlussfolgerung

Die vorliegende Arbeit sollte verschiedene z. T. etablierte klinische Knorpelersatzmaterialien in vitro und in vivo untersuchen. Die gewonnen Ergebnisse sollten anschließend in die Entwicklung von standardisierten Verfahren für die Prüfung von TE Konstrukten für den orthopädisch-unfallchirurgischen Einsatz einfließen.

Unter Berücksichtigung aller Ergebnisse lassen sich folgende Schlussfolgerungen ziehen:

- Das hier verwendete in vitro Modell bietet sehr gute Versuchsbedingungen für die Kultivierung von innovativen TE Konstrukten oder klinisch etablierten Knorpelersatzmaterialien über einen Zeitraum von bis zu 12 Wochen. Die verschiedenen biomechanischen, molekularbiologischen und histologischen Untersuchungen ermöglichen es einerseits, die bei der Knorpelregeneration stattfindenden molekularen Prozesse zu entschlüsseln und andererseits das Einwachsen des Knorpelersatzmaterials in das umliegende Gewebe zu beurteilen (push-out-Versuche), um so Vorhersagen für die in vivo „Performance“ der Konstrukte zu treffen.
- Dieses in vitro Modell scheint allerdings nur begrenzt für die Testung von resorbierbaren Materialien wie Bioseed®-C in Frage zu kommen. Eine auf diesem in vitro Modell basierende Vorhersage der in vivo Performance scheint aufgrund der schnellen Resorbierbarkeit des PGA-Vlieses (42 Tage) nicht möglich. Für resorbierbare Materialien müsste das vorliegende in vitro System so modifiziert werden, dass ein zentraler Knorpeldefekt in einem zuvor entnommenen Knorpel-Knochen Zylinder generiert und anschließend bis zu 12 Wochen kultiviert wird. Die vollständige Entfernung der Knorpelschicht ohne Schädigung der subchondralen Lamelle ist dabei jedoch technisch sehr anspruchsvoll.
- Die Auswertung der in vivo Proben zeigte trotz klarer klinischer Erfolge mit BioSeed-C im Schafmodell noch keine eindeutige Ausbildung von vollwertigem Knorpelgewebe. Zum Teil sind jedoch klare Unterschiede zwischen den Verumdefekten und den Leerdefekten mit einer potenziell prädiktiven Aussage für die in vivo Einheilung zu erkennen (eigene Daten).
- Mit dem NIRS-B Messsystem ist es möglich, optisch nicht erkennbare Unterschiede der Knorpeleigenschaften im Knie des Großtiermodells Schaf zerstörungsfrei zu detektieren. In einem weiteren Schritt scheint es zudem möglich zu sein, eine nichtinvasive Beurteilung der Knorpeldicke und der Knorpeleigenschaften in vivo an regeneriertem Knorpel durchzuführen, um so die Qualität des Regeneratgewebes zu beurteilen. Allerdings wurde die Kalibrierung des Messsystems bisher nur an

normalem und nicht degenerierten Knorpel durchgeführt. Es ist zu erwarten, dass die Situation bei degeneriertem Knorpel anders und komplexer ist und somit neue Analysen und Kalibrierungen erfordert, bevor das System beispielsweise als „hand-guided“ System bei humanen Operationen zum Einsatz kommt

In der vorliegenden Arbeit konnte gezeigt werden, dass die standardisierte Untersuchung von innovativen bzw. klinisch etablierten TE Konstrukten mit dem vorliegenden in vitro Modell über einen Zeitraum von bis zu 12 Wochen möglich ist, um mit den gewonnenen Ergebnissen (molekularbiologisch und biomechanisch) Vorhersagen für die die in vivo „Performance“ von Knorpelersatzmaterialien zu treffen. Die Auswertung der biomechanischen Untersuchungen der in vivo Proben erfolgte in Kooperation mit den Verbundpartnern des BMBF Projektes. Auf der Basis aller gewonnenen Erkenntnisse sollen nunmehr mit den Kooperationspartnern standardisierte Verfahren für die Prüfung von TE Konstrukten für den orthopädisch-unfallchirurgischen Einsatz entwickelt werden.

7. Literaturverzeichnis

Afara I, Singh S, Oloyede A. 2013a. Application of near infrared (NIR) spectroscopy for determining the thickness of articular cartilage. Med Eng Phys, 35 (1) (1):88-95.

Afara I, Singh S, Oloyede A. 2013b. Load-unloading response of intact and artificially degraded articular cartilage correlated with near infrared (NIR) absorption spectra. J Mech Behav Biomed Mater, 20:249-258.

Afara I, Prasadam I, Crawford R, Xiao Y, Oloyede A. 2012. Non-destructive evaluation of articular cartilage defects using near-infrared (NIR) spectroscopy in osteoarthritic rat models and its direct relation to Mankin score. Osteoarthritis Cartilage, 20 (11) (11):1367-1373.

Ahrem H, Pretzel D, Endres M, Conrad D, Courseau J, Muller H, Jaeger R, Kaps C, Klemm DO, Kinne RW. 2014. Laser-structured bacterial nanocellulose hydrogels support ingrowth and differentiation of chondrocytes and show potential as cartilage implants. Acta Biomater, 10 (3):1341-1353.

Andereya S, Maus U, Gavenis K, Muller-Rath R, Miltner O, Mumme T, Schneider U. 2006. [First clinical experiences with a novel 3D-collagen gel (CaReS) for the treatment of focal cartilage defects in the knee]. Z Orthop Ihre Grenzgeb, 144 (3):272-280. Andersson J, Stenhamre H, Backdahl H, Gatenholm P. 2010. Behavior of human chondrocytes in engineered porous bacterial cellulose scaffolds. J Biomed Mater Res A, 94 (4):1124-1132.

Astley OM, Chanliaud E, Donald AM, Gidley MJ. 2001. Structure of Acetobacter cellulose composites in the hydrated state. International journal of biological macromolecules, 29 (3):193-202.

Avila HM, Schwarz S, Feldmann EM, Mantas A, von Bomhard A, Gatenholm P, Rotter N. 2014. Biocompatibility evaluation of densified bacterial nanocellulose hydrogel as an implant material for auricular cartilage regeneration. Appl Microbiol Biotechnol, 98 (17):7423-7435.

Avila HM, Feldmann EM, Pleumeekers MM, Nimeskern L, Kuo W, de Jong WC, Schwarz S, Muller R, Hendriks J, Rotter N, van Osch GJ, Stok KS, Gatenholm P. 2015. Novel bilayer bacterial nanocellulose scaffold supports neocartilage formation in vitro and in vivo. Biomaterials, 44:122-133.

Bachmann G, Basad E, Lommel D, Steinmeyer J. 2004. [MRI in the follow-up of matrix-supported autologous chondrocyte transplantation (MACI) and microfracture]. Radiologe, 44 (8):773-782.

Bagratashvili VN, Sobol EN, Sviridov AP, Popov VK, Omel'chenko AI, Howdle SM. 1997. Thermal and diffusion processes in laser-induced stress relaxation and reshaping of cartilage. J Biomech, 30 (8) (8):813-817.

Bartlett W, Skinner J, Gooding C, Carrington R, Flanagan A, Briggs T, Bentley G. 2005. Autologous chondrocyte implantation versus matrix-induced autologous chondrocyte implantation for osteochondral defects of the knee: a prospective, randomised study. Bone & Joint Journal, 87 (5):640-645.

Bartlett W. KSP, Skinner J. A. , Carrington R. W. J. , Briggs T. W. R. , Bentley G. . 2006. Collagen-covered versus matrix-induced autologous chondrocyte implantation for osteochondral defects of the knee: a comparison of tourniquet times. European Journal of Orthopaedic Surgery & Traumatology, 16 (4):315-317.

Bartz C, Meixner M, Giesemann P, Roel G, Bulwin GC, Smink JJ. 2016. An ex vivo human cartilage repair model to evaluate the potency of a cartilage cell transplant. J Transl Med, 14 (1):317.

Baumgaertner MR, Cannon WD, Jr., Vittori JM, Schmidt ES, Maurer RC. 1990. Arthroscopic debridement of the arthritic knee. Clin Orthop Relat Res, (253):197-202.

Baykal D, Irrechukwu O, Lin PC, Fritton K, Spencer RG, Pleshko N. 2010. Nondestructive assessment of engineered cartilage constructs using near-infrared spectroscopy. Appl Spectrosc, 64 (10) (10):1160-1166.

Behrens P, Bosch U, Bruns J, Erggelet C, Esenwein SA, Gaissmaier C, Krackhardt T, Lohnert J, Marlovits S, Meenen NM, Mollenhauer J, Nehrer S, Niethard FU, Noth U, Perka C, Richter W, Schafer D, Schneider U, Steinwachs M, Weise K. 2004. [Indications and implementation of recommendations of the working group "Tissue Regeneration and Tissue Substitutes" for autologous chondrocyte transplantation (ACT)]. Z Orthop Ihre Grenzgeb, 142 (5):529-539.

Benninghoff A. 1925. Form und Bau der Gelenkknorpel in ihren Beziehungen zur Funktion. Zeitschrift für Zellforschung und mikroskopische Anatomie, 2 (5):783-862.

Bentley G, Biant LC, Carrington RW, Akmal M, Goldberg A, Williams AM, Skinner JA, Pringle J. 2003. A prospective, randomised comparison of autologous chondrocyte implantation versus mosaicplasty for osteochondral defects in the knee. J Bone Joint Surg Br, 85 (2):223-230.

Bobic V. 1996. Arthroscopic osteochondral autograft transplantation in anterior cruciate ligament reconstruction: a preliminary clinical study. Knee Surg Sports Traumatol Arthrosc, 3 (4):262-264.

Bodin A, Concaro S, Brittberg M, Gatenholm P. 2007. Bacterial cellulose as a potential meniscus implant. J Tissue Eng Regen Med, 1 (5):406-408.

Brittberg M, Peterson L, Sjogren-Jansson E, Tallheden T, Lindahl A. 2003. Articular cartilage engineering with autologous chondrocyte transplantation. A review of recent developments. J Bone Joint Surg Am, 85-A Suppl 3:109-115.

Brittberg M, Lindahl A, Nilsson A, Ohlsson C, Isaksson O, Peterson L. 1994. Treatment of deep cartilage defects in the knee with autologous chondrocyte transplantation. N Engl J Med, 331 (14):889-895.

Brown A. 1886a. The chemical action of pure cultivation of Bacterium aceti. J Chem Soc, 49:432-439.

Brown AJ. 1886b. XLIII.—On an acetic ferment which forms cellulose. Journal of the Chemical Society, Transactions, 49:432-439.

Buchner E, Brauer R, Schmidt C, Emmrich F, Kinne RW. 1995. Induction of flare-up reactions in rat antigen-induced arthritis. J Autoimmun, 8 (8) (1):61-74.

Buckwalter J, Mankin H. 1998. Articular cartilage: degeneration and osteoarthritis, repair, regeneration, and transplantation. Instructional course lectures, 47:487-504.

Buckwalter JA. 2002. Articular cartilage injuries. Clin Orthop Relat Res, (402):21-37.

Buckwalter JA, Lohmander S. 1994. Operative treatment of osteoarthrosis. Current practice and future development. J Bone Joint Surg Am, 76 (9):1405-1418.

Bullough P, Goodfellow J. 1968. The significance of the fine structure of articular cartilage. J Bone Joint Surg Br, 50 (4):852-857.

Bungartz M, Maenz S, Kunisch E, Horbert V, Xin L, Gunnella F, Mika J, Borowski J, Bischoff S, Schubert H, Sachse A, Illerhaus B, Gunster J, Bossert J, Jandt KD, Kinne RW, Brinkmann O. 2016. First-time systematic postoperative clinical assessment of a minimally invasive approach for lumbar ventrolateral vertebroplasty in the large animal model sheep. Spine J, 16 (10):1263-1275.

Burkart A, Schoettle PB, Imhoff A. 2001. Surgical therapeutic possibilities of cartilage damage. Der Unfallchirurg, 104 (9):798-807.

Cake MA, Appleyard RC, Read RA, Ghosh P, Swain MV, Murrell GC. 2003. Topical administration of the nitric oxide donor glyceryl trinitrate modifies the structural and biomechanical properties of ovine articular cartilage. Osteoarthritis Cartilage, 11 (12):872-878.

Carpenter AE, Jones TR, Lamprecht MR, Clarke C, Kang IH, Friman O, Guertin DA, Chang JH, Lindquist RA, Moffat J, Golland P, Sabatini DM. 2006. CellProfiler: image analysis software for identifying and quantifying cell phenotypes. Genome Biol, 7 (10):R100.

Chami G, Ward J, Wills D, Phillips R, Sherman K. 2006. Smart tool for force measurements during knee arthroscopy: in vivo human study. Stud Health Technol Inform, 119:85-89.

Chandrasekhar S, Esterman MA, Hoffman HA. 1987. Microdetermination of proteoglycans and glycosaminoglycans in the presence of guanidine hydrochloride. Anal Biochem, 161 (1):103-108.

Convery FR, Akeson WH, Keown GH. 1972. The repair of large osteochondral defects. An experimental study in horses. Clin Orthop Relat Res, 82:253-262.

Darling EM, Athanasiou KA. 2005. Rapid phenotypic changes in passaged articular chondrocyte subpopulations. Journal of Orthopaedic Research, 23 (2):425-432. Dell'Accio F, De Bari C, El Tawil NM, Barone F, Mitsiadis TA, O'Dowd J, Pitzalis C. 2006. Activation of WNT and BMP signaling in adult human articular cartilage following mechanical injury. Arthritis Res Ther, 8 (5):R139.

Dewan AK, Gibson MA, Elisseeff JH, Trice ME. 2014. Evolution of autologous chondrocyte repair and comparison to other cartilage repair techniques. Biomed Res Int, 2014:272481.

Dunzel A, Rudiger T, Pretzel D, Kopsch V, Endres M, Kaps C, Fohr P, Burgkart RH, Linss S, Kinne RW. 2013. [The bovine cartilage punch model: a tool for the in vitro analysis of biomaterials and cartilage regeneration]. Orthopade, 42 (4):254-261.

Efe T, Theisen C, Fuchs-Winkelmann S, Stein T, Getgood A, Rominger MB, Paletta JR, Schofer MD. 2012. Cell-free collagen type I matrix for repair of cartilage defects-clinical and magnetic resonance imaging results. Knee Surg Sports Traumatol Arthrosc, 20 (10):1915-1922.

Enders JT, Otto TJ, Peters HC, Wu J, Hardouin S, Moed BR, Zhang Z. 2009. A model for studying human articular cartilage integration in vitro. J Biomed Mater Res A, 94 (2):509-514.

Endres M, Neumann K, Schroder SE, Vetterlein S, Morawietz L, Ringe J, Sittinger M, Kaps C. 2007. Human polymer-based cartilage grafts for the regeneration of articular cartilage defects. Tissue Cell, 39 (5):293-301.

Endres M, Neumann K, Zhou B, Freymann U, Pretzel D, Stoffel M, Kinne RW, Kaps C. 2012. An ovine in vitro model for chondrocyte-based scaffold-assisted cartilage grafts. J Orthop Surg Res, 7:37.

Erggelet C, Browne J, Fu F, Mandelbaum B, Micheli L, Mosely J. 2000. Autologous chondrocyte transplantation for treatment of cartilage defects of the knee joint. Clinical results. Zentralblatt fur Chirurgie, 125 (6):516-522.

Erggelet C, Endres M, Neumann K, Morawietz L, Ringe J, Haberstroh K, Sittinger M, Kaps C. 2009. Formation of cartilage repair tissue in articular cartilage defects pretreated with microfracture and covered with cell-free polymer-based implants. J Orthop Res, 27 (10):1353-1360.

Evans BR, O'Neill HM, Greenbaum E. 2005. Electron Transfer by Enzymes and Photosynthetic Proteins Immobilized in Polysaccharide Composites.

Farndale RW, Buttle DJ, Barrett AJ. 1986. Improved quantitation and discrimination of sulphated glycosaminoglycans by use of dimethylmethylene blue. Biochim Biophys Acta, 883 (2):173-177.

Feldmann EM, Sundberg JF, Bobbili B, Schwarz S, Gatenholm P, Rotter N. 2013. Description of a novel approach to engineer cartilage with porous bacterial nanocellulose for reconstruction of a human auricle. J Biomater Appl, 28 (4):626-640.

Furukawa T, Eyre DR, Koide S, Glimcher MJ. 1980. Biochemical studies on repair cartilage resurfacing experimental defects in the rabbit knee. J Bone Joint Surg Am, 62 (1):79-89.

Gaissmaier C, Fritz J, Benz K, Stoop R, Schewe B, Weise K. 2003. Biomaterialien für die Transplantation chondrogener Zellen zur biologischen Rekonstruktion artikulärer Knorpeldefekte. SFA-Arthroskopie aktuell, 16:4-14.

Gama M, Gatenholm P, Klemm D. 2012. Bacterial nanocellulose: a sophisticated multifunctional material. CRC Press.

Gavenis K, Schmidt-Rohlfing B, Mueller-Rath R, Andereya S, Schneider U. 2006. In vitro comparison of six different matrix systems for the cultivation of human chondrocytes. In Vitro Cell Dev Biol Anim, 42 (5-6):159-167.

Gavenis K, Heussen N, Hofman M, Andereya S, Schneider U, Schmidt-Rohlfing B. 2014. Cell-free repair of small cartilage defects in the Goettinger minipig: the effects of BMP-7 continuously released by poly(lactic-co-glycolid acid) microspheres. J Biomater Appl, 28 (7):1008-1015.

Gavenis K, Schneider U, Maus U, Mumme T, Muller-Rath R, Schmidt-Rohlfing B, Andereya S. 2012. Cell-free repair of small cartilage defects in the Goettinger minipig: which defect size is possible? Knee Surg Sports Traumatol Arthrosc, 20 (11):2307-2314.

Gillogly SD, Wheeler KS. 2015. Autologous Chondrocyte Implantation With Collagen Membrane. Sports Med Arthrosc, 23 (3):118-124.

Gobbi A, Chaurasia S, Karnatzikos G, Nakamura N. 2015. Matrix-Induced Autologous Chondrocyte Implantation versus Multipotent Stem Cells for the Treatment of Large Patellofemoral Chondral Lesions: A Nonrandomized Prospective Trial. Cartilage, 6 (2):82-97.

Gomoll AH, Farr J, Gillogly SD, Kercher J, Minas T. 2010. Surgical management of articular cartilage defects of the knee. J Bone Joint Surg Am, 92 (14):2470-2490.

Haaland DM, Thomas EV. 1988. Partial least-squares methods for spectral analyses. 1. Relation to other quantitative calibration methods and the extraction of qualitative information. Anal Chem, 60 (11) (11):1193-1202.

Haddo O, Mahroof S, Higgs D, David L, Pringle J, Bayliss M, Cannon SR, Briggs TW. 2004. The use of chondrogide membrane in autologous chondrocyte implantation. Knee, 11 (1):51-55.

Haggart GE. 1947. Surgical treatment of degenerative arthritis of the knee joint. N Engl J Med, 236 (26):971-973.

Haigler CH, White AR, Brown RM, Cooper KM. 1982. Alteration of in vivo cellulose ribbon assembly by carboxymethylcellulose and other cellulose derivatives. The Journal of cell biology, 94 (1):64-69.

Halbwirth F, Niculescu-Morzsa E, Zwickl H, Bauer C, Nehrer S. 2015. Mechanostimulation changes the catabolic phenotype of human dedifferentiated osteoarthritic chondrocytes. Knee Surg Sports Traumatol Arthrosc, 23 (1):104-111.

Hangody L, Karpati Z, Szerb I, Eberhard R. 1996. Autologous osteochondral mosaic like graft technique for replacing weight bearing cartilage defects. ESSKA, 96:10-15.

Henderson I, Francisco R, Oakes B, Cameron J. 2005. Autologous chondrocyte implantation for treatment of focal chondral defects of the knee—a clinical, arthroscopic, MRI and histologic evaluation at 2 years. The Knee, 12 (3):209-216.

Heßler N. 2008. Bakterielle Nanocellulose: Struktur-und Formdesign während der Biosynthese.

Hestrin S, Schramm M. 1954. Synthesis of cellulose by Acetobacter xylinum. 2. Preparation of freeze-dried cells capable of polymerizing glucose to cellulose. Biochemical Journal, 58 (2):345.

Hoffmann M, Lange M, Reuter T, Meuche F, Plettenberg HKW. 2010. Measuring system to study the biomechanical and spectral behaviourn of cartilage. 18-19 May, 15 ITG/GMA Fachtagung, Nuernberg, Germany.

Hoffmann M, Lange M, Meuche F, Reuter T, Plettenberg HKW, Spahn G, Ponomarev I. 2012 Comparison of Optical and Biomechanical Properties of Native and Artificial Equine Joint Cartilage under Load using NIR Spectroscopy. Biomed Tech, Berlin, 57 (Suppl. 1):1059-1061.

Horbert V, Xin L, Foehr P, Brinkmann O, Bungartz M, Burgkart RH, Graeve T, Kinne RW. 2018. In Vitro Analysis of Cartilage Regeneration Using a Collagen Type I Hydrogel (CaReS) in the Bovine Cartilage Punch Model. Cartilage:1947603518756985.

Hunter CJ, Levenston ME. 2004. Maturation and integration of tissue-engineered cartilages within an in vitro defect repair model. Tissue Eng, 10 (5-6):736-746.

Hunziker EB. 2002. Articular cartilage repair: basic science and clinical progress. A review of the current status and prospects. Osteoarthritis Cartilage, 10 (6):432-463.

Imhoff AB, Ottl GM, Burkart A, Traub S. 1999. [Autologous osteochondral transplantation on various joints]. Orthopade, 28 (1):33-44.

Iwasa J, Engebretsen L, Shima Y, Ochi M. 2009. Clinical application of scaffolds for cartilage tissue engineering. Knee Surgery, Sports Traumatology, Arthroscopy, 17 (6):561-577.

Jeyakumar V, Halbwirth F, Niculescu-Morzsa E, Bauer C, Zwickl H, Kern D, Nehrer S. 2017. Chondrogenic Gene Expression Differences between Chondrocytes from Osteoarthritic and Non-OA Trauma Joints in a 3D Collagen Type I Hydrogel. Cartilage, 8 (2):191-198.

Johnson LL. 1986. Arthroscopic abrasion arthroplasty historical and pathologic perspective: present status. Arthroscopy, 2 (1):54-69.

Jonas R, Farah LF. 1998. Production and application of microbial cellulose. Polymer Degradation and Stability, 59 (1-3):101-106.

Jurvelin JS, Rasanen T, Kolmonen P, Lyyra T. 1995. Comparison of optical, needle probe and ultrasonic techniques for the measurement of articular cartilage thickness. J Biomech, 28 (2):231-235.

Kaps C, Frauenschuh S, Endres M, Ringe J, Haisch A, Lauber J, Buer J, Krenn V, Haupl T, Burmester GR, Sittinger M. 2006. Gene expression profiling of human articular cartilage grafts generated by tissue engineering. Biomaterials, 27 (19):3617-3630.

Kempson GE, Muir H, Pollard C, Tuke M. 1973. The tensile properties of the cartilage of human femoral condyles related to the content of collagen and glycosaminoglycans. Biochim Biophys Acta, 297 (2):456-472.

Khan IM, Gilbert SJ, Singhrao SK, Duance VC, Archer CW. 2008. Cartilage integration: evaluation of the reasons for failure of integration during cartilage repair. A review. Eur Cell Mater, 16:26-39.

Kim HK, Moran ME, Salter RB. 1991. The potential for regeneration of articular cartilage in defects created by chondral shaving and subchondral abrasion. An experimental investigation in rabbits. J Bone Joint Surg Am, 73 (9):1301-1315.

Klemm D, Schumann D, Udhardt U, Marsch S. 2001. Bacterial synthesized cellulose — artificial blood vessels for microsurgery. Progress in Polymer Science, 26 (9):1561-1603.

Klemm D, Schumann D, Kramer F, Heßler N, Hornung M, Schmauder H-P, Marsch S. 2006. Nanocelluloses as innovative polymers in research and application. Polysaccharides Ii. Springer, 49-96.

Klemm D, Kramer F, Moritz S, Lindstrom T, Ankerfors M, Gray D, Dorris A. 2011. Nanocelluloses: a new family of nature-based materials. Angew Chem Int Ed Engl, 50 (24):5438-5466.

Knutsen G, Drogset JO, Engebretsen L, Grontvedt T, Isaksen V, Ludvigsen TC, Roberts S, Solheim E, Strand T, Johansen O. 2007. A randomized trial comparing autologous chondrocyte implantation with microfracture. Findings at five years. J Bone Joint Surg Am, 89 (10):2105-2112.

Kon E, Verdonk P, Condello V, Delcogliano M, Dhollander A, Filardo G, Pignotti E, Marcacci M. 2009. Matrix-assisted autologous chondrocyte transplantation for the repair of cartilage defects of the knee: systematic clinical data review and study quality analysis. Am J Sports Med, 37 Suppl 1:156S-166S.

Kopsch V, Kroker A, Plettenberg HKW, Bischoff S, Pietsch S, Kinne RW. Topografische Charakterisierung der Knorpeleigenschaften der medialen Femurkondyle im

Großtiermodell Schaf mittels Nahinfrarotspektroskopie (NIRS). AGA 2013, 19-21 September, Wiesbaden, Germany.

Korkala OL. 1988. Periosteal primary resurfacing of joint surface defects of the patella due to injury. Injury, 19 (3):216-218.

Kowalska-Ludwicka K, Cala J, Grobelski B, Sygut D, Jesionek-Kupnicka D, Kolodziejczyk M, Bielecki S, Pasieka Z. 2013. Modified bacterial cellulose tubes for regeneration of damaged peripheral nerves. Arch Med Sci, 9 (3):527-534.

Kramer F. 2008. Bakterielle Nanocellulose und Nanocellulosekomposite für die Entwicklung geformter Biomaterialien.

Kreuz PC, Müller S, Ossendorf C, Kaps C, Erggelet C. 2009. Treatment of focal degenerative cartilage defects with polymer-based autologous chondrocyte grafts: four-year clinical results. Arthritis research & therapy, 11 (2):R33.

Kuettner KE. 1992. Biochemistry of articular cartilage in health and disease. Clinical biochemistry, 25 (3):155-163.

Kunisch E, Maenz S, Knoblich M, Ploeger F, Jandt KD, Bossert J, Kinne RW, Alsalameh S. 2017. Short-time pre-washing of brushite-forming calcium phosphate cement improves its in vitro cytocompatibility. Tissue Cell, 49 (6):697-710.

Lang N, Merkel E, Fuchs F, Schumann D, Klemm D, Kramer F, Mayer-Wagner S, Schroeder C, Freudenthal F, Netz H, Kozlik-Feldmann R, Sigler M. 2015. Bacterial nanocellulose as a new patch material for closure of ventricular septal defects in a pig model. Eur J Cardiothorac Surg, 47 (6):1013-1021.

Lopes J, Machado J, Castanheira L, Granja P, Gama F, Dourado F, Gomes J. 2011. Friction and wear behaviour of bacterial cellulose against articular cartilage. Wear, 271 (9-10):2328-2333.

Lotz MK, Kraus VB. 2010. New developments in osteoarthritis. Posttraumatic osteoarthritis: pathogenesis and pharmacological treatment options. Arthritis Res Ther, 12 (3):211.

Lotz MK, Otsuki S, Grogan SP, Sah R, Terkeltaub R, D'Lima D. 2010. Cartilage cell clusters. Arthritis Rheum, 62 (8):2206-2218.

Madry H, Pape D. 2008. [Autologous chondrocyte transplantation]. Orthopade, 37 (8):756-763.

Madry H, Zurakowski D, Trippel SB. 2001. Overexpression of human insulin-like growth factor-I promotes new tissue formation in an ex vivo model of articular chondrocyte transplantation. Gene Ther, 8 (19):1443-1449.

Madry H, Grun UW, Knutsen G. 2011. Cartilage repair and joint preservation: medical and surgical treatment options. Dtsch Arztebl Int, 108 (40):669-677.

Maenz S, Kunisch E, Muhlstadt M, Bohm A, Kopsch V, Bossert J, Kinne RW, Jandt KD. 2014. Enhanced mechanical properties of a novel, injectable, fiber-reinforced brushite cement. J Mech Behav Biomed Mater, 39:328-338.

Maenz S, Hennig M, Muhlstadt M, Kunisch E, Bungartz M, Brinkmann O, Bossert J, Kinne RW, Jandt KD. 2016. Effects of oxygen plasma treatment on interfacial shear strength and post-peak residual strength of a PLGA fiber-reinforced brushite cement. J Mech Behav Biomed Mater, 57:347-358.

Maenz S, Brinkmann O, Kunisch E, Horbert V, Gunnella F, Bischoff S, Schubert H, Sachse A, Xin L, Gunster J, Illerhaus B, Jandt KD, Bossert J, Kinne RW, Bungartz M. 2017. Enhanced bone formation in sheep vertebral bodies after minimally invasive treatment with a novel, PLGA fiber-reinforced brushite cement. Spine J, 17 (5):709-719.

Magnuson PB. 1974. The classic: Joint debridement: surgical treatment of degenerative arthritis. Clin Orthop Relat Res, (101):4-12.

Manfredini M, Zerbinati F, Gildone A, Faccini R. 2007. Autologous chondrocyte implantation: a comparison between an open periosteal-covered and an arthroscopic matrix-guided technique. Acta Orthopaedica Belgica, 73 (2):207.

Mankin HJ. 1982. The response of articular cartilage to mechanical injury. J Bone Joint Surg Am, 64 (3):460-466.

Markstedt K, Mantas A, Tournier I, Martinez Avila H, Hagg D, Gatenholm P. 2015. 3D Bioprinting Human Chondrocytes with Nanocellulose-Alginate Bioink for Cartilage Tissue Engineering Applications. Biomacromolecules, 16 (5):1489-1496.

Martinez H, Brackmann C, Enejder A, Gatenholm P. 2012. Mechanical stimulation of fibroblasts in micro-channeled bacterial cellulose scaffolds enhances production of oriented collagen fibers. J Biomed Mater Res A, 100 (4):948-957.

Matthews LS, Hirsch C. 1972. Temperatures measured in human cortical bone when drilling. J Bone Joint Surg Am, 54 (2):297-308.

Maus U, Schneider U, Gravius S, Muller-Rath R, Mumme T, Miltner O, Bauer D, Niedhart C, Andereya S. 2008. [Clinical results after three years use of matrix-associated ACT for the treatment of osteochondral defects of the knee]. Z Orthop Unfall, 146 (1):31-37.

Meachim G, Roberts C. 1971. Repair of the joint surface from subarticular tissue in the rabbit knee. J Anat, 109 (Pt 2):317-327.

Messner K, Maletius W. 1996. The long-term prognosis for severe damage to weight-bearing cartilage in the knee: a 14-year clinical and radiographic follow-up in 28 young athletes. Acta Orthop Scand, 67 (2):165-168.

Micheli LJ, Browne JE, Erggelet C, Fu F, Mandelbaum B, Moseley JB, Zurakowski D. 2001. Autologous chondrocyte implantation of the knee: multicenter experience and minimum 3-year follow-up. Clin J Sport Med, 11 (4):223-228.

Mika J, Clanton TO, Ambrose CG, Kinne RW. 2017. Surgical Preparation for Articular Cartilage Regeneration in the Osteoarthritic Knee Joint. Cartilage, 8 (4):365-368.

Mika J, Clanton TO, Pretzel D, Schneider G, Ambrose CG, Kinne RW. 2011. Surgical preparation for articular cartilage regeneration without penetration of the subchondral bone plate: in vitro and in vivo studies in humans and sheep. Am J Sports Med, 39 (3):624-631.

Minas T. 1998. Chondrocyte implantation in the repair of chondral lesions of the knee: economics and quality of life. Am J Orthop (Belle Mead NJ), 27 (11):739-744.

Mitchell N, Shepard N. 1987. Effect of patellar shaving in the rabbit. J Orthop Res, 5 (3):388-392.

Mithoefer K, Williams RJ, 3rd, Warren RF, Potter HG, Spock CR, Jones EC, Wickiewicz TL, Marx RG. 2005. The microfracture technique for the treatment of articular cartilage lesions in the knee. A prospective cohort study. J Bone Joint Surg Am, 87 (9):1911-1920.

Mollenhauer J, Aurich M. 2003. Grundlegendes zum Gelenkknorpel. Praxisleitfaden der Knorpelreparatur. Springer, 3-10.

Morales TI. 2007. Chondrocyte moves: clever strategies? Osteoarthritis Cartilage, 15 (8):861-871.

Moretti M, Wendt D, Schaefer D, Jakob M, Hunziker EB, Heberer M, Martin I. 2005. Structural characterization and reliable biomechanical assessment of integrative cartilage repair. J Biomech, 38 (9):1846-1854.

Moritz S, Wiegand C, Wesarg F, Hessler N, Muller FA, Kralisch D, Hipler UC, Fischer D. 2014. Active wound dressings based on bacterial nanocellulose as drug delivery system for octenidine. Int J Pharm, 471 (1-2):45-55.

Moseley JB, Jr., Anderson AF, Browne JE, Mandelbaum BR, Micheli LJ, Fu F, Erggelet C. 2010. Long-term durability of autologous chondrocyte implantation: a multicenter, observational study in US patients. Am J Sports Med, 38 (2):238-246.

Muller FA, Muller L, Hofmann I, Greil P, Wenzel MM, Staudenmaier R. 2006. Cellulose-based scaffold materials for cartilage tissue engineering. Biomaterials, 27 (21):3955-3963.

Musumeci G, Castrogiovanni P, Leonardi R, Trovato FM, Szychlinska MA, Di Giunta A, Loreto C, Castorina S. 2014. New perspectives for articular cartilage repair treatment through tissue engineering: A contemporary review. World J Orthop, 5 (2):80-88.

Nakayama A, Kakugo A, Gong JP, Osada Y, Takai M, Erata T, Kawano S. 2004. High mechanical strength double-network hydrogel with bacterial cellulose. Advanced Functional Materials, 14 (11):1124-1128.

Napavichayanun S, Yamdech R, Aramwit P. 2016. The safety and efficacy of bacterial nanocellulose wound dressing incorporating sericin and polyhexamethylene biguanide: in vitro, in vivo and clinical studies. Arch Dermatol Res, 308 (2):123-132.

Nehrer S, Domayer S, Dorotka R, Schatz K, Bindreiter U, Kotz R. 2006. Three-year clinical outcome after chondrocyte transplantation using a hyaluronan matrix for cartilage repair. European journal of radiology, 57 (1):3-8.

Newman AP. 1998. Articular cartilage repair. Am J Sports Med, 26 (2):309-324.

Niemeyer P, Kostler W, Salzmann GM, Lenz P, Kreuz PC, Sudkamp NP. 2010. Autologous chondrocyte implantation for treatment of focal cartilage defects in patients age 40 years and older: A matched-pair analysis with 2-year follow-up. Am J Sports Med, 38 (12):2410-2416.

Niemeyer P, Andereya S, Angele P, Ateschrang A, Aurich M, Baumann M, Behrens P, Bosch U, Erggelet C, Fickert S. 2013. Autologous chondrocyte implantation (ACI) for cartilage defects of the knee: a guideline by the working group" Tissue Regeneration" of the German Society of Orthopaedic Surgery and Traumatology (DGOU). Z Orthop Unfall, 151 (1):38-47.

Nieminen HJ, Toyras J, Laasanen MS, Jurvelin JS. 2006. Acoustic properties of articular cartilage under mechanical stress. Biorheology, 43 (3-4):523-535.

Nimeskern L, Martinez Avila H, Sundberg J, Gatenholm P, Muller R, Stok KS. 2013. Mechanical evaluation of bacterial nanocellulose as an implant material for ear cartilage replacement. J Mech Behav Biomed Mater, 22:12-21.

Norman AG, Dougherty WM, Chansky HA, Simonian PT, Sidles JA, Clark JM. 1999. A new technique for mapping articular cartilage contour and thickness. 1-4 February, 45th Annual Meeting of the Orthopaedic Research Society, Anaheim , CA, USA.

Noyes FR, Stabler CL. 1989. A system for grading articular cartilage lesions at arthroscopy. Am J Sports Med, 17 (4):505-513.

O'Driscoll SW, Fitzsimmons JS. 2001. The role of periosteum in cartilage repair. Clin Orthop Relat Res, (391 Suppl):S190-207.

Obradovic B, Martin I, Padera RF, Treppo S, Freed LE, Vunjak-Novakovic G. 2001. Integration of engineered cartilage. J Orthop Res, 19 (6):1089-1097.

Padalkar MV, Spencer RG, Pleshko N. 2013. Near infrared spectroscopic evaluation of water in hyaline cartilage. Ann Biomed Eng, 41 (11) (11):2426-2436.

Passler HH. 2000. [Microfracture for treatment of cartilage detects]. Zentralbl Chir, 125 (6):500-504.

Pastoureau P, Leduc S, Chomel A, De Ceuninck F. 2003. Quantitative assessment of articular cartilage and subchondral bone histology in the meniscectomized guinea pig model of osteoarthritis. Osteoarthritis Cartilage, 11 (6) (6):412-423.

Patrascu JM, Kruger JP, Boss HG, Ketzmar AK, Freymann U, Sittinger M, Notter M, Endres M, Kaps C. 2013. Polyglycolic acid-hyaluronan scaffolds loaded with bone marrow-derived mesenchymal stem cells show chondrogenic differentiation in vitro and cartilage repair in the rabbit model. J Biomed Mater Res B Appl Biomater, 101 (7):1310-1320.

Pepin SR, Wijdicks CA, Griffith CJ, Goerke U, Michaeli S, McNulty MA, Parker JB, Carlson CS, Ellermann J, LaPrade RF. 2009. Comparison of 7.0 Tesla MRI and Histology Measurments in Knee Articular Cartilage in an in vivo Canine Model. 22-25 February, 55th Annual Meeting of the Orthopaedic Research Society, Las Vegas, NV, USA.

Peterson L, Vasiliadis HS, Brittberg M, Lindahl A. 2010. Autologous chondrocyte implantation: a long-term follow-up. The American journal of sports medicine, 38 (6):1117-1124.

Peterson L, Brittberg M, Kiviranta I, Åkerlund EL, Lindahl A. 2002. Autologous chondrocyte transplantation: biomechanics and long-term durability. The American journal of sports medicine, 30 (1):2-12.

Peterson L, Minas T, Brittberg M, Nilsson A, Sjogren-Jansson E, Lindahl A. 2000. Two- to 9-year outcome after autologous chondrocyte transplantation of the knee. Clin Orthop Relat Res, (374):212-234.

Petri M, Broese M, Simon A, Liodakis E, Ettinger M, Guenther D, Zeichen J, Krettek C, Jagodzinski M, Haasper C. 2013. CaReS (MACT) versus microfracture in treating symptomatic patellofemoral cartilage defects: a retrospective matched-pair analysis. J Orthop Sci, 18 (1):38-44.

Pillai CK, Sharma CP. 2010. Review paper: absorbable polymeric surgical sutures: chemistry, production, properties, biodegradability, and performance. J Biomater Appl, 25 (4):291-366.

Plettenberg HKW. 2007. Entwicklung eines Messsystems zur Untersuchung arthrotischer Knorpelschäden mittels naher Infrarot-Spektroskopie für den Einsatz in der Arthroskopie: Technische Universitaet Ilmenau, Germany.

Poole AR, Kojima T, Yasuda T, Mwale F, Kobayashi M, Laverty S. 2001. Composition and structure of articular cartilage: a template for tissue repair. Clin Orthop Relat Res, (391 Suppl):S26-33.

Pretzel D, Pohlers D, Weinert S, Kinne RW. 2009. In vitro model for the analysis of synovial fibroblast-mediated degradation of intact cartilage. Arthritis Res Ther, 11 (1):R25.

Pretzel D, Linss S, Ahrem H, Endres M, Kaps C, Klemm D, Kinne RW. 2013. A novel in vitro bovine cartilage punch model for assessing the regeneration of focal cartilage defects with biocompatible bacterial nanocellulose. Arthritis Res Ther, 15 (3):R59.

Putz R. 2008. Aufbau und Funktion des Gelenkknorpels. Aktuelle Rheumatologie, 33 (01):22-28.

Ressler N, Ziauddin C, Vygantas W, K. K. 1976. Improved techniques for near-infrared study of water binding by globular proteins and intact tissues. Appl Spectrosc, 30:295–302.

Richter W, Diederichs S. 2009. Regenerative Medizin in der Orthopädie. Der Orthopäde, 38 (9):859-869.

Roemer FW, Eckstein F, Guermazi A. 2009. Magnetic resonance imaging-based semiquantitative and quantitative assessment in osteoarthritis. Rheum Dis Clin North Am, 35 (3) (3):521-555.

Rosen CL, Steinberg GK, DeMonte F, Delashaw JB, Jr., Lewis SB, Shaffrey ME, Aziz K, Hantel J, Marciano FF. 2011. Results of the prospective, randomized, multicenter clinical trial evaluating a biosynthesized cellulose graft for repair of dural defects. Neurosurgery, 69 (5):1093-1103; discussion 1103-1094.

Ruediger T, Dunzel A, Burgkart RH, Walter M, Kinne RW. 2013. Evaluation of the articular cartilage thickness - A comparative study of different animal models for cartilage repair and regeneration. 23-24 May, Biomat 2013, Weimar, Germany.

Ruettger A, Neumann S, Wiederanders B, Huber R. 2010. Comparison of different methods for preparation and characterization of total RNA from cartilage samples to uncover osteoarthritis in vivo. BMC Res Notes, 3:7.

Saska S, Teixeira LN, de Castro Raucci LMS, Scarel-Caminaga RM, Franchi LP, Dos Santos RA, Santagneli SH, Capela MV, de Oliveira PT, Takahashi CS, Gaspar AMM, Messaddeq Y, Ribeiro SJL, Marchetto R. 2017. Nanocellulose-collagen-apatite composite associated with osteogenic growth peptide for bone regeneration. Int J Biol Macromol, 103:467-476.

Schneider U, Schmidt-Rohlfing B, Gavenis K, Maus U, Mueller-Rath R, Andereya S. 2011a. A comparative study of 3 different cartilage repair techniques. Knee Surg Sports Traumatol Arthrosc, 19 (12):2145-2152.

Schneider U, Rackwitz L, Andereya S, Siebenlist S, Fensky F, Reichert J, Loer I, Barthel T, Rudert M, Noth U. 2011b. A prospective multicenter study on the outcome of type I collagen hydrogel-based autologous chondrocyte implantation (CaReS) for the repair of articular cartilage defects in the knee. Am J Sports Med, 39 (12):2558-2565.

Schramm M, Hestrin S. 1954a. Synthesis of cellulose by Acetobacter xylinum. 1. Micromethod for the determination of celluloses. Biochemical Journal, 56 (1):163.

Schramm M, Hestrin S. 1954b. Factors affecting production of cellulose at the air/liquid interface of a culture of Acetobacter xylinum. J Gen Microbiol, 11 (1):123-129.

Schramm M, Gromet Z, Hestrin S. 1957. Synthesis of cellulose by Acetobacter Xylinum. 3. Substrates and inhibitors. Biochemical Journal, 67 (4):669.

Schuettler KF, Struewer J, Rominger MB, Rexin P, Efe T. 2013. Repair of a chondral defect using a cell free scaffold in a young patient--a case report of successful scaffold transformation and colonisation. BMC Surg, 13:11.

Schumann DA, Wippermann J, Klemm DO, Kramer F, Koth D, Kosmehl H, Wahlers T, Salehi-Gelani S. 2009. Artificial vascular implants from bacterial cellulose: preliminary results of small arterial substitutes. Cellulose, 16 (5):877-885.

Schuttler KF, Schenker H, Theisen C, Schofer MD, Getgood A, Roessler PP, Struewer J, Rominger MB, Efe T. 2014. Use of cell-free collagen type I matrix implants for the treatment of small cartilage defects in the knee: clinical and magnetic resonance imaging evaluation. Knee Surg Sports Traumatol Arthrosc, 22 (6):1270-1276.

Secretan C, Bagnall KM, Jomha NM. 2010. Effects of introducing cultured human chondrocytes into a human articular cartilage explant model. Cell Tissue Res, 339 (2):421-427.

Seifert M. 2004. Modifizierung der Struktur von Bakteriencellulose durch die Zusammenstellung des Nährmediums bei der Kultivierung von Acetobacter xylinum [Dissertation]. Jena: Friedrichi1Schilleri1Universität.

Shapiro F, Koide S, Glimcher MJ. 1993. Cell origin and differentiation in the repair of full-thickness defects of articular cartilage. J Bone Joint Surg Am, 75 (4):532-553. Shepherd D, Seedhom B. 1999. Thickness of human articular cartilage in joints of the lower limb. Ann Rheum Dis, 58 (1) (1):27-34.

Sophia Fox AJ, Bedi A, Rodeo SA. 2009. The basic science of articular cartilage: structure, composition, and function. Sports Health, 1 (6):461-468.

Steadman JR, Rodkey WG, Singleton SB, Briggs KK. 1997. Microfracture technique forfull-thickness chondral defects: Technique and clinical results. Operative techniques in orthopaedics, 7 (4):300-304.

Steadman JR, Rodkey WG, Briggs KK, Rodrigo JJ. 1999. [The microfracture technic in the management of complete cartilage defects in the knee joint]. Orthopade, 28 (1):26-32.

Steinwachs M, Kreuz PC. 2007. Autologous chondrocyte implantation in chondral defects of the knee with a type I/III collagen membrane: a prospective study with a 3-year follow-up. Arthroscopy, 23 (4):381-387.

Steinwachs MR, Guggi T, Kreuz PC. 2008. Marrow stimulation techniques. Injury, 39 (1) (1):26-31.

Stockwell RA. 1979. Biology of cartilage cells. CUP Archive.

Stumpfe ST, Pester JK, Steinert S, Marintschev I, Plettenberg HKW, Aurich M, Hofmann GO. 2013. Is there a correlation between biophotonical, biochemical, histological, and visual changes in the cartilage of osteoarthritic knee-joints? Muscles Ligaments Tendons J, 3 (3):11157-11165.

Sugisaki M, Misawa A, Ikai A, Young-Sung K, Tanabe H. 2001. Sex differences in the hemoglobin oxygenation state of the resting healthy human masseter muscle. J Orofac Pain, 15 (4):320-328.

Suh JK, Youn I, Fu FH. 2001. An in situ calibration of an ultrasound transducer: a potential application for an ultrasonic indentation test of articular cartilage. J Biomech, 34 (10):1347-1353.

Svensson A, Nicklasson E, Harrah T, Panilaitis B, Kaplan DL, Brittberg M, Gatenholm P. 2005. Bacterial cellulose as a potential scaffold for tissue engineering of cartilage. Biomaterials, 26 (4):419-431.

Theodoropoulos JS, De Croos JN, Park SS, Pilliar R, Kandel RA. 2011. Integration of tissue-engineered cartilage with host cartilage: an in vitro model. Clin Orthop Relat Res, 469 (10):2785-2795.

Tiderius CJ, Jessel R, Kim YJ, Burstein D. 2007. Hip dGEMRIC in asymptomatic volunteers and patients with early osteoarthritis: the influence of timing after contrast injection. Magn Reson Med, 57 (4):803-805.

Vaquero J, Forriol F. 2012. Knee chondral injuries: clinical treatment strategies and experimental models. Injury, 43 (6):694-705.

Vinardell T, Thorpe SD, Buckley CT, Kelly DJ. 2009. Chondrogenesis and integration of mesenchymal stem cells within an in vitro cartilage defect repair model. Ann Biomed Eng, 37 (12):2556-2565.

Weise K, Krackhardt T, Gaissmaier C. 2000. Die operative Behandlung von Gelenkknorpeldefekten unter besonderer Berücksichtigung der autologen Knorpelzelltransplantation: Grundlagen-Ergebnisse-Ausblick. Op-Journal, 16 (02):150-159.

Welsch GH, Mamisch TC, Zak L, Blanke M, Olk A, Marlovits S, Trattnig S. 2010. Evaluation of cartilage repair tissue after matrix-associated autologous chondrocyte transplantation using a hyaluronic-based or a collagen-based scaffold with morphological MOCART scoring and biochemical T2 mapping: preliminary results. Am J Sports Med, 38 (5):934-942.

Wippermann J, Schumann D, Klemm D, Kosmehl H, Salehi-Gelani S, Wahlers T. 2009a. Preliminary Results of Small Arterial Substitute Performed with a New Cylindrical Biomaterial Composed of Bacterial Cellulose. European Journal of Vascular and Endovascular Surgery, 37 (5):592-596.

Wippermann J, Schumann D, Klemm D, Kosmehl H, Salehi-Gelani S, Wahlers T. 2009b. Preliminary results of small arterial substitute performed with a new cylindrical biomaterial composed of bacterial cellulose. Eur J Vasc Endovasc Surg, 37 (5):592-596.

Wirth CJ, Rudert M. 1996. Techniques of cartilage growth enhancement: a review of the literature. Arthroscopy, 12 (3):300-308.

Ye K, Di Bella C, Myers DE, Choong PF. 2014. The osteochondral dilemma: review of current management and future trends. ANZ J Surg, 84 (4):211-217.

Zheng YP, Niu HJ, Arthur Mak FT, Huang YP. 2005. Ultrasonic measurement of depth-dependent transient behaviors of articular cartilage under compression. J Biomech, 38 (9):1830-1837.

Zierbock S, Plettenberg H, Schmitt M, Liebold S, Hoffmann M, Popp J. 2012. NIR spectroscopic analyses of chemical osteoarthritic cartilage models. NIRNews, 23 (3):6-8.

Zscharnack M, Krause C, Aust G, Thummler C, Peinemann F, Keller T, Smink JJ, Holland H, Somerson JS, Knauer J, Schulz RM, Lehmann J. 2015. Preclinical good laboratory practice-compliant safety study to evaluate biodistribution and tumorigenicity of a cartilage advanced therapy medicinal product (ATMP). J Transl Med, 13:160.

Zwickl H, Niculescu-Morzsa E, Nehrer S. 2010. Investigation of Collagen Transplants Seeded with Human Autologous Chondrocytes at the Time of Transplantation. Cartilage, 1 (3):194-199.

Zwickl H, Niculescu-Morzsa E, Halbwirth F, Bauer C, Jeyakumar V, Reutterer A, Berger M, Nehrer S. 2016. Correlation Analysis of SOX9, -5, and -6 as well as COL2A1 and Aggrecan Gene Expression of Collagen I Implant-Derived and Osteoarthritic Chondrocytes. Cartilage, 7 (2):185-192.

8. Anhang

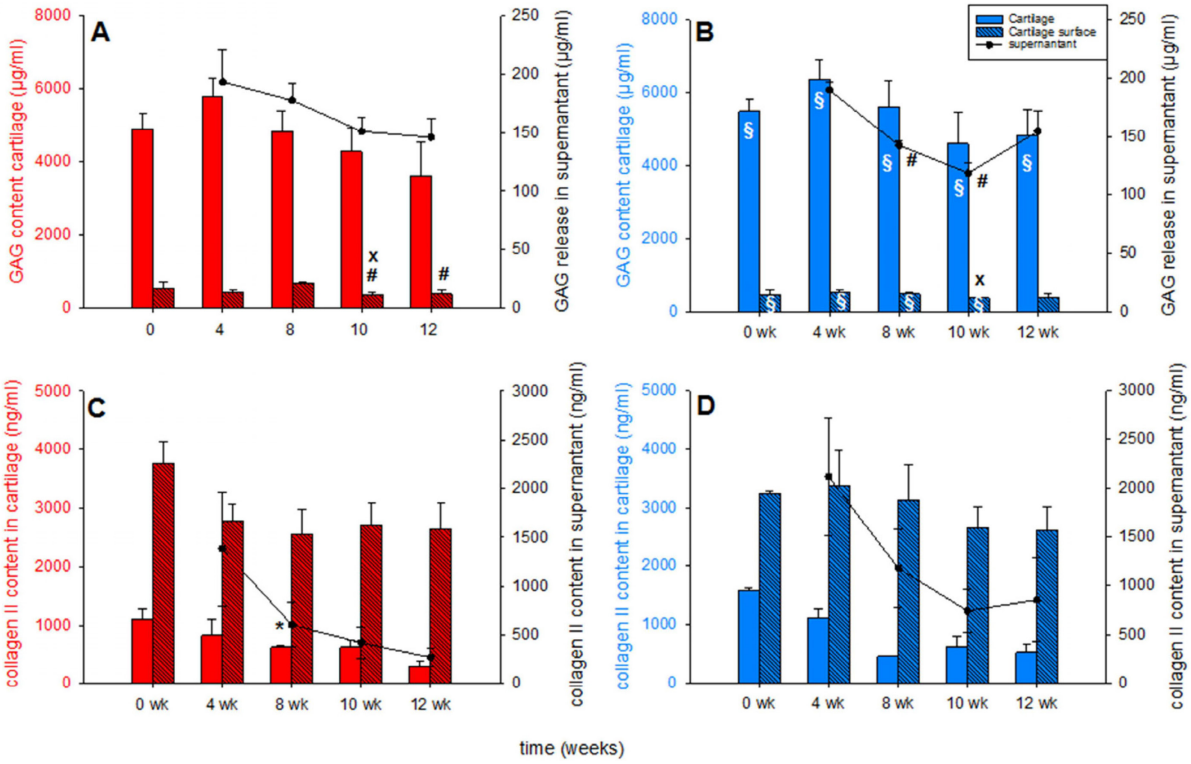

Suppl. Fig. 1: Quantitative analysis of proteoglycan content or release (DMB assay) or newly synthesized collagen 2 (ELISA) in cartilage-implant constructs (cell-free or cell-loaded implants). Proteoglycans (DMB assay) and newly synthesized collagen 2 (ELISA) were quantified in fresh and cultured 'host' cartilage matrix (cartilage), in cells located on the cartilage surface (cartilage surface), and in the culture supernatant (supernatant), when using cell-free collagen implants (A for proteoglycan; C for collagen 2) or cell-loaded collagen implants (B for proteoglycan; D for collagen 2); values are expressed as means ± SEM; symbols indicate $p \leq 0.05$ versus * 0 weeks; # 4 weeks; x 8 weeks; § versus cell-free.

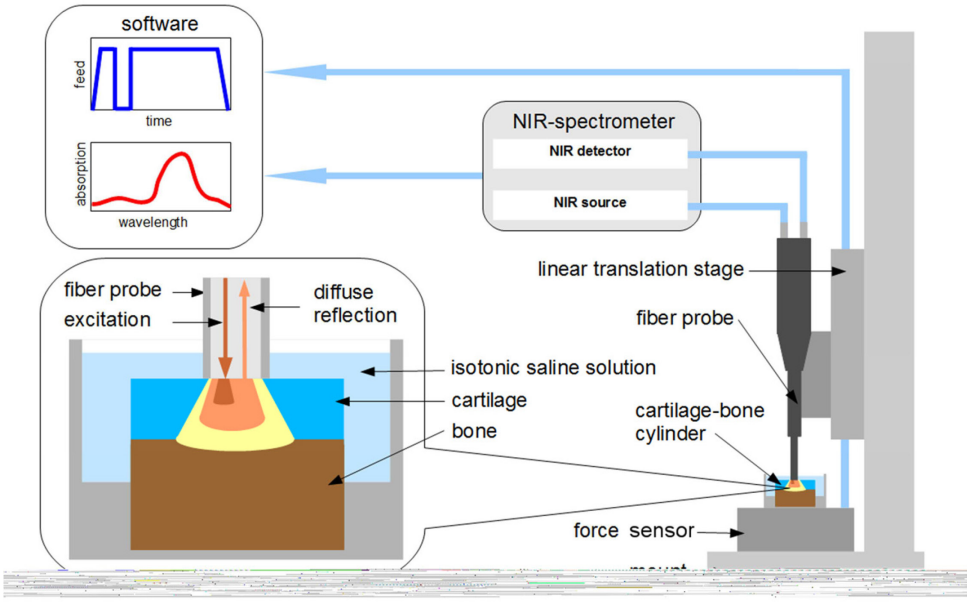

Suppl. Fig. 2: **Experimental setup.** NIRS-B was performed on the cartilage surface of the osteochondral cylinders in isotonic saline using a NIR-spectrometer, synchronized with a linear translation stage driving a 2 mm diameter fiber probe, and a force meter to measure the force caused by indentation.

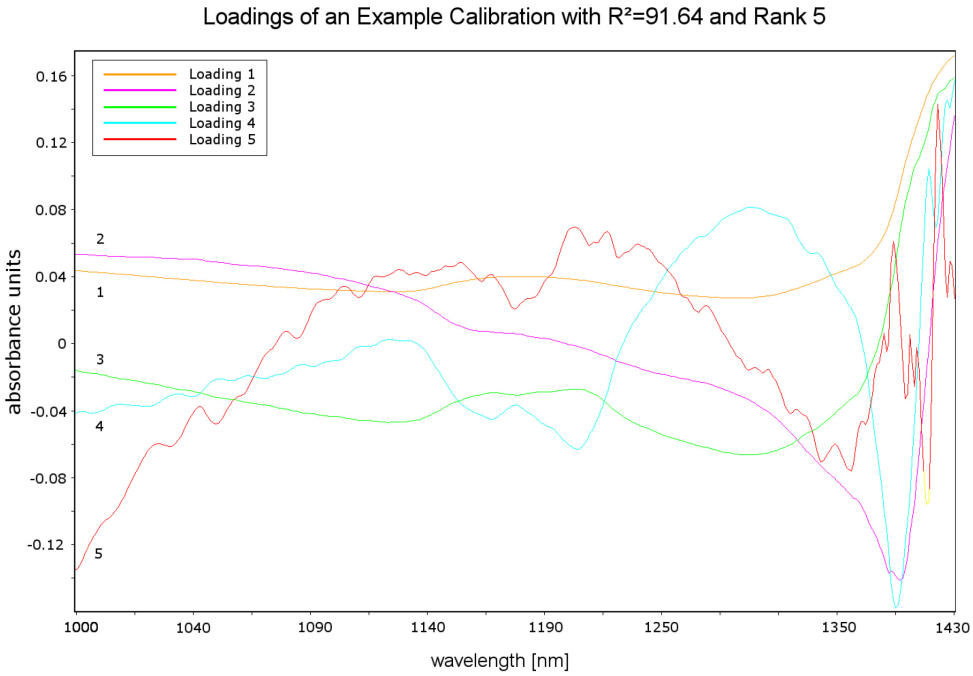

Suppl. Fig. 3: Exemplary depiction of the factors (loadings; n = 5; named 1 to 5) and factor weights (scores) of several principal components based on the factor analysis of one NIR spectra. The data matrix of the NIR spectra is fragmented into factors and scores (in this example with 5 factors and 40 spectra, i.e., a total of 200 scores) to develop Model 2s (smoothed) for NIRS-B thickness prediction based on needle indentation.

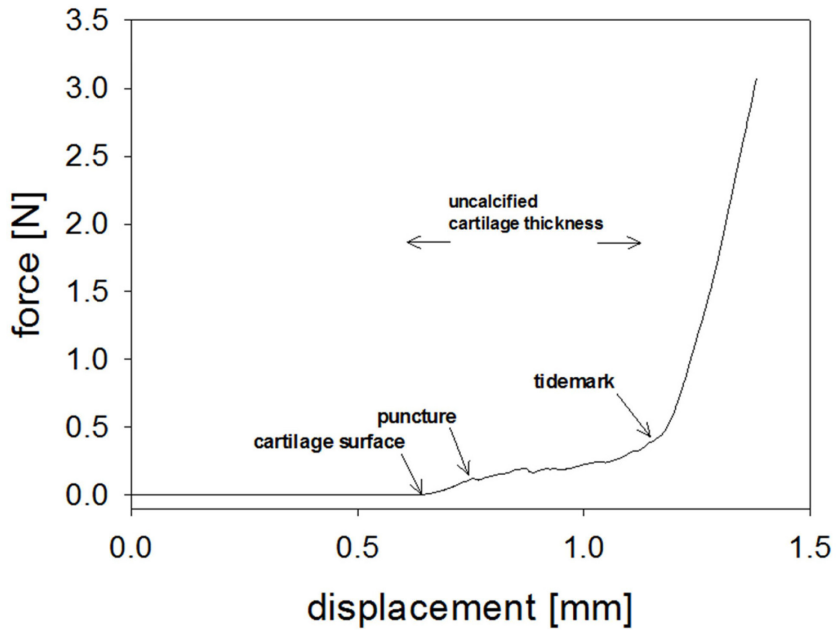

Suppl. Fig. 4: Determination of the cartilage thickness by the gold standard needle indentation. Force [N] – displacement [mm] curve used for the identification of the tidemark and the subsequent determination of the thickness of the uncalcified cartilage.

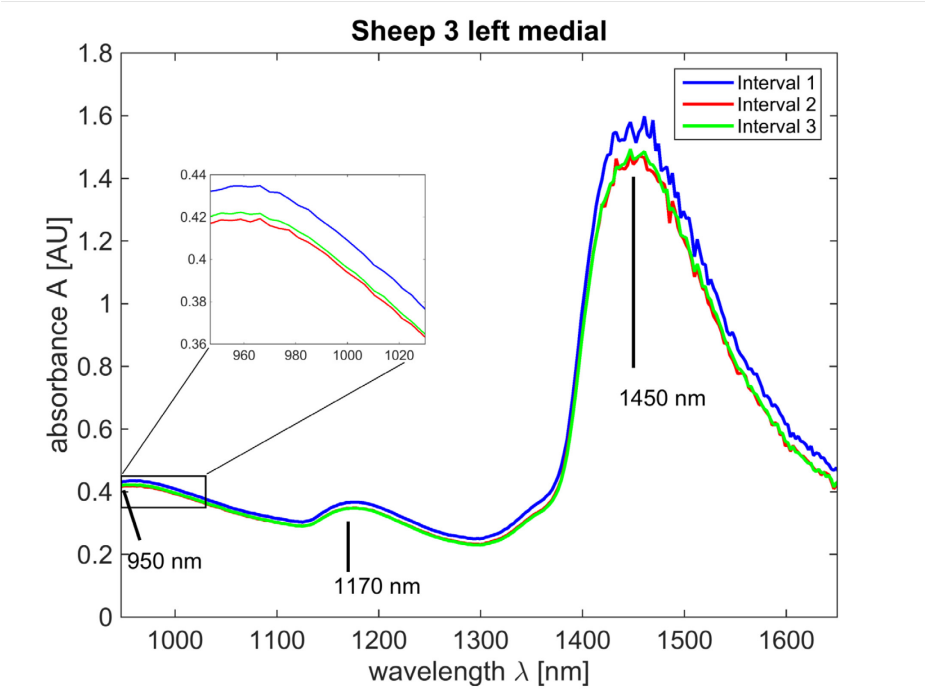

Suppl. Fig. 5: NIRS absorbance spectrum for the same location in the intervals 1 (minimal indentation), 2 (maximal indentation), and 3 (relaxation). The complete NIRS absorbance spectrum displays the characteristic wavelength pattern of cartilage with maxima at λ = 950 nm, λ = 1170 nm, and λ = 1450 nm (the insert shows a magnification of the spectra at 950 nm).

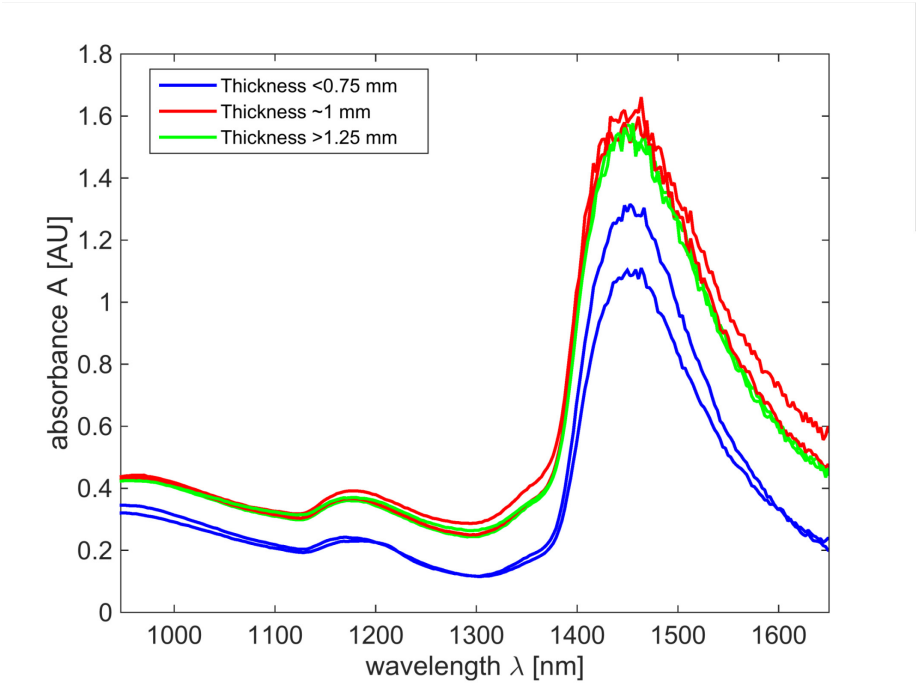

Suppl. Fig. 6: NIR spectra from cartilage samples of varying thickness (n = 6; three areas with different cartilage thickness)

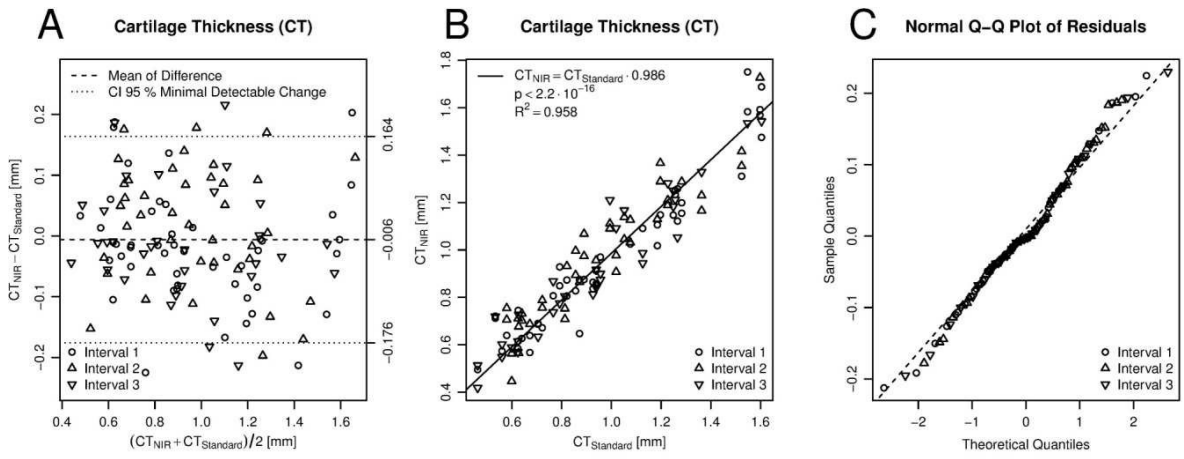

Suppl. Fig. 7: Independent linear analysis for repeated measures of the NIRS performance (model 4r; n = 120). (A) Confidence intervals close to the prediction accuracy of NIRS-B (approx. 0.17 mm); (B) highly significant, positive correlation between needle indentation and NIRS-B; (A-C) no significant indications for an offset of the values for the 2 methods from zero (B), for a significant inter-observer variability (B), or a deviation from a normal distribution (C).

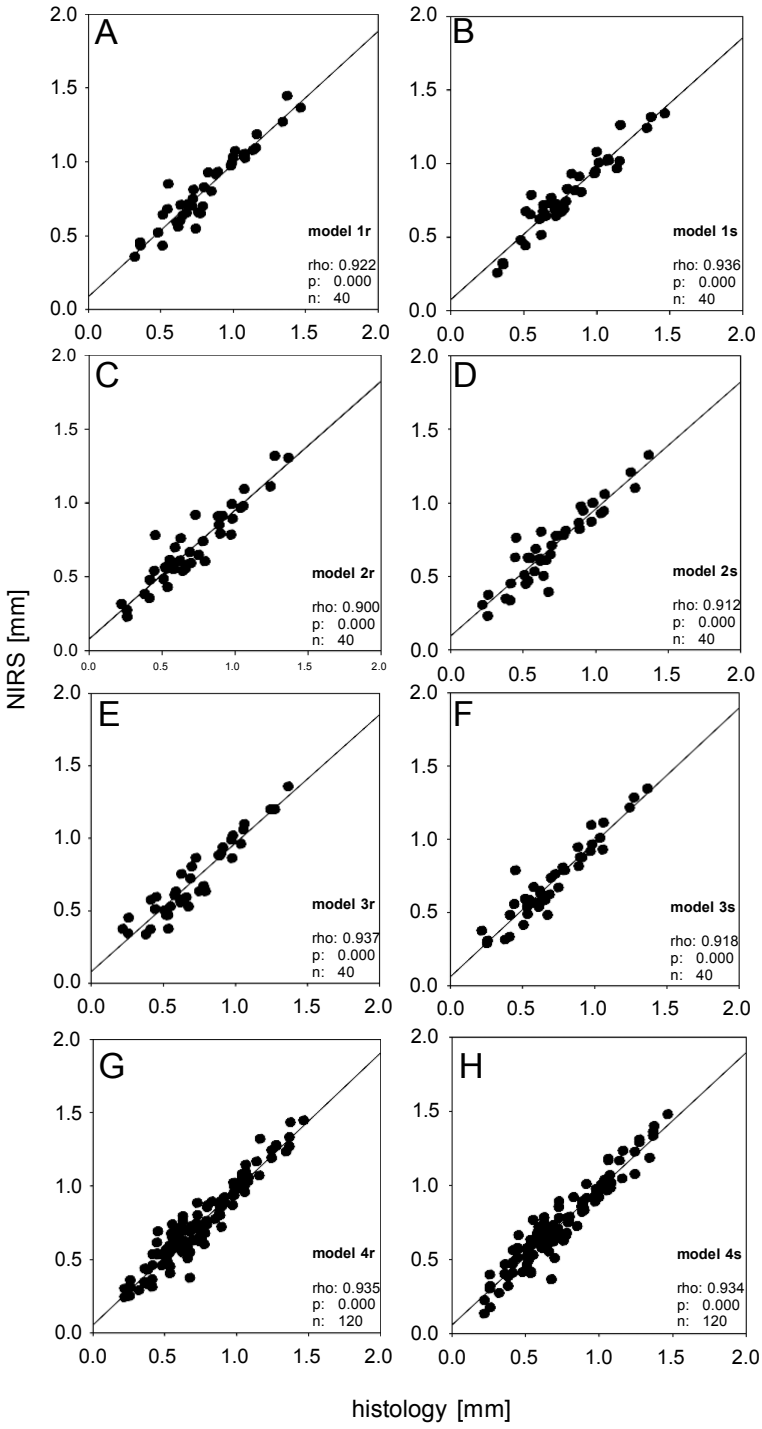

Suppl. Fig. 8: Correlations between the values obtained by NIRS and histology. Visual depiction of the correlations between the values obtained by NIRS and histology for the different prediction models (including rho, p, and n for each correlation; compare with Table 4).

Wissenschaftliche Veröffentlichungen

Fachzeitschriften (Peer-Reviewed, veröffentlicht)

1. A. Dunzel, T.Rüdiger, D.Pretzel, **V.Kopsch**, M.Endres, C.Kaps, R.H.Burgkart, S.Linß, R.W.Kinne. “The bovine cartilage punch model: a tool for the in vitro analysis of biomaterials and cartilage regeneration”. Orthopade. 2013 Apr ;42(4):254-61.

2. S.Maenz, E.Kunisch, M.Mühlstädt, A.Böhm, **V.Kopsch**, J.Bossert, R.W.Kinne, K.D.Jandt.” Enhanced mechanical properties of a novel, injectable, fiber-reinforced brushite cement.” J Mech Behav Biomed Mater. 2014 Nov;39:328-38.

3. M.Bungartz, S.Maenz, E.Kunisch, **V.Horbert**, L.Xin, F. Gunnella, J.Mika, J.Borowski, S.Bischoff, H.Schubert, A.Sachse, B.Illerhaus, J.Günster, J.Bossert, K.D.Jandt, R.W.Kinne, O.Brinkmann.“ First-time systematic postoperative clinical assessment of a minimally invasive approach for lumbar ventrolateral vertebroplasty in the large animal model sheep.“ Spine J. 2016 Oct;16(10):1263-1275.

4. L.Xin, M.Bungartz, S.Maenz, **V.Horbert**, M.Hennig, B.Illerhaus, J.Günster, J.Bossert, S.Bischoff, J.Borowski, H.Schubert, K.D.Jandt, E.Kunisch, R.W.Kinne, O.Brinkmann.“ Decreased extrusion of calcium phosphate cement versus high viscosity PMMA cement into spongious bone marrow-an ex vivo and in vivo study in sheep vertebrae.“ Spine J. 2016 Dec;16(12):1468-1477.

5. S.Maenz, O.Brinkmann, E.Kunisch, **V.Horbert**, F.Gunnella, S.Bischoff, H.Schubert, A.Sachse, L.Xin, J.Günster, B.Illerhaus, K.D.Jandt, J.Bossert, R.W.Kinne, M.Bungartz.“ Enhanced bone formation in sheep vertebral bodies after minimally invasive treatment with a novel, PLGA fiber-reinforced brushite cement.“ Spine J. 2017 May;17(5):709-719

6. **V.Horbert**, M.Lange, T.Reuter, M.Hoffmann, S.Bischoff, J.Borowski, H.Schubert, D.Driesch, J.Mika, C.Hurschler, R.W.Kinne.“ Comparison of Near-Infrared Spectroscopy with Needle Indentation and Histology for the Determination of Cartilage Thickness in the Large Animal Model Sheep.” Cartilage. 2017 Oct 1:1947603517731851.

7. F.Gunnella, E.Kunisch, M.Bungartz, S.Maenz, **V.Horbert**, L.Xin, J.Mika, J.Borowski, S.Bischoff, H.Schubert, P.Hortschansky, A.Sachse, B.Illerhaus, J.Günster, J.Bossert, K.D.Jandt, F.Plöger, R.W.Kinne, O.Brinkmann.“ Low-dose BMP-2 is sufficient to enhance the bone formation induced by an injectable, PLGA fiber-reinforced, brushite-forming cement in a sheep defect model of lumbar osteopenia.“ Spine J. 2017 Nov;17(11):1699-1711

8. M.Bungartz, E.Kunisch, S.Maenz, **V.Horbert**, L.Xin, F.Gunnella, J.Mika, J.Borowski, S.Bischoff, H.Schubert, A.Sachse, B.Illerhaus, J.Günster, J.Bossert, K.D.Jandt, F.Plöger, R.W.Kinne, O.Brinkmann.“ GDF5 significantly augments the bone formation induced by an injectable, PLGA fiber-reinforced, brushite-forming cement in a sheep defect model of lumbar osteopenia.“ Spine J. 2017 Nov;17(11):1685-1698.

9. F.Gunnella, E.Kunisch, S.Maenz, **V.Horbert**, L.Xin, J.Mika, J.Borowski, S.Bischoff, H.Schubert, A.Sachse, B.Illerhaus, J.Günster, J.Bossert, K.D.Jandt, F.Plöger, R.W.Kinne, O.Brinkmann, M.Bungartz.“ The GDF5 mutant BB-1 enhances the bone formation induced by an injectable, poly(l-lactide-co-glycolide) acid (PLGA) fiber-

reinforced, brushite-forming cement in a sheep defect model of lumbar osteopenia.“ Spine J. 2018 Feb;18(2):357-369.

10. **V.Horbert**, L.Xin, P.Foehr, O.Brinkmann, M.Bungartz, R.H.Burgkart, T.Graeve, R.W.Kinne.“ In Vitro Analysis of Cartilage Regeneration Using a Collagen Type I Hydrogel (CaReS) in the Bovine Cartilage Punch Model.” Cartilage. 2018 Feb 1:1947603518756985.

11. **V.Horbert**, P.Foehr, F.Kramer, U.Udhardt, M.Bungartz, O.Brinkmann, R.H.Burgkart, D.O.Klemm, R.W.Kinne.”In vitro analysis of the potential cartilage implant bacterial nanocellulose using the bovine cartilage punch model.” Cellulose. 2019; 26: 631. https://doi.org/10.1007/s10570-019-02260-z

12. **V.Horbert**, J.Böttcher, P.Foehr, F.Kramer, U.Udhardt, M.Bungartz, O.Brinkmann, R.H.Burgkart, D.O.Klemm, R.W.Kinne.” Laser perforation and cell seeding improve bacterial nanocellulose as a potential cartilage implant in the in vitro cartilage punch model” Cellulose. 2019; 26: 647. https://doi.org/10.1007/s10570-019-02286-3

Fachzeitschriften (Peer-Reviewed, eingereicht)

1. L.Xin, **V.Horbert**, S.Bischoff, H.Schubert, J.Borowski, S.Maenz, B.Illerhaus, R.W.Kinne, J.Mika.” First-time systematic post-operative clinical assessment of a minimally-invasive sheep large animal model for the treatment of osteochondral defects.” Journal of Orthopaedic Research

Fachzeitschriften (Peer-Reviewed, in Bearbeitung)

1. **V. Horbert**, J. Mika, L. Bischoff, J. Borgwardt, C. Witte, S. Bischoff, J. Borowski , M. Endres , H. Schubert , S. Pietsch , R.W. Kinne.”Long-term chondrogenesis without initial dedifferentiation following matrix-associated chondrocyte transplantation (MACT)”.

Vorträge (Fachtagungen)

1. **V. Kopsch**, P. Foehr, R.H. Burgkart, F. Kramer, U. Udhardt, D. Klemm, R.W. Kinne.“ In vitro analysis of bacterial nanocellulose implants using the bovine cartilage punch model”. MSE Darmstadt, 2014

2. **V. Kopsch**, M. Lange, T. Reuter, M. Hoffmann, S. Bischoff, J. Adolph, H. Schubert, J. Mika, C. Hurschler, R.W. Kinne.“ Non-invasive determination of cartilage thickness in the large animal model sheep by near-infrared spectroscopy”. ICRS Chicago, 2015

Poster (Fachtagungen)

2. **V.Kopsch**, A.Kroker, S.Pietsch, S.Bischoff, H.K.W.Plettenberg, R.W.Kinne.“Topografische Charakterisierung der Knorpeleigenschaften der medialen Femurkondyle im Großtiermodell Schaf mittels Nahinfrarot-spektroskopie (NIRS)“. AGA Wiesbaden, 2013

3. **V.Kopsch**, T. Ruediger, A. Dunzel, P. Foehr, R.H. Burgkart, T. Graeve, R.W. Kinne." In vitro analysis of biomaterial/cartilage regeneration using the bovine cartilage punch model". BioMat Weimar, 2013

4. **V.Kopsch**, T. Ruediger, A. Dunzel, P. Foehr, R.H. Burgkart, T. Graeve, R.W. Kinne." In vitro Analyse der Biomaterial/Knorpel-Regeneration mit dem bovinen Knorpel-Stanzen Modell". DKOU Berlin, 2013

5. **V.Kopsch**, P. Foehr, R.H. Burgkart, C. Kaps, M. Endres, R.W. Kinne." In vitro Testung eines PGA-Implantates in einem Knorpel-Regenerations-Modell". DKOU Berlin, 2014

6. **V. Kopsch**, M. Lange, T. Reuter, M. Hoffmann, S. Bischoff, J. Adolph, H. Schubert, J. Mika, C. Hurschler, R.W. Kinne." Non-invasive determination of cartilage thickness in the large animal model sheep by near-infrared spectroscopy". BioMat Weimar, 2015

7. **V. Kopsch**, J. Mika, L. Bischoff, J. Borgwardt, C. Witte, S. Bischoff, J. Adolph , M. Endres , C. Kaps, H. Schubert , S. Pietsch , R.W. Kinne."Long-term chondrogenesis without initial dedifferentiation following matrix-associated chondrocyte transplantation (MACT)". ICRS Chicago, 2015

8. **V. Horbert**, J. Mika, L. Bischoff, J. Borgwardt, S. Bischoff, C. Kaps, S. Pietsch, R.W. Kinne." Long-term chondrogenesis without initial dedifferentiation following matrix-associated chondrocyte transplantation (MACT)". DKOU Berlin, 2015

9. **V. Horbert**, L. Xin, C. Prinz, S. Bischoff, M. Endres, C. Ortmann, T. Vogl , R.W. Kinne." µCT analysis of a novel, cell-free osteochondral implant in the large animal model sheep - 6 and 12 month results". DKOU Berlin, 2016

10. **V. Horbert**, L. Xin, C. Prinz, S. Bischoff, M. Endres, C. Ortmann, T. Vogl , R.W. Kinne." µCT analysis of osteochondral regeneration with a novel, cell-free titanium implant in a sheep model - 6 and 12 month results". DKOU Berlin, 2017

Danksagung

An dieser Stelle möchte ich mich bei allen bedanken, die zum Gelingen dieser Arbeit beigetragen haben:

Mein besonderer Dank gilt Herrn Prof. Dr. med. Raimund W. Kinne für die Überlassung des Themas, die herzliche Aufnahme in die Arbeitsgruppe, für die interessanten Gespräche während der Bearbeitung, die engagierte Betreuung sowie der Begutachtung dieser Arbeit.

Weiterhin möchte ich mich bei Herrn Prof. Dr. Reinhard Wetzker für sein Interesse an dieser Arbeit sowie deren Begutachtung bedanken.

Ein herzliches Dankeschön geht außerdem an alle Mitarbeiterinnen und Mitarbeiter der AG „Experimentelle Rheumatologie“ für das offene und freundschaftliche Arbeitsklima. Stellvertretend möchte ich Frau Ulrike Körner und Frau Cordula Müller danken, die mit Ihrer Expertise in allen molekularbiologischen und histologischen Belangen entscheidend zum Gelingen dieser Arbeit beigetragen haben.

Außerdem möchte ich meinen Eltern danken, die mir mein Studium ermöglicht und mich mein Leben lang bei all meinen Vorhaben unterstützt haben.

Zuletzt möchte ich meinem lieben Ehemann Peter und meinen beiden Kindern Konstantin und Alexander dafür danken, dass Sie der größte Rückhalt in meinem Leben sind. Ich danke meiner gesamten Familie für die entgegengebrachte Geduld während der Erstellung dieser Arbeit.

Ehrenwörtliche Erklärung

Hiermit erkläre ich, dass mir die Promotionsordnung der Medizinischen Fakultät der Friedrich-Schiller-Universität bekannt ist,

ich die Dissertation selbst angefertigt habe und alle von mir benutzten Hilfsmittel, persönlichen Mitteilungen und Quellen in meiner Arbeit angegeben sind,

mich folgende Personen bei der Auswahl und Auswertung des Materials sowie bei der Herstellung des Manuskripts unterstützt haben: Prof. Dr. Raimund W. Kinne,

die Hilfe eines Promotionsberaters nicht in Anspruch genommen wurde und dass Dritte weder unmittelbar noch mittelbar geldwerte Leistungen von mir für Arbeiten erhalten haben, die im Zusammenhang mit dem Inhalt der vorgelegten Dissertation stehen,

dass ich die Dissertation noch nicht als Prüfungsarbeit für eine staatliche oder andere wissenschaftliche Prüfung eingereicht habe und

dass ich die gleiche, eine in wesentlichen Teilen ähnliche oder eine andere Abhandlung nicht bei einer anderen Hochschule als Dissertation eingereicht habe.

Jena, den 17. 10.2018 Victoria Horbert